EDITORIAL STAFF

R. J. McKay, Chairman, Publication Committee
Cecil V. King, Editor
Herman Hackerman, Technical Editor
Ruth G. Sterns, Managing Editor
U. B. Thomas, News Editor
Natalie Michalski, Assistant Editor

DIVISIONAL EDITORS

W. C. Vosburgh, Battery
J. E. Draley, Corrosion
John J. Chapman, Electric Insulation
Abner Brenner, Electrodeposition
H. C. Froelich, Electronics
D. H. Baird, Electronics—Semiconductors
Sherlock Swann, Jr., Electro-Organic
John M. Blocher, Jr., Electrothermics and Metallurgy, I
A. U. Seybolt, Electrothermics and Metallurgy, II
W. C. Gardiner, Industrial Electrolytic
C. W. Tobias, Theoretical Electrochemistry, I
A. J. de Bethune, Theoretical Electrochemistry, II

REGIONAL EDITORS

Howard T. Francis, Chicago
Joseph Schulein, Pacific Northwest
J. C. Schumacher, Los Angeles
G. W. Heise, Cleveland
G. H. Fetterley, Niagara Falls
Oliver Osborn, Houston
Earl A. Gulbransen, Pittsburgh
A. C. Holm, Canada
J. W. Cuthbertson, Great Britain
T. L. Rama Char, India

ADVERTISING OFFICE

Jack Bain, Advertising Manager
545 Fifth Avenue, New York 17, N. Y.

ECS OFFICERS

Herman Hackerman, President
University of Texas, Austin, Texas
Sherlock Swann, Jr., Vice-President
University of Illinois, Urbana, Ill.
W. C. Gardiner, Vice-President
Olin Mathieson Chemical Corp., Niagara Falls, N. Y.
R. A. Schaefer, Vice-President
Cleveland Graphite Bronze Div., Clevite Corp., Cleveland, Ohio
Lyle I. Gilbertson, Treasurer
Air Reduction Co., Murray Hill, N. J.
Henry B. Linford, Secretary
Columbia University, New York, N. Y.
Robert K. Shannon, Assistant Secretary
National Headquarters, The ECS, 1860 Broadway, New York 23, N. Y.

Journal of the Electrochemical Society

JULY 1957 **VOL. 104 • NO. 7**

CONTENTS

Editorial

Training a Chemist 138C

Technical Papers

The Overpotential of the Manganese Dioxide Electrode, II. Acid Electrolytes. *Shiro Yoshizawa and W. C. Vosburgh* 399

Anodic Corrosion and Hydrogen and Oxygen Overvoltage on Lead and Lead Antimony Alloys. *P. Rüetschi and B. D. Cahan* 406

Oxidation of Iron-Nickel Alloys, II. Electron Diffraction at High Temperature. *R. T. Foley, C. J. Guare, and H. R. Schmidt* 413

Dissolution of Iron in Acidified Chromic Chloride Solutions. *Robert Skomoroski and C. V. King* 417

The Activation and Passivation of Stainless Steel in Aerated Sulfuric Acid. *G. H. Cartledge* 420

Ionic Conductivity of Anodic Films at High Field Strengths: Transient Behavior. *D. A. Vermilyea* 427

Metal-Water Reactions, V. Kinetics of the Reaction between Magnesium and Water Vapor. *H. J. Svec and D. S. Gibbs* 434

Enhanced Surface Reactions. *M. J. D. Low and H. A. Taylor* 439

Luminescence of Modified Tin-Activated Strontium Orthophosphate. *H. Koelmans and A. P. M. Cox* 442

Energy Transport by Cascade and Resonance Processes in Doubly Activated Phosphors. *E. W. Claffy and C. C. Klick* 445

Electrolytic Production of Bromates. *T. Osuga and K. Sugino* 448

High Temperature Oxidation of High Purity Nickel between 750° and 1050°C. *E. A. Gulbransen and K. F. Andrew* 451

Impedance at Polarized Platinum Electrodes in Various Electrolytes. *J. N. Sarmousakis and M. J. Prager* 454

Technical Note

Electrodeposition of Lead from the Pyrophosphate Bath. *J. Vaid and T. L. Rama Char* 460

Technical Review

A Review of Patents on Silicon Carbide Furnacing. *J. C. McMullen* 462

Current Affairs

R. J. McKay Appointed Publication Committee Chairman 141C

Abstracts of Electronics—Semiconductor "Recent News" Papers Presented at Washington Meeting 142C

Section News 143C
New Members 144C
Personals 146C
News Items 146C
Book Reviews 148C
Announcements from Publishers 149C
Meetings of Other Organizations 150C
Employment Situations 150C

Published monthly by The Electrochemical Society, Inc., from Manchester, N. H., **Executive Offices, Editorial Office** and **Circulation Dept.** at 1860 Broadway, New York 23, N. Y., **Advertising Office** at 545 Fifth Ave., New York, N. Y., combining the JOURNAL and TRANSACTIONS OF THE ELECTROCHEMICAL SOCIETY. Statements and opinions given in articles and papers in the JOURNAL OF THE ELECTROCHEMICAL SOCIETY are those of the contributors, and The Electrochemical Society assumes no responsibility for them. Nondeductible subscription to members $5.00; subscription to nonmembers $18.00. Single copies $1.25 to members, $1.75 to nonmembers.

Copyright 1957 by The Electrochemical Society, Inc.

Entered as second-class matter at the Post Office at Manchester, N. H., under the act of August 24, 1912.

THE ELECTROCHEMICAL SOCIETY, INC.

The Electrochemical Society is an international organization of individuals and companies concerned with or interested in Electrochemistry and allied subjects.

The Society is dedicated to the advancement of the theory and practice of Electrochemistry and related subjects, as shown in the following divisions:

Battery	Electro-Organic
Corrosion	Electrothermics and Metallurgy
Electric Insulation	Industrial Electrolytic
Electrodeposition	Theoretical Electrochemistry
Electronics	

Among the means to this end are the holding of meetings for the reading and discussion of professional and scientific papers on these subjects, the publication of such papers, discussions, and communications as may seem appropriate, and cooperation with chemical, electrical, and other scientific and technical societies.

It is an incorporated society without capital stock. The affairs of the Society are managed by a Board of Directors under a Constitution and Bylaws. Officers are nominated by a nominating committee appointed by the Board of Directors and elected by the members.

Direct all general correspondence and inquiries regarding membership to Society headquarters at 1860 Broadway, New York 23, N. Y.

Officers of the Society

President	NORMAN HACKERMAN
Past President	HANS THURNAUER
Vice-President	SHERLOCK SWANN, JR.
Vice-President	W. C. GARDINER
Vice-President	R. A. SCHAEFER
Treasurer	LYLE I. GILBERTSON
Secretary	HENRY B. LINFORD

Plating Electrotype Shells

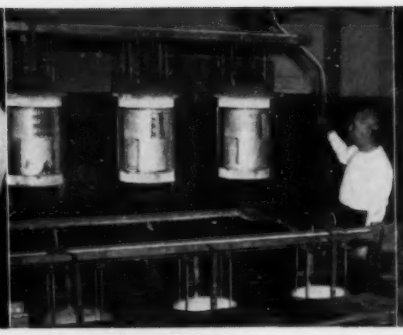

Plating Stereotypes

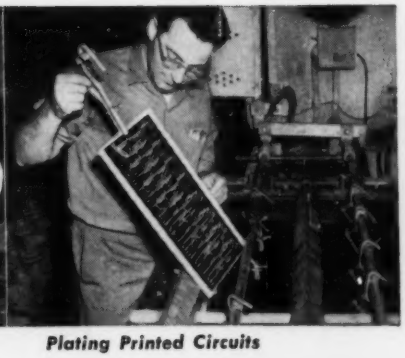

Plating Printed Circuits

Building Up Worn Parts

Plating Versatile Lead-Tin Alloys

High Speed Wire Plating

You can electroplate 10 ways better

with B&A FLUOBORATE Plating Solutions

LEAD

TIN

IRON

COPPER

NICKEL

CADMIUM

INDIUM

1. No mixing or dissolving necessary . . . supplied in concentrated solution form
2. Easier bath preparation
3. Stability of bath composition
4. Ease of control
5. Practically 100% anode and cathode efficiencies
6. High conductivity
7. Good covering power
8. Fine-grained deposits of good color
9. Faster, high-speed operation
10. Readily adaptable for alloy deposits: lead-tin and lead-tin-copper alloys

FINE CHEMICALS

B'A

STANDARD OF PURITY

REAGENTS

AND MANY MORE ADVANTAGES . . .

. . . enabling you to increase production . . . lower your operating costs . . . get easier, simpler operations. In addition to the advantages listed, each fluoborate bath offers a number of special advantages for its particular applications.

Here is the *modern* way to electroplate. Mail the coupon now for complete information.

JE-7

BAKER & ADAMSON® *Fine Chemicals*
GENERAL CHEMICAL DIVISION
ALLIED CHEMICAL & DYE CORPORATION
40 Rector Street, New York 6, N. Y.

Please send me, without cost or obligation, complete technical data on the use of fluoborate solutions for the following plating applications

_____

Name_____

Title_____

Company_____

Address_____

City_____ Zone____ State_____

Editorial

Training a Chemist

THE India Section of The Electrochemical Society prides itself on the fact that it is the only Section which has its own publication. The Bulletin of the India Section appears quarterly, and is now in its sixth year. It is not a large publication, but each issue contains a few technical papers, news of Indian and other electrochemical industries, book lists and reviews, abstracts of articles of interest, and an editorial which usually deals with some aspects of chemistry or the chemical industry which are peculiar to India. The technical papers are abstracted by *Chemical Abstracts*.

The India Section is small in numbers, but bold in spirit and endeavor, and should be congratulated on its efforts to improve its great country through the medium of chemistry. In addition to its members, the Section has the support of some 21 industrial Patrons in India. It deserves the support and encouragement of ECS members in other countries. This might take many forms, from subscribing to the Bulletin, donating books or apparatus, to more ambitious plans such as raising funds for fellowships, or cooperating with the Section in arranging for exchange of personnel.

The January 1957 Bulletin contained an editorial with the above title, "Training a Chemist." While at first glance the questions discussed seem peculiar to India, further scrutiny reveals that they are universal problems. The author points out that while science graduates may be equipped with good basic knowledge, they should also have been "led to see and think in the way of a true scientific mind." He also fears that employers often find that graduates lack the kind of training essential for a successful operating chemist. He suggests that the chemical industries establish a system of apprenticeships, or that they lend experienced men to give intensive courses in practical training, to deal with the latter difficulty.

In the United States, employers must, of course, usually provide some practical training, or allow time for the new employee to become acclimated. We are fortunate in having a wide variety of institutions which offer training at almost any level. An intelligent high-school graduate who likes chemistry can take an intensive two-year course which will fit him for many positions in the industry, or he can spend 8 years in acquiring a Ph.D. degree. The Universities, especially in the graduate schools, do much soul-searching with regard to the curriculum: shall we concentrate on a few fundamental courses, or shall we in addition offer specialized courses, as in Electrochemistry, Colloids and Polymers, Catalysis, and the like?

The trend seems to be to emphasize the fundamental courses. If an employer wants a technician, he can go to the proper institution. Many large industrial employers can say no, we do not especially want graduates of a particular technical course. We have our own problems and will have to train your graduate in our own methods, anyway. Give us a man as well trained in fundamentals as possible, with laboratory experience and experimental skill, with good and adaptable personality, and who at least shows promise of originality and independent thinking. . . .

Every employer would like his scientists to have been ". . . led to see and think in the way of a true scientific mind."

—CVK

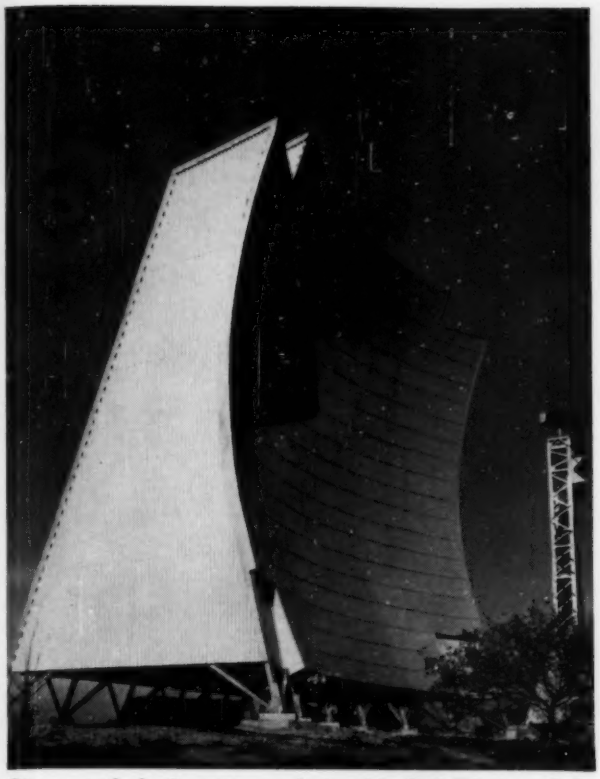

Giant over-the-horizon antenna designed by Bell Telephone Laboratories for "White Alice," Air Force Alaskan defense communications network.

How UHF radio got seven-league boots

THE huge antenna systems which project ultra-high frequency radio communications beyond the horizon began when a Bell Telephone Laboratories engineer became intrigued with a strange phenomenon. Although these radio waves were supposed to be useful only over line-of-sight distances, the waves displayed a mysterious tendency to take off in a giant stride to antennas beyond the horizon.

This phenomenon had been studied both here and abroad, but no practical use was seen until the engineer became interested and thoroughly sifted the experimental data. He came up with the stimulating conclusion that over-the-horizon transmission is far stronger and much more dependable than was generally supposed. Further he predicted that it could be utilized to supply dependable broadband communications. He and his associates at Bell Laboratories confirmed the prediction experimentally, then drew up requirements for the first over-the-horizon UHF transmission system.

This pioneer work at Bell Telephone Laboratories has greatly increased the usefulness of UHF communications. For example, over-the-horizon transmission now provides critically important communications between remote military outposts in the Arctic and in the far north.

For the Bell System it can provide important new links for telephone conversations and television.

Kenneth Bullington, B.S.E.E., University of New Mexico; M.S., Massachusetts Institute of Technology; recipient of the 1956 Morris Liebmann Memorial Prize and the 1956 Stuart Ballantine Medal for his contributions in the field of over-the-horizon ultra-high frequency radio transmission.

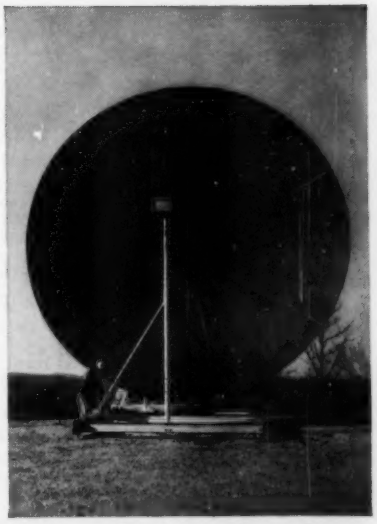

Experimental antenna used in early over-the-horizon UHF radio transmission research. Research extended transmission from 30 miles line-of-sight to 200 miles.

BELL TELEPHONE LABORATORIES

WORLD CENTER OF COMMUNICATIONS RESEARCH AND DEVELOPMENT

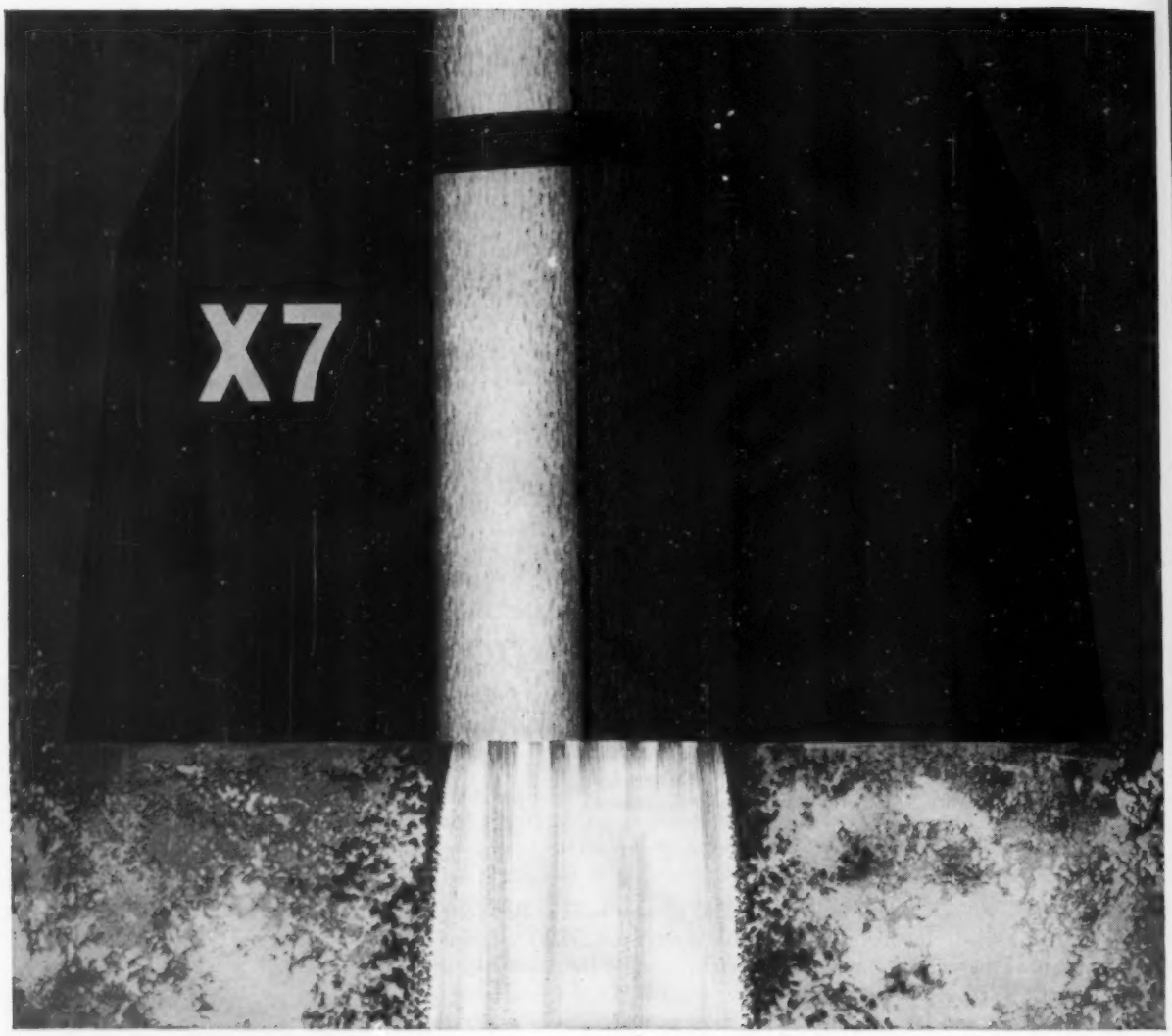

New punch for missile propellants

High heat of reaction, other characteristics point to magnesium for high-energy fuels

Magnesium, in its finely divided form, may well be suitable for new types of rocket fuels. It has long been known that a tremendous amount of chemical energy is locked within the metal. Upon further examination, finely divided magnesium has many significant characteristics that are important to the development of an efficient fuel:

High heat of reaction
Chemically reactive
High energy per unit volume
High theoretical flame temp.
Can be dispersed in various media
Products of combustion are: inert, relatively non-abrasive and present no toxicity problem
Inexhaustible raw material supply

Magnesium's heat of reaction, for example, compares to that of other fuel materials as follows: magnesium, 14,200 B.T.U. per lb. of oxygen required for combustion; aluminum, 13,370; lithium, 10,980; boron 9,670 (all at 2900°K). This plus magnesium's high theoretical flame temperature indicates that magnesium is especially adaptable for short-range applications where high initial thrust is desirable.

In addition, magnesium can also be considered as an intermediate in the manufacture of other metallic and organometallic fuels.

For information about finely divided magnesium, contact your nearest Dow sales office or write THE DOW CHEMICAL COMPANY, Midland, Michigan, Department MA1438QQ-1.

YOU CAN DEPEND ON DOW

The Overpotential of the Manganese Dioxide Electrode

II. Acid Electrolytes

Shiro Yoshizawa[1] and W. C. Vosburgh

Duke University, Durham, North Carolina

ABSTRACT

The overpotential of electrodes prepared by electrodeposition on graphite was measured in solutions of sulfuric acid and manganese(II) and sodium sulfates as a function of acidity, current density, and temperature. The relation of overpotential to current density and the shapes of the growth and decay curves can be explained quantitatively, on the assumption that the primary reduction product is MnOOH on the MnO_2 surface and the electrode potential is dependent on the ratio of MnOOH to MnO_2 on the surface.

The overpotential of the MnO_2 electrode in NH_4Cl electrolyte at *p*H 5 and *p*H 7 was measured by Chreitzberg and Vosburgh (1). The overpotential was defined as the difference between the open-circuit potential in the steady state attained after a discharge and the closed-circuit potential at the end of the discharge. The outstanding features observed in this and previous work (2) were (*a*) the overpotential increases slowly at the beginning of a discharge, (*b*) the decay after breaking the circuit is slow, (*c*) the relation between overpotential and the logarithm of the current density is not linear, and (*d*) the overpotential is a linear function of the logarithm of the ammonium ion concentration at constant ionic strength. These facts seemed best explained qualitatively on the basis of two assumptions: (*a*) the potential of a MnO_2 electrode depends on the composition of the oxide at the surface exposed to the solution (3, 4); (*b*) during or after discharge the lower oxide formed at the surface can diffuse into the higher oxide below, perhaps by a process involving the movement of only protons and electrons (2, 5). In addition, when enough of a suitable electrolyte is present it is known that considerable managanese(II) ion goes into solution during a discharge, and this reaction continues for a time after the circuit is broken (4, 6). In solutions of high *p*H the manganese(II) ion in solution should eventually react with any MnO_2 remaining on the electrode to bring the system to complete equilibrium.

The slow growth of the overpotential is considered to result from the reduction of MnO_2 at the surface exposed to the solution at a rate faster than that at which the lower oxide produced is removed. In the steady state of polarization these two rates become equal, with more lower oxide on the surface than at open-circuit equilibrium. After breaking the circuit the excess lower oxide continues to be removed from the surface by the two processes, inward diffusion and reaction with the electrolyte to give manganese(II) ion. The effect of the ammonium ion concentration is explained as an effect on the rate of reaction of ammonium ion with the lower oxide.

With two independent processes for the removal of lower oxide from the surface, the discharge is more complicated than desirable for a quantitative explanation. By changing the conditions, one or the other of the processes can be reduced in importance or eliminated. In a sufficiently acid solution containing considerable manganese(II) ion the MnO_2 electrode potential after a discharge returns to a value equal to that before discharge (7). This indicates that all of the lower oxide produced has reacted with the acid.

Discharges in several acid solutions have been carried out. The overpotentials have been measured and the discharge and recovery curves observed. It has been possible to develop equations for the variation of the overpotential with current density and for the growth and decay of the overpotential.

Experimental Methods

The preparation of MnO_2 electrodes by electrodeposition on graphite rods and the preparation of cells were as previously described (1, 8). The electrodes were made of cylindrical graphite rods with 8 cm^2 of exposed area on which was electrodeposited 0.2 mmole of MnO_2. The cells consisted of a centrally located MnO_2 electrode in a vessel holding about 190 ml of electrolyte with a cylindrical Pb electrode lining the wall of the vessel. A Luggin capillary was provided for a reference electrode which was of Hg and Hg_2SO_4 with an electrolyte the same as, or similar to, that of the cell.

Constant current for discharges was provided by four dry cells in series, with hand regulation of the resistance in the circuit. Both current and the potential difference between the MnO_2 and Hg_2SO_4 electrodes were measured by a recording potentiometer sensitive to about 1 mv. The cells were maintained at 25° ± 0.5°C in an air bath during measure-

[1] Present address: Department of Industrial Chemistry, Kyoto University, Kyoto, Japan.

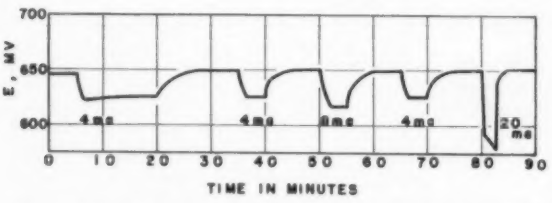

Fig. 1. Open- and closed-circuit potentials of a single electrode in electrolyte 1. The equilibrium open-circuit potential was 650 mv, while the closed-circuit potential depended on the current as shown. The curve was redrawn from a recording potentiometer graph.

ments and the electrolyte was stirred during measurements by a magnetic stirrer.

Overpotential Measurements

The cells were allowed to stand over-night before measurements were begun. After 15 min or more on open circuit a current was passed until constancy was attained. With an electrolyte 1M in H_2SO_4 and 0.1M in $MnSO_4$ constancy of closed-circuit potential was ordinarily attained within 2 min, except in the first discharge, as shown in Fig. 1. On breaking the circuit, constancy of open-circuit potential was usually attained in about 6 min. The difference between the constant closed-circuit potential and the constant open-circuit potential after the discharge was taken as the overpotential. Several successive measurements were possible with a single electrode as illustrated in Fig. 1, which was copied from part of a recorder graph.

Overpotentials at the same current density either on a single electrode or on different electrodes seldom differed by more than 1 mv. In the first discharge of a fresh electrode the potential usually passed through a pronounced minimum before becoming constant as shown in Fig. 1. In subsequent discharges made soon after the first a minimum was detected only when a more sensitive recording potentiometer was used, in which case there was a faint minimum in each discharge curve. When the first discharge was at very small current density there was usually only a small minimum, but a larger one appeared later when a sufficiently large current was passed. When an excessively large current was passed the closed-circuit potential did not become constant, as illustrated in the 20-ma discharge at 83 min in Fig. 1. Such a discharge always damaged the electrode so that overpotentials measured afterward at lower current densities were too large. With lower acid concentration the attainment of equilibrium was a little slower and the reproducibility not quite so good, but the overpotential was larger and the relative error about the same. When the electrolyte contained 0.01M H_2SO_4, 0.99M Na_2SO_4 and 0.10M $MnSO_4$, closed-circuit potentials became constant in 3-4 min and, after a discharge, 30-45 min was required for constancy of the open-circuit potential.

Overpotential measurements were made at several current densities and with five electrolytes containing H_2SO_4, the compositions of which are given in Table I. In column 4 of Table II the observed overpotentials are given. An approximate calculation of the concentration overpotential showed that only at the highest current densities was this appreciable. When the calculated value was over 0.5 mv a correction was made, but no corrections were over 1 mv. The iR drop included in the measurements was a little larger. This was calculated in two parts, that along the graphite rod, and that through the solution; the two were of approximately equal magnitude. The larger part of the difference between the observed and corrected values in Table II is this correction. The last column was calculated by Eq. (XXVI).

Table I. Composition of acid electrolytes

No.	Composition, M H_2SO_4	Na_2SO_4	$MnSO_4$	pH
1	1.00	—	0.10	0.12[c]
2	0.50	0.50	0.10	0.55[c]
3	0.10	0.90	0.10	1.55[c]
4	0.05	0.95	0.10	2.12[c]
5	0.01	0.99	0.10	2.59[c]
6	[b]	0.33	—	4.0[a]
SH1	0.04	—	0.01	1.39[c]
SH2	0.0125	0.015[d]	0.01	1.94[c]

[a] Measured with a glass electrode. [b] Acetic acid, 0.1M, and 0.01M sodium acetate. [c] Calculated. [d] K_2SO_4.

Table II. Variation of overpotential with current density and acidity. 25°C.

No. of electrodes	No. of measurements	Current density ma/electrode	Overpotential, mv Obs.	Corr.	Calc.
		Part 1. Electrolyte No. 1.			
1	1	0.40	8	8	8
1	1	0.50	10	10	10
1	2	1.00	16	16	15
3	4	2.0	20	20	21
3	5	4.0	25	24	29
1	1	8.0	32	31	37
1	1	16.0	46	44	45
1	1	24.0	54	51	50
		Part 2. Electrolyte No. 2			
2	2	1.00	14	14	11
2	2	2.0	18	18	17
2	2	4.0	22	21	23
2	2	8.0	30	29	31
2	2	16.0	42	40	40
2	2	32.0	51	47	49
		Part 3. Electrolyte No. 3			
1	1	0.50	10	10	10
1	1	1.00	14	14	17
1	1	2.0	21	21	23
1	3	4.0	29	28	31
1	1	6.0	39	38	36
1	1	8.0	42	40	40
1	1	10.0	45	43	43
1	1	12.0	53	51	46
		Part 4. Electrolyte No. 4			
1	3	1.00	22	—	—
1	1	2.0	28	—	—
1	1	4.0	33	—	—
		Part 5. Electrolyte No. 5			
2	2	0.70	19	19	19
3	5	1.00	21	21	22
3	4	2.0	28	27	31
3	4	4.0	39	37	41
1	1	6.0	50	47	47
1	1	8.0	56	53	52

Table III. Variation of overpotential with current density in an electrolyte of 0.33M Na_2SO_4, 0.1M acetic acid, and 0.01M sodium acetate, pH 4.0, 25°C

Current ma	Obs. overpotential, mv, at 100 ma-min	200 ma-min	300 ma-min
0.4	30	33	39
0.5	38	39	40
1.0	52	52	—
2.0	68	68	68
3.0	(57)	78	78
5.0	90	92	95
1.0*	44	50	56
2.0*	64	67	69

* Ammonium sulfate instead of sodium sulfate in the electrolyte.

In Table III are shown some overpotentials in an electrolyte of 0.33M Na_2SO_4, 0.1M acetic acid, and 0.01M sodium acetate (electrolyte 6). The establishment of a steady state of polarization was slower in this electrolyte, and measurements were made on each electrode after 100, 200, and 300 ma-min of discharge at a single current density. At the lowest current density the overpotential increased appreciably as the discharge proceeded, but usually the increase was small up to 300 ma-min of discharge. In two discharges ammonium sulfate was substituted for the sodium sulfate, with only a small effect in the direction of less overpotential.

With electrolyte 6, trouble was experienced in getting constant initial open-circuit potentials, and it was suspected that peroxide formation was responsible (9). Exclusion of oxygen by a current of nitrogen led to satisfactory constancy.

Overpotential and Acidity

The relation of overpotential to the acidity of the electrolyte is shown in Table IV. In the second column are given the total H_2SO_4 concentrations of all but two of the electrolytes. The acid must have been ionized mostly to H_3O^+ and HSO_4^-. The pH values of electrolytes 1-6 and the C and V electrolyte were measured by means of a glass electrode. Those of SH1 and SH2 were calculated, these electrolytes having an ionic strength of only 0.1.

The overpotentials in the fifth column were calculated by the empirical equation $\Delta E_c = 17 + 7$ pH. This expresses the results well for electrolytes 2-5

Table IV. Variation of overpotential with acidity; current density 4 ma/8 cm^2; 25°C

Electrolyte[a]	H_2SO_4 M	pH	Overpotential, mv Corr.[b]	Calc'd (1)	Calc'd (2)
1	1.00	0.1	24	18	19
2	0.50	0.6	21	21	22
3	0.10	1.6	28	28	28
4	0.05	2.1	32	32	31
5	0.01	2.6	37	35	37
SH1	0.04	1.3	35	26	32
SH2	0.0125	1.9	36	30	36
C and V	*c*	7	70	66	—
6	*d*	4.0	85	45	—

[a] *See* Table I for composition of electrolytes.
[b] Corrections for *IR* drop and concentration polarization not exceeding a total of 2 mv have been applied.
[c] The source of protons for the reaction was 2M NH_4Cl (1).
[d] The source of protons was 0.1M acetic acid.

and C and V, but fails for the others. The assumption that the overpotential is determined by the nature and concentration of the source of protons for the electrode reaction leads to a better equation. It is sufficient for present purposes to assume that the H_3O^+ and HSO_4^- ions are equivalent and to relate the overpotential to twice the total H_2SO_4 concentration. This gives the equation $\Delta E_c = 22 - 9\log 2c$ in which c is the concentration. The last column of Table IV shows that this equation gives good calculated values for all of the electrolytes containing H_2SO_4 except electrolytes 1 and SH1, for which the calculated values are 5 and 3 mv too low, respectively. These two solutions were the only ones that contained no cations other than H_3O^+ and Mn^{++}.

Growth and Decay of Polarization

For the investigation of the shapes of the growth and decay curves a recording potentiometer with a chart speed of about 5 cm/min and a sensitivity of about 0.01 mv was used. This instrument had a range of only 0-10 mv, so most of the electromotive force was balanced by a hand-operated potentiometer.

The curves showed evidence of a small *iR* drop in agreement with the calculated values and negligible for these experiments. Some curves are shown in connection with their discussion below.

The discharge curves all showed minima like that in the first discharge in Fig. 1. The minima in second and subsequent discharges made soon after the first were too small to have been recognized in the measurements of Fig. 1.

Evidence for the Presence of Lower Oxide on the Electrode Surface

If polarization is the result of the accumulation of lower oxide on the surface it should be possible to demonstrate its presence. An electrode was discharged in electrolyte 1 to a steady state of polarization at a current of 1 ma/8 cm^2. It was then quickly removed from the electrolyte, washed, and placed in a test tube containing 1M H_2SO_4 without added manganese sulfate. After 5 min it was transferred to a second portion of the same solution, and after increasing periods of time to a third, fourth, and fifth portion. Mn was determined colorimetrically in each portion of the solution. The electrode was replaced in the cell with electrolyte 1 and the experiment repeated with a discharge at 4 ma. Two more experiments were made with 4-ma discharges of another electrode. Blank experiments were made by bringing the two electrodes to open-circuit equilibrium with electrolyte 1 and then transferring to the successive portions of 1M H_2SO_4. Results are shown in the three upper curves of Fig. 2.

All three curves show that manganese(II) ion is extracted continuously for more than 80 min both after a discharge and in the blanks. The curves for the discharged electrodes lie above those for the blanks as the result of the extraction of more manganese(II) ion in the first 5 min. After 5 min all are approximately parallel. The experiment was repeated with electrolyte 5 with similar results. It may be concluded that there is an excess of lower

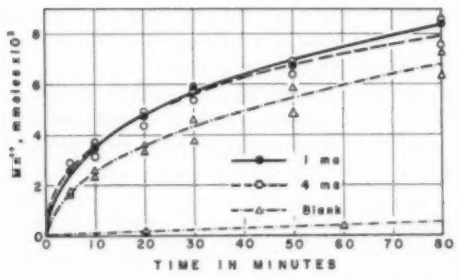

Fig. 2. Manganese(II) ion dissolved from partially discharged and undischarged electrodes. In the experiments represented by the three upper curves the electrodes were transferred from a solution containing 0.1M $MnSO_4$ and 1M H_2SO_4 to one of 1M H_2SO_4. The lowest curve represents an electrode at constant potential in 1M H_2SO_4 transferred to 1M H_2SO_4.

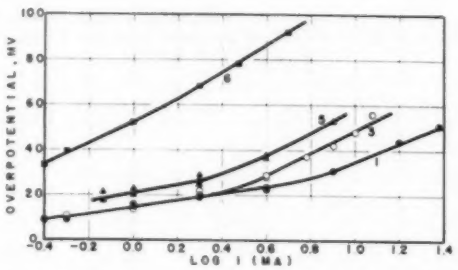

Fig. 3. Relation between overpotential and the logarithm of the current density (ma/8 cm^2). The numbers indicate the electrolytes, compositions of which are given in Table I.

oxide on the surface of a freshly discharged electrode.

The continuous extraction of manganese(II) ion from the electrodes is largely the result of the transfer of the electrode from a solution containing 0.1M $MnSO_4$ to one free from Mn. In the first solution the electrode takes up manganese(II) ion and in the second solution releases it slowly. A corresponding slow change in electrode potential takes place when the electrode is transferred from one solution to the other.

When an electrode was kept in 1M H_2SO_4 free from Mn, with occasional change of solution, until there was no further change of potential, it released only a little manganese(II) ion to fresh 1M H_2SO_4. The record of such an experiment is given in the lower blank curve of Fig. 2. A sample at 180 min confirmed the linear relationship shown. This may be a true self-discharge and is equivalent to a current density of 0.02 ma/8 cm^2.

Effect of Temperature

Measurements similar to those in Table II were made at different temperatures. Some of the results are shown in Fig. 8, below, in connection with their discussion. The 15°-values are in poor agreement with the others. Similar measurements were made with electrolyte 5.

The effect of temperature can be compared with that at pH 7. The ratio of the overpotential at 5°C to that at 25°C is 1.4 at pH 7 (1) with a current density of 1.6 ma/electrode, while with electrolyte 1 the corresponding ratio is 2.2 for 1 ma/electrode and 2.7 for 2 ma/electrode. For electrolyte 5 the ratios for 15° and 25°C are 1.7 and 1.9 as compared with 1.2 for pH 7. The ratios increase with acidity. Electrolytes 1 and 5 can be compared at temperatures 25° and 50°C; the ratio for a current of 2 ma/electrode is 2.3 for electrolyte 1 and 1.4 for electrolyte 5.

Effect of Thickness of MnO_2

A few electrodes were made with thinner and thicker deposits of MnO_2 by plating for 15 min or 2 hr instead of the usual 30 min at 25 ma/electrode. The overpotential for a 4-ma discharge was 29 mv for a 15-min electrode, 24 mv for a 30-min electrode, and 11 mv for a 2-hr electrode. Comparison of the discharge curves for a 1-ma discharge of a 30-min and a 2-hr electrode shows that the minimum value comes considerably later for the 2-hr electrode, at 12 min after the beginning of the discharge instead of 5 min. The minimum usually comes at about the same stage of discharge as measured in ma-min (1). This suggests that the true current density may be smaller for the 2-hr electrode, because of larger surface area. A smaller current density should give a smaller overpotential in qualitative agreement with experiment. However, ratios of surface area estimated from the minima and from the overpotentials did not agree.

Discussion

The Tafel Equation.—In Fig. 3 the relation between the overpotential and the logarithm of the current density for electrolytes 1, 3, 5, and 6 is shown. The curves for the more acid solutions might be considered to consist of two interesting straight lines. All resemble the relation in NH_4Cl electrolyte at pH 7 except that the overpotential decreases considerably with the large increase in acidity (1). The slope of the low-current portion for electrolytes 1 and 3 is 15 mv/log I. At lower acidity the slope is larger but approaches this value as the current decreases. For the lead dioxide electrode the corresponding slope is about 18 mv/log I (10).

A theory of the overpotential similar to that for the hydrogen evolution reaction (11) does not account for the slow growth and decay of polarization and predicts too high a slope for the Tafel equation. An alternative theory has been developed that accounts for the slow decay of polarization and is also in accord with the observed relation of current and overpotential.

Decay of Polarization.—The postulates adopted are as follows. (*A*) The potential of a MnO_2 electrode is determined in part by the composition of the surface exposed to the electrolyte (3, 4). (*B*) Overpotential results from an excess of the reaction product on the surface. (*C*) In a steady state of discharge in sufficiently acid electrolytes the reaction product is removed by reaction with the acid as fast as it is formed. (*D*) The primary reaction product is MnOOH, which reacts with the acid of the electrolyte according to the equation:

$$2MnOOH + 2H^+ \rightleftarrows MnO_2 + Mn^{++} + 2H_2O \qquad (A)$$

Consider the concentrations of hydrogen and manganese(II) ions and the ionic strength constant,

which was approximately true in the experiments. Let L be the mole fraction of MnOOH in the electrode surface and $(1-L)$ the mole fraction of MnO_2. Tne rate at which MnOOH is removed from the surface in accordance with Eq. (A) can be expressed by

$$-\frac{dL}{dt} = k_1L^2 - k_2(1-L) \qquad (I)$$

in which k_1 and k_2 are the velocity constants of the forward and reverse reactions. These constants include the constant hydrogen and manganese ion concentrations. If the postulates are correct, Eq. (I) should apply to the reaction of excess lower oxide on the electrode surface with acid, on open circuit, that is, to the decay of polarization. At equilibrium, $-dL/dt$ is zero and L becomes L_e, the mole fraction of lower oxide in the surface at equilibrium on open circuit. It will be assumed that L_e is small with acid electrolytes. Then, at equilibrium

$$\frac{k_1}{k_2} = \frac{1-L_e}{L_e^2} \cong \frac{1}{L_e^2} \qquad (II)$$

Integration of (I) and simplification using (II) and assuming L_e^2 negligible compared with L, gives

$$\ln\frac{L+L_e}{L-L_e} = t\sqrt{(k_2)^2 + 4\,k_1k_2} + C \qquad (III)$$

in which C is the integration constant. Taking L_e as negligible when added to or subtracted from unity, (III) can be arranged to give

$$\ln\frac{\dfrac{1}{L_e}+\dfrac{1-L}{L}}{\dfrac{1}{L_e}-\dfrac{1-L}{L}} = kt + C \qquad (IV)$$

in which $k = \sqrt{(k_2)^2 + 4\,k_1k_2}$

It is assumed, in agreement with postulate (A), that the electrode potential E is determined by L and $1-L$ in accordance with the equation

$$E = E^\circ - \frac{RT}{F}\ln\frac{L}{1-L} \qquad (V)$$

In the steady state of polarization $L = L_p$ and $E = E_p$, and at open-circuit equilibrium $L = L_e$ and $E = E_e$. The increase of potential at any time after opening the circuit is $E - E_p = \Delta E$ and the overpotential is $E_e - E_p = \Delta E_e$. It follows that

$$\Delta E = \frac{RT}{F}\ln\frac{1-L}{L}\cdot\frac{L_p}{1-L_p} \qquad (VI)$$

$$\Delta E_e = \frac{RT}{F}\ln\frac{1-L_e}{L_e}\cdot\frac{L_p}{1-L_p} \cong \frac{RT}{F}\ln\frac{L_p}{L_e(1-L_p)} \qquad (VII)$$

Combining (IV), (VI), and (VII)

$$\ln\frac{\exp\left[(\Delta E_e)F/RT\right] + \exp\left[(\Delta E)F/RT\right]}{\exp\left[(\Delta E_e)F/RT\right] - \exp\left[(\Delta E)F/RT\right]} = kt + C \qquad (VIII)$$

Since $\Delta E = 0$ when the circuit is opened at $t = 0$,

$$C = \ln\frac{\exp\left(\Delta E_e\right)F/RT + 1}{\exp\left(\Delta E_e\right)F/RT - 1} \qquad (IX)$$

Eqs. (VIII) and (IX) give the change in ΔE with time when the polarized electrode is allowed to stand in the electrolyte on open circuit.

Decay curves were determined as described above. From the initial and final values of the electrode potential ΔE_e was calculated, and k was evaluated from one value of ΔE after 2-5 min. It was then possible to calculate the curves. If the left-hand term of Eq. (VIII) is plotted against the time, a straight line is obtained, with a few of the early points and some of the last ones deviating from the line. Since errors in the later observations are magnified in this plot, it is more satisfactory to plot ΔE against time, as in Fig. 4 and 5. The equation holds well for electrolyte 1, except near the beginning, and less well for electrolyte 5. The considerably smaller acid concentration in electrolyte 5 and slower rate of dissolving of the lower oxide may make possible an appreciable amount of diffusion of lower oxide into the interior of the MnO_2 thus complicating the decay of polarization.

Growth of polarization.—One may now proceed on the assumption that the overpotential is determined by a balance between the formation of lower oxide and its dissolution by the electrolyte. In the

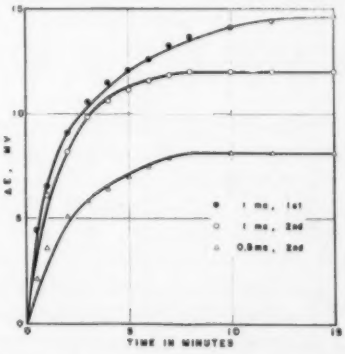

Fig. 4. Decay of polarization, electrolyte 1; the increase in potential after opening the circuit, ΔE, plotted against time. The lines were calculated by means of Eqs. (VIII) and (IX) and the points were taken from the recorded decay curves. The topmost curve followed the first discharge of an electrode, while the other two followed second discharges.

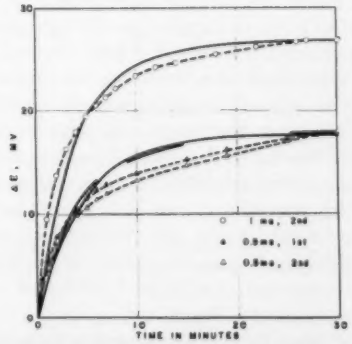

Fig. 5. Decay of polarization, electrolyte 5. The solid curves were calculated by means of Eqs. 8 and 9 and the dashed curves are drawn to pass through the experimental points. First and second refer to first and second discharges of a particular electrode. The discontinuous line is the theoretical curve for the second discharge at 0.5 ma.

early part of a discharge the rate of increase, dL/dt, of the lower oxide concentration on the electrode surface is equal to the difference between the rate of production of lower oxide by the electrochemical reaction, which may be represented by $k' I$, and the rate of dissolution, which is given by Eq. (I).

$$\frac{dL}{dt} = k' I - k_1 L^2 + k_2(1 - L) \qquad (X)$$

Eq. (X) becomes Eq. (I) when $I = 0$. In the steady state of polarization at constant current $dL/dt = 0$, and $L = L_p$. Substituting in (X) and rearranging

$$k' I = k_1 L_p^2 + k_2 L_p - k_2 \qquad (XI)$$

Combining (X) and (XI)

$$\frac{dL}{dt} = k_1\left(L_p - L\right)\left(L_p + L + \frac{k_2}{k_1}\right) \qquad (XII)$$

Integrating (XII),

$$\frac{1}{2L_p + k_2/k_1} \ln \frac{L_p + L + k_2/k_1}{L_p - L} = k_1 t + C \qquad (XIII)$$

In a sufficiently acid solution k_2/k_1 should be small, while L_p should be fairly large. Neglecting k_2/k_1 and noting that $L = L_i$ when $t = 0$

$$\ln \frac{L_p + L}{L_p - L} - \ln \frac{L_p + L_i}{L_p - L_i} = 2k_1 L_p t \qquad (XIX)$$

Combining with (V) and defining E_i as the electrode potential at $t = 0$, $\Delta E_i = E_i - E$, and $\Delta E_p = E_i - E_p$

$$\ln \frac{2L_i(1 - L_i) + e^{-x} + e^{-a}}{e^{-x} - e^{-a}} = 2k_1 L_p t + \ln \frac{L_p + L_i}{L_p - L_i} \qquad (XX)$$

in which $x = (\Delta E_i)F/RT$ and $a = (\Delta E_p)F/RT$. If $2L_i/(1 - L_i)$ can be neglected, which will be shown later to be justified when ΔE_i is small,

$$\frac{e^{-x} + e^{-a}}{e^{-x} - e^{-a}} = 2k_1 L_p t + \ln \frac{L_p + L_i}{L_p - L_i} \qquad (XXI)$$

The left-hand term can be changed to the form of the corresponding term of Eq. (VIII), but the meanings of x and a are slightly different.

Eq. (XXI) is in approximate agreement with discharge curves that do not pass through the pronounced minimum of a first discharge, which is illustrated in Fig. 1. It does not predict the small minima found by the more accurate measurements in the later discharges. However, a simple empirical correction can be applied for the unknown process causing the minimum, and this leads to excellent agreement of calculated and observed values. A calculated curve and some experimental points taken from the recorded discharge curves of two electrodes are shown in Fig. 6.

The first step in the empirical correction was to extrapolate the portion of the experimental curve at the right of the minimum back to zero time, giving a curve like that ending at 16.5 mv in Fig. 6. This intercept was arbitrarily assumed to be ΔE_p, the value of ΔE_i at the steady state of polarization

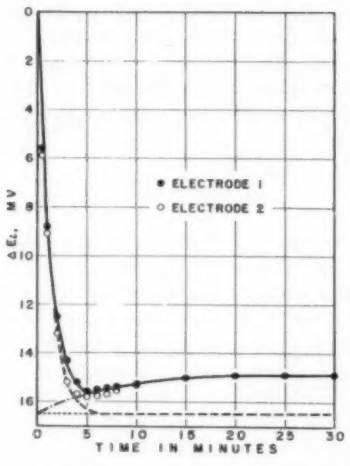

Fig. 6. Growth of polarization. The dashed curve is the theoretical curve for a discharge with no minimum. The solid curve is the theoretical curve corrected empirically to include the minimum.

if the process leading to the minimum had not taken place. The process leading to the minimum is assumed to start at $t = 0$ and its effect on ΔE_i at any time to be given by the difference between 16.5 mv and the appropriate point on either the extrapolated or the real portion of the discharge curve. Addition of these differences to the corresponding averages of the two sets of experimental values gives the dashed curve, which is the hypothetical discharge curve uncomplicated by the second process. This should be in accord with Eq. (XXI). The graphical method gave only a first aproximation to the correction shown in Fig. 6. From the first approximation the left-hand term in Eq. (XXI) was calculated and plotted against the time. This should give a straight line, but the plot was very sensitive to small differences in ΔE_p and only one value gave a satisfactory line, 16.5 mv in Fig. 6. From this value and the slope and intercept of the straight line the final dashed curve was calculated. When from this final curve the proper differences were subtracted the solid curve was obtained, agreeing with both sets of experimental points well within a millivolt for the most part, or as well as the two experimental curves agree.

This shows that it is possible to explain the discharge curves with the smaller minima as a combination of the curve predicted by the above theory and another process. This other process might be a change of physical form of the lower oxide (10).

The same treatment was applied to some discharges in electrolyte 5. Here, the corrections were much larger than for electrolyte 1; in one case the estimated theoretical ΔE_p was 45 mv while the actual steady-state value was 25 mv. However, the corrected curve was in good agreement with the observed values, better than would be expected on the basis of the decay of polarization in electrolyte 5. The approximations in the derivation of Eq. (XXI) are somewhat questionable here, and there is the possible complication of the inward diffusion of lower oxide. The empirical correction seems to correct for both of these.

Overpotential and current density.—At the steady state of polarization $dL/dt = 0$ in Eq. (X) and

$$I = K_1 L_p^2 - K_2(1 - L_p) \qquad \text{(XXII)}$$

in which K_1 and K_2 are equal to $k_1 k'$ and $k_2 k'$, respectively. Solving Eq. (VII) for L_p

$$L_p = \frac{1}{1 + [(1 - L_e)/L_e]e^{-y}} \qquad \text{(XXIII)}$$

in which $y = (\Delta E_e)F/RT$, and combining (XXII) and (XXIII)

$$I = \frac{K_1}{\{1 + [(1 - L_e)/L_e]e^{-y}\}^2} - \frac{K_2[(1 - L_e)/L_e]e^{-y}}{1 + [(1 - L_e)/L_e]e^{-y}} \qquad \text{(XXIV)}$$

Constant K_1 can be eliminated, since at open-circuit equilibrium

$$\frac{k_1}{k_2} = \frac{K_1}{K_2} = \frac{1 - L_e}{L_e^2} \qquad \text{(XXV)}$$

Combining (XXIV) and (XXV) and simplifying gives

$$I = \frac{K_2(1 - L_e)}{[L_e + (1 - L_e)\ e^{-y}]^2} - \frac{K_2(1 - L_e)\ e^{-y}}{L_e + (1 - L_e)\ e^{-y}} \qquad \text{(XXVI)}$$

When the acid concentration is large and ΔE_e is small, $L_e/(1 - L_e) << e^{-y}$ and (XXVI) can be simplified to

$$I = \frac{K_2}{1 - L_e} \exp\left[\frac{2(\Delta E_e)F}{RT}\right] - K_2 \qquad \text{(XXVII)}$$

The applicability of Eq. (XXVII) is shown in Fig. 7 and 8, in which exp $[2(\Delta E_e)F/RT]$ is plotted against I. In Fig. 8 the lines are drawn to fit the points, with most weight given to small values of ΔE_e. In a preliminary drawing of Fig. 7 values of K_2 and $(1 - L_e)$ were determined from the slopes and intercepts. Using the values so obtained as first approximations it was found by repeated trial in Eq. (XXVI) which values gave the best agreement with experiment. The values adopted are given in Table V and were used in drawing the lines in Fig. 7. The values of ΔE_e calculated by Eq. (XXVI) are given in the last column of Table II.

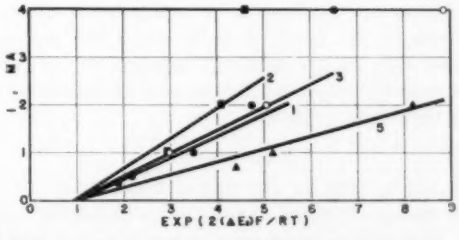

Fig. 7. Test of Eq. (XXVII) for the relation of overpotential (ΔE_e) and current density; exp $[2(\Delta E_e)F/RT]$ plotted against the current/8 cm² of electrode surface. The lines were drawn after finding the best values for the slopes and intercepts by use of Eq. (XXVI).

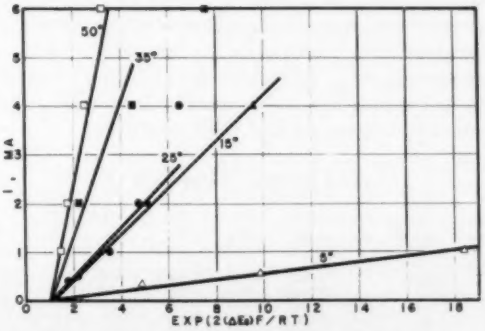

Fig. 8. Application of Eq. (XXVII) to overpotentials at various temperatures (°C).

Table V. Values of K_2 and $1 - L_e$ in Eq. (XXVI) at 25°C

Electrolyte No.	1	2	3	5
K_2	0.46	0.78	0.46	0.25
$1\text{-}L_e$	1.00	0.99	0.97	0.95

Calculated and experimental values of ΔE_e agree quite well except at 4 and 8 ma for electrolyte 1. There are smaller deviations in the same direction for the other electrolytes at these currents, or at 2 and 4 ma, while the agreement at the smallest and largest currents is generally better. It is possible that the approximations in the theory are responsible.

It is worthy of note that electrolyte 1 seems to be out of place in Fig. 7 and its value for K_2 does not fit in with the series of values for the other electrolytes. It will be recalled that electrolyte 1 also did not agree well with the others in the relation of overpotential to acidity.

Variation with temperature.—In Fig. 8 Eq. (XXVII) is applied to the data for the overpotential in electrolyte 1 at the temperatures 5°, 15°, 25°, 35°, and 50°C. The values of K_2 found graphically are 0.064, 0.41, 0.46, 1.25, and 2.60. When log K_2 is plotted against $1/T$ in accordance with the Arrhenius equation a straight line is obtained, with the 15° value deviating more than expected. The value of the Arrhenius constant derived from the slope of the line is 14.6 kcal. This is in the range for chemical reactions rather than diffusion processes.

For electrolyte 5 the values of K_2 found from a plot similar to Fig. 8 were 0.17, 0.25, 0.46, and 0.82 for temperatures 15°, 25°, 35°, and 50°C. From these the value 9.5 kcal was obtained for the Arrhenius constant.

Acknowledgment

The authors are indebted to Dr. Stanley Hills for some preliminary experiments and two of the values in Table IV. This work was supported in part by Contract Nonr-1016 (00) with the Office of Naval Research and in part by a research grant from Duke University.

Manuscript received August 22, 1956. This paper was prepared for delivery before the Cleveland Meeting, Sept. 29 to Oct. 4, 1956.

Any discussion of this paper will appear in a Discussion Section to be published in the June 1958 JOURNAL.

REFERENCES

1. A. M. Chreitzberg, Jr., and W. C. Vosburgh, *This Journal*, **104**, 1 (1957).
2. D. T. Ferrell, Jr., and W. C. Vosburgh, *This Journal*, **98**, 334 (1951).

3. A. Kozawa and K. Sasaki, *J. Electrochem. Soc., Japan*, **22**, 569 (1954).
4. A. M. Chreitzberg, Jr., D. R. Allenson, and W. C. Vosburgh, *This Journal*, **102**, 557 (1955).
5. J. J. Coleman, *Trans. Electrochem. Soc.*, **90**, 545 (1946).
6. N. C. Cahoon, *This Journal*, **99**, 343 (1952).
7. S. Hills, Ph.D. Thesis, Duke University (1955).
8. W. C. Vosburgh, R. S. Johnson, John S. Reiser, and D. R. Allenson, *This Journal*, **102**, 151 (1955).
9. W. C. Vosburgh, D. R. Allenson, and Stanley Hills, *ibid.*, **103**, 91 (1956).
10. W. H. Beck, P. Jones, and W. F. K. Wynne-Jones, *Trans. Faraday Soc.*, **50**, 1249 (1954).
11. H. Eyring, S. Glasstone, and K. J. Laidler, *J. Chem. Phys.*, **7**, 1053 (1939).

Anodic Corrosion and Hydrogen and Oxygen Overvoltage on Lead and Lead Antimony Alloys

P. Rüetschi and B. D. Cahan

Research Department, The Electric Storage Battery Company, Philadelphia, Pennsylvania

ABSTRACT

Constant current techniques permit rapid evaluation of the anodic corrosion of lead and lead antimony alloys. The amount of PbO_2 formed during anodization can be evaluated by measuring the length of the potential plateau of the $PbO_2/PbSO_4$ couple produced during discharge. The rate of self-discharge and the degree of utilization of the lead dioxide must be taken into account in order to obtain correct corrosion figures. Methods for evaluating the self-discharge and degree of utilization of the PbO_2 are described.

X-ray diffraction patterns were taken of the anodized Pb and Pb-Sb alloy samples. Patterns of $PbSO_4$, Pb, α-PbO_2, and β-PbO_2 were observed, but there was no indication that PbO was formed on any sample. The principal anodization product was α-PbO_2, a new crystalline modification of PbO_2. Hydrogen and oxygen overvoltages were measured on various alloys of the Pb-Sb system, using interrupter techniques. Overvoltage and anodic corrosion of single crystal faces of Pb were also investigated.

The anodic corrosion of Pb and Pb-Sb alloys is of fundamental importance to the lead-acid battery industry. Positive grid corrosion is one of the principal reasons why lead-acid batteries wear out in service. The standard method in the battery industry for evaluating positive grid corrosion is the SAE overcharge test. This is essentially a constant current experiment performed in the region of oxygen evolution.

In this study constant current techniques were used to study the anodic behavior of Pb and Pb-Sb alloys under precisely defined conditions.

Lander (1,2) and Wolf and Bonilla (3) investigated corrosion by constant potential techniques. The former finds tetragonal β-PbO_2 is formed by the reaction of H_2O and Pb but this PbO_2 is unstable on electrochemical grounds and goes to PbO and $PbSO_4$.

Formation of PbO as a product of anodic corrosion in H_2SO_4 has also been reported by Burbank (4). These findings are in contrast with the views of Wynne-Jones and co-workers (5) who find that PbO_2 and $PbSO_4$ are the only possible reaction products. Kabanov, *et.al.* (6) determined the rate of anodic corrosion by measuring the capacity of the PbO_2 layer formed. A similar technique was used in this study. It has been shown that the hydrogen overvoltage of metals can be correlated to the strength of the intermetallic bond (7), and, therefore, to anodic corrosion. According to this theory the hydrogen overvoltage decreases with increasing bond strength. The oxygen overvoltage also depends in a similar way on the characteristics of the electrode material so that it decreases with increasing strength of the bond M-O between the metal and oxygen (8). In the present investigation on anodic corrosion, hydrogen and oxygen overvoltage studies were therefore included.

Experimental

Pb alloys used for the experiments were cast into strips using identical casting conditions for all alloys. The strips measured 2 cm x 2 cm x 2 mm with an 8 cm x 1 cm x 2 mm tab for handling and electrical connection. One flat surface of the strips was cut with a highly polished carbon steel microtome blade. To minimize cold-working and surface oxidation effects, five additional cuts of 2 μ depth were taken less than 5 min prior to insertion into the experimental cell. Measurements showed the final depth of roughness to be smaller than 1/10μ. Table I lists the alloys used and their analyses.

Table I. Analyses of alloys used (%)

Alloy #	Sb	As	Sn	Cu	Bi	Ag	Fe	Ni
1	0.0001	—	0.0001	0.0001	0.0005	0.0001	—	0.0001
2	1.08	—	0.0001	0.003	0.05	0.003	0.0005	0.0003
3	2.16	0.008	0.0001	0.003	0.01	0.004	0.0005	0.0003
4	3.48	0.03	0.0001	0.003	0.018	0.005	0.0005	0.0003
5	5.76	0.025	0.0002	0.01	0.015	0.004	0.0005	0.0003
6	7.26	0.015	0.0001	0.008	0.008	0.005	0.0005	0.0008
7	8.76	0.015	0.0001	0.01	0.003	0.004	0.0005	0.001
8	10.98	0.015	0.0001	0.005	0.008	0.002	0.0005	0.001

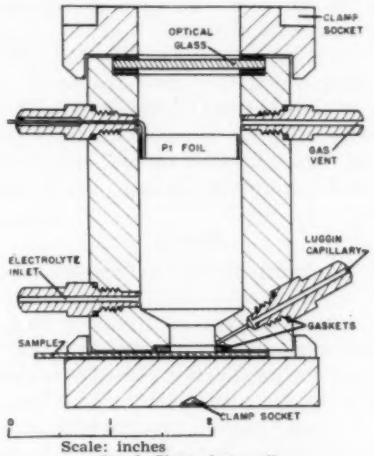

Fig. 1. Electrolytic cell

Large single crystals of Pb were prepared using differential cooling (9) and cut with the (100), (110), and (111) faces parallel to the surface. Orientations of the planes were determined by etch-pit analysis (10) and checked with x-ray back reflection. The planes were oriented with an accuracy of 1-2%.

Fig. 1 is a sectional view of the special electrolytic cell designed for rapid mounting of specimens. The cell exposes a defined electrode area of 0.95 cm^2 to the electrolyte. The Luggin capillary intersects the cylindrical anode compartment at the specimen surface and thus causes a minimal distortion of the uniform electric field in the electrolyte.

Fig. 2 is the schematic diagram of the circuit used to provide interrupted current studies of the *IR* drop during overvoltage measurements. A standard power supply (V_1 and V_2) supplied + 325 v D.C. and +200 v D.C., respectively. V_3 is a thyratron oscillator adjustable by means of R_{10} and C_{6-12} to a frequency range of 5 cps to 50 kc. The resultant sawtooth wave is differentiated by C_{13} and R_{15}, producing a sharp negative pulse which triggers the monostable multivibrator V_{4a} and V_{4b}. A positive and a negative pulse are produced across the coil L_1 in the plate circuit of V_{4b}. These pulses are amplified and inverted by V_{5a} and fed to the cathode follower V_{5b}. The first of the two pulses triggers the sweep of an oscilloscope, and the second is fed to the pulse shaper V_{6a}. This produces a sharp negative pulse which passes through the gate diode V_{7a} and triggers the output multivibrator V_{6b}, V_8, and V_9. This multivibrator is arranged so that V_8 is normally conducting. The cell to be investigated is placed in the plate circuit of V_8. The screen voltage of the output tubes is held constant by the VR tubes V_{10} and V_{11}. In this way the output current is held at a constant value, except when the multivibrator is triggered. The diode V_{12} serves to couple the cathodes of the multivibrator, and increases the cutoff speed by rapidly turning V_{6b} on and off at a given cathode voltage of V_8. Constant or interrupted currents variable from 15 to 100 ma were produced with the apparatus just described, with an accuracy of ±0.5%.

Currents below 15 ma were produced by the dual control heptode V_{13}, whose screen grids are held at

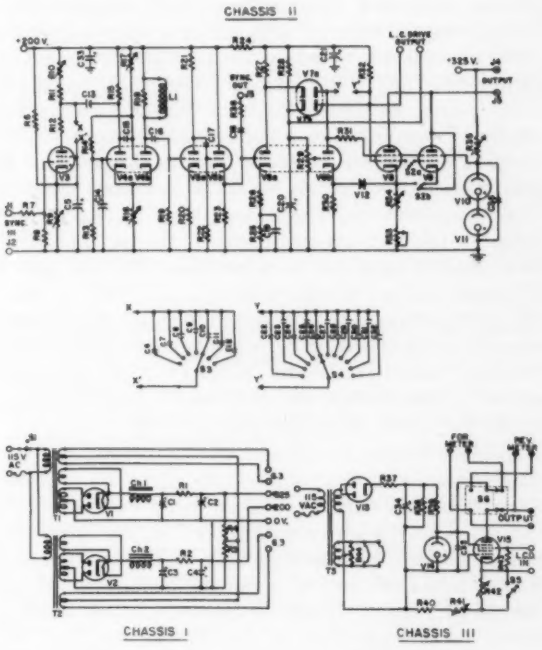

Fig. 2. Schematic diagram of the electronic interrupter. Power supply (Chassis I), oscillator and interrupter (Chassis II), low current output (Chassis III).

R1, 2, 12 — 100 2w
R3 — 39k ½w
R4 — .22M ½w
R6 — .18M ½w
R7) — Determined by ampli-
R8) — tude of sync pulses
R9, 41 — 5K pot 2w
R10 — 2M pot 2w
R11, 25, 30 — .27M ½w
R13 — 27K ½w
R14, 36, 38 — .1M ½w
R15 — 4.7K 1w
R16 — 10K pot 2w
R17 — .25M pot 2w
R18 — 470 1w
R19, 22 — 1.2M ½w
R20, 24 — 1K 1w
R21 — 3900 1w
R23 — 5600 1w
R26, 40 — 100 ½w
R27, 31 — 4.7K ½w
R28, 32 — .39M ½w
R29 — 50K pot 2w
R33 — 1K pot 10w
R34 — 100 10w adj.
R35 — 5K pot 4w
R37 — 100 2w
R39 — 390 2w
R42 — 5M pot ½w
R43 — .47M ½w
R44 — 100 pot ½w
C1, 2, 3, 4-40-40 mfd 475V elec
C5 — 50 mfd 25V
C6 — .25 mfd 400 V
C7 — .15 mfd 400 V
C8, 25 — .05 mfd 400 V
C9 — .015 mfd ceramic
C10 — .005 mfd ceramic
C11, 28 — .002 mfd ceramic
C12 — .008 mfd ceramic
C13 — 50 mfd ceramic
C14, 18, 19, 26 — .01 mfd ceramic
C15 — 200 mmfd ceramic
C16, 17 — .001 mfd ceramic
C20 — 4 mfd 150V elec
C21 — 10 mfd 350 V
C22 — 1 mfd 200 V
C23 — .5 mfd 200 V
C24 — .1 mfd 200 V
C27 — .006 mfd ceramic
C29 — 680 mmfd ceramic
C30 — 300 mmfd ceramic
C31 — 82 mmfd ceramic
C32 — 10 mmfd ceramic
C33 — 20 mfd 300 V elec
C34 — 40 mfd 350 V elec
C35, 36 — .02 mfd ceramic
S1, 5 — SPST Toggle Switch
S2 — DPDT Toggle Switch
S3 — 7 pos. switch
S4 — 11 pos. switch
S6 — DPDT Switch with off position
Ch 1, 2 — 4Hy @ 120 mA choke
T_1 — 750CT @ 150mA, 5V @ 3A 6.3CT @ 4.5A
T_2 — 500CT @ 70mA, 5V @ 3A, 6.3CT @ 4.5A
T_3 — 117 @ 70 mA, 6.3 @ 2A
L_1 — 2mH coil
V1, 2 — 5V4G
V3 — 2D21
V4, 6 — GL6463
V5 — 12AU7
V7 — 6AL5
V8, 9 — 6CM6
V10, 11, 14 — OC3
V12 — CK742 Hi Current Diode
V13 — 6X4
V15 — 5915A or 6CB6

105 v by an OC3 voltage regulator tube. The currents were constant to ±0.5%. The tube V_{15} acts as a constant current device until a negative pulse is impressed on its second control grid. This shuts off the tube until the pulse is removed. The driving pulse is produced across the diode V_{7b}. Off times as short as 0.5 μ sec with cutoff times of 0.2 μ sec were produced by this apparatus.

All experiments were made in a constant temperature bath at 30° ±0.02°C. The H_2SO_4 used in the cell had a specific gravity of 1.225 (at 20°C corresponding to 308g H_2SO_4/1000g of solution) prepared from C. P. H_2SO_4 and triple distilled water with a

specific resistance greater than 2×10^6 ohm-cm. Potentials were measured with either a hydrogen electrode or a mercury-mercurous sulfate electrode calibrated at 0.607 v to hydrogen. Potentials were recorded by a #42200-F Model S Micromax recorder operated together with a high input impedance (10^{14} ohm) electrometer amplifier circuit from a L & N Electrochemograph Unit No. 7673. A voltage divider of 60 megohms impedance was built to change the range of the instrument. A bias-adjuster consisting of a 100,000 ohm ten-turn precision Helipot and a constant voltage source was placed in series with the voltage divider. Transient and high speed phenomena were recorded by a Minneapolis-Honeywell ½ second recorder, Model Y153X(19)V-X-156, operated in conjunction with a General Radio Electrometer Voltmeter amplifier type 1230-A.

X-ray diffraction patterns were taken with a GE XRD-3 Geiger Diffractometer. Anodized Pb samples were removed from the electrolytic cell, washed, and dried with acetone within 3 sec of the interruption of current. Readable patterns could be obtained within 5 min of removal from the cell, although no change was observed after a 2 week stand in the dry state.

Samples of α-PbO_2 and β-PbO_2 were prepared for x-ray analysis and potential measurements by several methods. The α-PbO_2 was prepared in the following ways:

1. Electrolysis on Pt foil, in a concentrated solution of NaOH, saturated with $Pb(OH)_2$, at a current density of 1-10 ma/cm^2. The adhering film sample was ground, washed with hot ammonium acetate solution and with conductivity water. Further purification was obtained by treating the washed product with 2% HNO_3 and H_2O_2 until violent reaction ceased. The material was then washed with water, hot ammonium acetate, and again with water.

2. Electrolysis of a strongly ammoniacal solution of concentrated ammonium acetate (50%) saturated with lead acetate with current densities of 0.1-10 ma/cm^2.

3. Precipitation at 15°C from an ammoniacal solution of lead acetate (200-300 g/l) in 50% ammonium acetate by ammonium persulfate solution (50 g/l).

4. Conversion from β-PbO_2 at a pressure of 125,000 psi.

β-PbO_2 was produced by the following methods:

1. Electrolysis of a saturated solution of lead nitrate containing excess HNO_3 at a current density of 0.1-10 ma/cm^2.

2. Baker C.P. PbO_2, washed with hot saturated ammonium acetate and water.

Samples of α- or β-PbO_2 used for potential measurements were further treated by digestion with 1.225 sp gr H_2SO_4 on a steam bath for 1 week, according to the procedure described by Hamer (11).

Current for anodization runs was obtained from the interrupter, with the oscillator disconnected. Samples were anodized for 1, 2, 3, 4, and 20 hr with a current density of 3 ma/cm^2. The formed PbO_2 layers were then discharged with currents of 100 μa, 500μa, or 2.5 ma, or left on open circuit where they underwent self-discharge.

Samples were removed from the cell immediately after formation and also after discharge to determine the quantity of PbO_2 present. The PbO_2 layers were treated with KI in sodium acetate containing acetic acid. The liberated iodine was titrated with standardized sodium thiosulfate, using semi-micro techniques.

Results

In this paper all current values are given for a specimen area of 0.95 cm^2. Alloy samples were anodized with a current of 3 ma for various time periods and were then discharged with varying currents. Before the anodization period was started, the sample was usually cathodized for 30-60 min with a current of 3 ma. During this cathodization period hydrogen overvoltage measurements were taken.

Fig. 3 shows the initial potential transients after reversing the current for a specimen of pure Pb (alloy No. 1). The plateau at the $Pb/PbSO_4$ potential has a length of about 8 sec. There is also a very slight break visible slightly above the theoretical potential of the Pb/PbO_2 couple as indicated by the arrow in Fig. 3 The cell reaction for this couple is

$$PbO_2 + 4H^+ + 4e \rightleftarrows 2H_2O + Pb \qquad (1)$$

corresponding to a reversible potential of +0.665 v. Therefore, it is theoretically possible that PbO_2 can be formed at potentials far below the $PbSO_4/PbO_2$ potential. The latter has a value of +1.685 v (11, 12). It will be shown later that the α-crystal modification of PbO_2 is probably formed by reaction (I), whereas β-PbO_2 is formed by oxidation of $PbSO_4$. The overshoot of the potential transient above the potential for oxygen evolution is approximately 360 mv. Since a current of 3 ma was used the resistance of the passivating sulfate layer was estimated to be 120 ohms. From the length of the $Pb/PbSO_4$ plateau (8 sec) one can calculate that approximately 1.25×10^{-7} moles $PbSO_4$ were formed, corresponding to a thickness of 640Å if a density of 6.2 g/cm^3 is assumed for the sulfate layer. The "mean specific re-

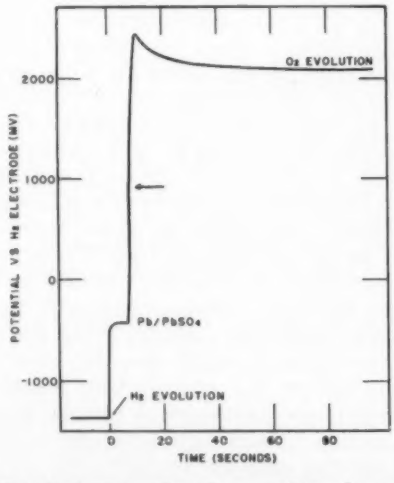

Fig. 3. Initial voltage transients for a specimen of pure Pb (alloy No. 1) anodized at 3 ma.

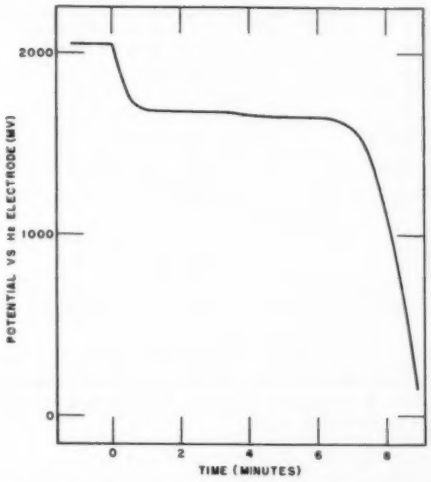

Fig. 4. Discharge curve of a sample with 1% Sb (alloy No. 2) after 20 hr of anodization at 3 ma; discharge current 500 ma.

sistance" of the sulfate was calculated to be 10^{9} ohm-cm and the electric field in the sulfate layer at the breakdown point 5×10^{4} v/cm. These very approximate calculations are valid only for a uniform surface. The potential of the positive electrode, after the initial peak, passed through a slight minimum and maximum and then decreased slowly with time. This behavior has previously been described by Wynne-Jones and co-workers (13). After anodization for 1, 2, 3, 4, or 20 hr, the extent of anodic corrosion was determined by discharging the PbO_2 formed on the electrode.

A typical discharge curve is shown in Fig. 4. This curve was obtained after anodization of a sample of 1% Sb (alloy No. 2) for 20 hr with a current of 3 ma in H_2SO_4 sp gr 1.225 and at a temperature of 30°C. The discharge current was 500 μa. A small drop in potential of 20 to 30 mv is visible approximately in the middle of the discharge curve. This small change in potential was observed in all discharge runs. Its position varied with the Sb concentration in the alloy. For pure Pb the change occurred near the end of the total discharge curve, whereas for alloys with Sb concentrations above 3% it was near the beginning of the curve. While the two plateaus might be explained possibly as a passivation phenomenon, it is more probable that they correspond to the two crystalline modifications α and β-PbO_2.

The formation and breakdown of the passivating sulfate layer produced initially upon anodization using a constant current was shown in Fig. 3. A similar study was made using an interrupted current of 3 ma and a repetition rate of about 1000 times/sec, whereby the length of current interruption was about 1/10 of the length of the current pulse. These current pulses were directed initially in the cathodic direction during which time the build up and decay of hydrogen overvoltage were studied. Voltage transients were observed on the screen of an oscilloscope and the ohmic component of the overvoltage was determined. Additional work is planned using this new technique for the study of passivation phenomena.

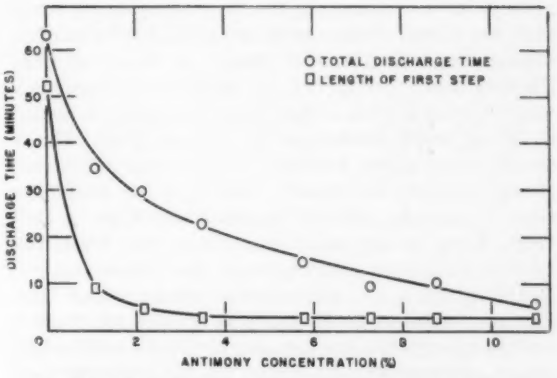

Fig. 5. Total discharge time and the length of the first step after 20 hr of anodization at 3 ma as a function of the antimony concentration; discharge current 100 μ a.

A large number of discharge runs similar to those in Fig. 4 were made; anodization was for 20 hr at 3 ma, while the discharge current was 100 μa. Results are shown in Fig. 5 to 8. Fig. 5 shows the length of the total discharge step (sum of the two plateaus) after anodization of samples containing various Sb concentrations. The length of the first plateau is also given, and this length is constant for all alloys with an Sb concentration higher than 3%. The value of 2.94% represents the limit of solid solubility of Sb in Pb at 257°C (14).

In Fig. 6 the length of the total discharge step after anodization for 4 hr at 3 ma has been plotted. The curve of the squares was obtained by measuring the potential decay on open circuit (self-discharge). The curve of the circles represents the length of the discharge steps applying discharge current of 100 μa. For any Sb concentration the length of the self-discharge step is of the same order of magnitude as the length of the 100 μa discharge step. Therefore, the total length of the discharge step is a fair measure of the extent of anodic corrosion only if the rate of self-discharge is properly taken into account.

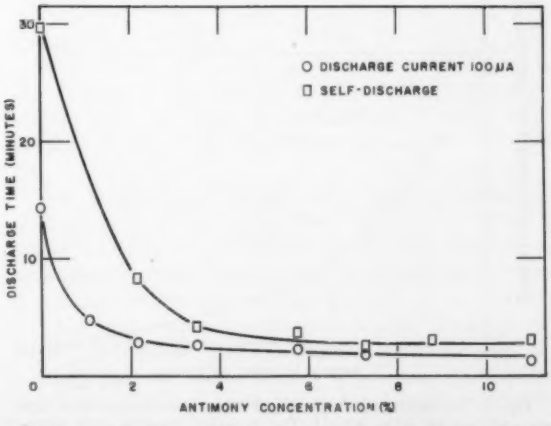

Fig. 6. Total discharge time and self-discharge time after 4 hr of anodization at 3 ma as a function of Sb concentration.

In order to determine the loss of capacity (amp sec) due to self-discharge of the PbO_2 layers the following experiments were made. A series of pure Pb specimens (alloy No. 1) which had previously been anodized with a current of 3 ma for a period of 20 hr were discharged at various rates. Fig. 7 shows a plot of the product $i \times t$ where i is the discharge current in amperes and t is the discharge time in seconds, against the discharge time in seconds. Even if the same amount of the PbO_2 remained in the corrosion layer at the end of the potential plateau, i.e. independent of discharge current or discharge time, this plot should not yield a horizontal straight line because the layer suffers different amounts of self-discharge for different discharge times. It can be seen that the available capacity thus increases with decreasing discharge time. By microtitration, it was found that the amount of PbO_2 left in the layer at the end of discharge was, indeed, practically independent of the discharge rate. A titration of the absolute amount of PbO_2 in a freshly formed oxide layer was inconclusive because self-discharge effects interfered during dissolution of the PbO_2 in the solution to be titrated. A much smaller error might be anticipated when discharged layers were titrated.

One can now assume that an extrapolation of the curve in Fig. 7 to zero discharge time yields the maximum obtainable capacity because self-discharge is now eliminated. The total amount of corrosion is obtained by adding to this limiting capacity value, the capacities corresponding to the amount of PbO_2 left in the layers as found by microtitration. Capacity values obtained by this procedure are marked with circles in Fig. 7 and correspond to the total amount of PbO_2 formed on the sample surface during the 20-hr anodization. This amount should, of course, be the same for the different discharge runs. An investigation as illustrated for pure Pb in Fig. 7 would essentially be necessary for each alloy studied in order to determine exactly the total amount of corrosion. This is anticipated for future work.

Fig. 8 shows the discharge time after various periods of anodization for pure Pb samples. The discharge current was 100 μa. Values for self-discharge

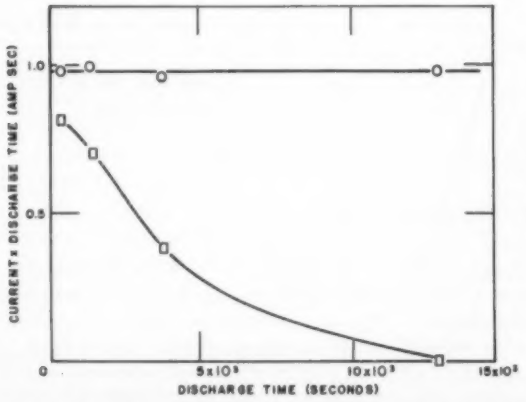

Fig. 7. Evaluation of the total amount of corrosion for a specimen of pure Pb (alloy No. 1). The available capacity as a function of discharge is shown by the squares; the circles indicate the amount of total corrosion.

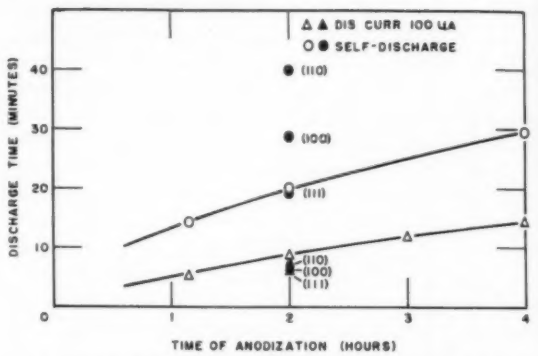

Fig. 8. Total discharge time and time for self-discharge as a function of time of anodization at 3 ma. Solid symbols show data obtained on single crystal faces.

are given. Data on single crystal faces (solid symbols) are also shown on Fig. 8. The extent of self-discharge varied significantly for different crystal faces, whereas only slight differences were observed with the 100 μa discharge.

It must be kept in mind that the actual corrosion values obtained by the procedure outlined above and illustrated in Fig. 7 give the amount of PbO_2 formed. The depth of attack can be calculated from these values using the specific gravities of the alloys. Specific gravities and conversion factors are given in Table II.

X-ray diffraction patterns were taken of a series of Pb-Sb alloys which had been anodized for varying time periods and of specimens which had been discharged to the end of the first potential plateau. The only patterns observable on any sample were those of $PbSO_4$, Pb, α-PbO_2, and β-PbO_2. The α-PbO_2 pattern was usually dominant. Also, after discharge of the samples to the end of the first potential plateau, the α-PbO_2 pattern was still quite strong, even though partially obscured by the $PbSO_4$ pattern. Fig. 9 shows a typical pattern of a sample (alloy No. 8) which had been anodized for 18 hr with a current of 3 ma in 1.225 sp gr H_2SO_4 at 30°C. Also shown are the pattern of electrolytically produced (*see* Experimental Procedure 1) α-PbO_2, Baker's C. P. β-PbO_2, and, for purposes of comparison, tetragonal PbO produced by the oxidation of lead ground in a ball mill.

Hydrogen overvoltage measurements were not very reproducible, due to apparent changes in the surface of the alloys. After polarization with currents larger than 5-10 ma/cm², the overvoltage usually decreased with time because the surface was

Table II. Specific gravities of Pb-Sb alloys

% Sb	Sp gr (g/cm³)	$\frac{cm^3}{g\ Pb}$	$\frac{cm^3}{g\ Pb\ in\ \%\ of\ pure\ Pb}$
0	11.35	0.0882	100
4	11.02	0.0945	107.1
6	10.89	0.0978	110.8
8	10.75	0.1011	114.7
9	10.67	0.1031	116.9
11	10.52	0.1068	121.0
12	10.44	0.1088	123.3

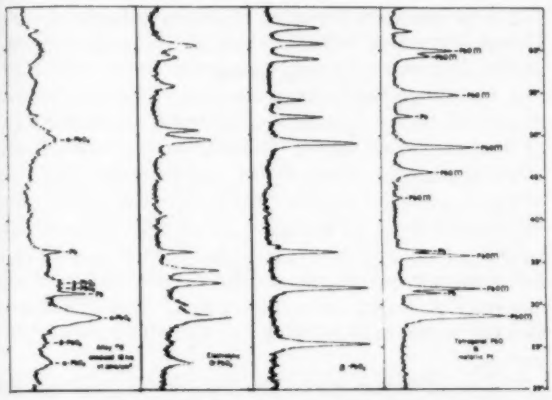

Fig. 9. X-ray diffraction patterns of PbO + Pb, β-PbO_2, α-PbO_2 and of alloy No. 8 after anodization with 3 ma for a period of 18 hr. The patterns were taken with G.E. XRD-3 diffraction unit.

increased by cathodic corrosion (15, 16). There was probably a slight simultaneous production of stibine. At current densities below 0.5-1 ma/cm² the hydrogen overvoltage decreased due to adsorption of anions (17). The Tafel-slopes were nearly the same (0.120) for all the alloys, in the current density range between 1 and 10 ma/cm². In order to compare the various surfaces, the overvoltage was measured as soon as possible after immersion of the sample, starting with currents of 3 ma/cm² and increasing to 10 ma/cm². Experiments with the interrupter showed that the ohmic resistance contributed less than 2 mv (at a current of 3 ma) to the total overvoltage in the cell described in Fig. 1. Experiments with single crystal faces of pure Pb showed that the differences in hydrogen overvoltage between the three planes investigated, namely (100), (111), and (110), were very small. Slopes of the Tafel lines were close to 0.120 on all three faces. The hydrogen overvoltage on the (111) face was only about 20 mv higher than on the (100) face at a current of 1 ma/cm². The hydrogen overvoltage on the (110) plane showed an unstable behavior and fluctuated periodically with time between the values for the (111) and (100) plane.

Hydrogen overvoltage decreased with increasing Sb concentration. However, this decrease was smaller than expected. It is conceivable that Sb in solid solution does not lower the hydrogen overvoltage as effectively as free Sb. Some results are given in Table III where i_o denotes the exchange current in amperes, α the transfer coefficient, and b the slope of the Tafel line, together with literature values [*see* also (18-22)] for pure Pb and pure Sb taken from the recent review by Bockris (23).

Table III. Hydrogen overvoltage on Pb-Sb alloys

Alloy	% Sb	i_o	α	b
1	0	1.8×10^{-13}	0.50	0.120
2	1.08	7.5×10^{-13}	0.46	0.130
3	2.16	1.4×10^{-12}	0.45	0.133
5	5.76	4.5×10^{-12}	0.44	0.136
Pb(23)	0	2×10^{-13}	0.48	
Sb(23)	100	10^{-6}	0.58	

Table IV. Oxygen overvoltage on Pb-Sb alloys

Alloy	% Sb	i_o	α	b
1	0	1.4×10^{-10}	0.55	0.110
2	1.08	8.9×10^{-11}	0.55	0.110
3	2.16	2.1×10^{-10}	0.55	0.110
5	5.76	4.4×10^{-10}	0.55	0.110

The oxygen overvoltage decreased with time. The decrease amounted usually to about 60 mv in 20 hr. This decrease has been previously described (13), and is due possibly to increased surface area. One would also expect different oxygen overvoltages for α-PbO_2 and β-PbO_2 and therefore a change of oxygen overvoltage with time as the relative amount of the two oxides on the surface changes with time. The ohmic component of the overvoltage was only about 1 mv (at 3 ma) as determined by the current interrupter technique.

The reversible potential of the oxygen electrode ($O_2 + 4H^+ + 4e \rightarrow 2H_2O$) is +1.260 v (for H_2SO_4 sp gr 1.225) as calculated from data given in references (12), (24), and (25). Overvoltage values are given relative to this potential. Table IV summarizes some results on oxygen overvoltage measurements using the same symbols as were used in Table III. These measurements have been taken after 20 hr anodization with 3 ma.

After 2 hr of anodization at 3 ma, the oxygen overvoltage of pure Pb was 0.840 v. The difference in oxygen overvoltage on the single crystal faces (100), (111), and (110) of the pure Pb specimen were less than 5 mv. The Tafel slope was the same for the three planes, namely 0.110.

Discussion

During x-ray diffraction analysis of formed positive lead acid battery plates, several diffraction peaks were noted that did not correspond to any known compounds of Pb. Further experimentation has positively identified this material as a new crystalline modification of lead dioxide, found independently by Cahan in this laboratory and Zaslavsky, *et al.* (26), called α-PbO_2 for the purpose of differentiating it from the more common tetragonal or rutile form, herein called β-PbO_2. The α-PbO_2 has an orthorhombic spatial group of Pbcn (or D_{2h}^{14}) with the axes $a = 4.938$Å, $b = 5.939$Å, $c = 5.486$Å (26).

Alpha-PbO_2 has been prepared by several means, as indicated in the experimental section. Noteworthy among these methods of preparation was the conversion of β-PbO_2 to α-PbO_2 at a pressure of 125,000 psi.

The pattern for α-PbO_2 also appears on x-ray diffraction studies of anodized Pb alloy surfaces. A study of Pb strips anodized for varying periods of time with current densities between 100 ma/cm² and 1 ma/cm² shows first the production of an intense pattern for $PbSO_4$, a gradual replacement of the $PbSO_4$ pattern by β-PbO_2, and the appearance of the α-PbO_2 pattern along with the gradual disappearance of the β-PbO_2 pattern. At higher current densities, the pattern of α-PbO_2 becomes more and more pronounced. Results of this study indicate that

anodic oxidation of $PbSO_4$ produces the β-form of PbO_2, while the α-form is produced by the direct oxidation of Pb metal to PbO_2. Since α-PbO_2 forms directly from the Pb metal, it can be produced at potentials between the reversible $PbSO_4$-PbO_2 potential (1.685 v) and the Pb-PbO_2 potential (0.67 v). Large hard black nodules consisting primarily of α-PbO_2 have been found in the examination of positive grids from lead-acid batteries after removal from service. This condition has been noticed by other investigators (1, 4, 27) but has been interpreted as formation of tetragonal PbO.

The major peak of the powder pattern of α-PbO_2 coincides with the major peak of tetragonal PbO (*see* Fig. 9). The thin films produced on anodization of Pb give very diffuse patterns, and in many instances the major peak is the only one clearly visible. It is, therefore, easy to misinterpret the pattern of α-PbO_2 on these films as belonging to tetragonal PbO.

Lander (1, 2, 27) and Burbank (4) have postulated the formation of tetragonal PbO as the result of a solid-state reaction between Pb and the PbO_2 formed on anodization. The existence of PbO in a strong H_2SO_4 solution is difficult to picture thermodynamically or kinetically and in no case has any tetragonal PbO been detected in this laboratory by x-ray diffraction of Pb corroded in H_2SO_4. Samples of Pb anodized for various periods of time have been removed from the electrolyte, dried, and x-rayed within 5 min. In all cases, the only products were α-PbO_2, β-PbO_2, $PbSO_4$, and no PbO. No change in these patterns was detected even after 2 or more weeks in the dry state. Liberation of iodine from KI solutions by these films even after several weeks of storage in the dry state indicate PbO_2 to be present. Discharge of these films showed voltage steps corresponding to the PbO_2-$PbSO_4$ potential. Even samples which showed no β-PbO_2 pattern after anodization liberated iodine from KI solutions and showed the PbO_2-$PbSO_4$ potentials during discharge.

The following mechanism is proposed for anodic corrosion. In the initial stages of anodization (Fig. 3) $PbSO_4$ is first formed from the Pb at the Pb/$PbSO_4$ potential. As this film is completed, the potential rises to the oxygen overvoltage value, where two reactions occur. $PbSO_4$ is converted to β-PbO_2, and the underlying grid metal, due to the high potential, is converted directly to α-PbO_2 according to a Cabrera-Mott type film formation. As the anodization progresses, the $PbSO_4$ is used up in the production of β-PbO_2.

Referring to Fig. 5 and 6, the total discharge time cannot give a correct measure of the anodic corrosion without taking into account the self-discharge. The results demonstrate that additions of Sb up to 3% strongly decrease anodic corrosion, whereas practically nothing is gained by further addition of Sb up to 11%. This behavior can be explained plausibly by keeping in mind that the solid solubility of Sb in Pb is 3%. For concentrations above 3% Sb all the alloys in the range studied have the same basic grain structure, the only difference being the relative proportion of free Sb in the interstices (28). It has been reported elsewhere that self-discharge increases with increasing Sb concentration (29). Therefore, by correcting the upper curve of Fig. 5 for self-discharge according to the procedure described in Fig. 7, one would obtain a leveling out of the corrosion curve. Indeed, such a correction could change the shape of the curve remarkably.

The corrosion results described above do not agree with those of Kabanov, *et al.* (6). This might be due to the fact that the latter authors used surfaces as-cast rather than microtomed and surface film effects might have interfered. These authors also neglected self-discharge and inefficiency of discharge.

The equilibrium value for the solubility of Sb in Pb is only 0.24% at 25°C (14). During the cooling and aging period, Sb crystals are precipitated from the 3% phase. The structure of the Pb grains, and hence the rate of corrosion, is the same for all the alloys with Sb concentration above 3% if the cooling rates are the same. Using conventional cooling rates, a major amount of Sb remains initially in solid solution and the lattice constants substantially decrease (14). According to the laws of electrochemical kinetics, the anodic corrosion in constant current experiments should increase with increasing potential (if passivation is not interfering) and with decreasing strength of the metallic bond. The addition of Sb causes a deformation of the Pb lattice and probably high bond strength.

It has been shown that the hydrogen overvoltage decreases with increasing strength of the bond between the metal atoms (7) while lower overvoltage values could be associated on this basis with higher corrosion resistance. One also must keep in mind that free Sb metal has a lower hydrogen overvoltage than Pb [Table III (23)].

Oxygen overvoltage can also be correlated to the rate of corrosion. According to the rate equation for electrochemical anodic attack the corrosion current depends exponentially on the electrode potential if no passivating effects interfere. Alloys with low oxygen overvoltage, therefore, should be more resistant to anodic corrosion during constant current experiments. Calculations from data on single crystals presented in Fig. 9 show that the (100) and (111) faces have practically the same corrosion resistance while the (110) face is more corrodible. McGivern, working with cylindrical single crystals has also concluded that the (110) face is least resistant to corrosion (30).

Acknowledgments

The authors are indebted to J. F. McGivern, H. Stoertz, and A. Pippel, of the Metallurgy Division, for their assistance in preparing single crystals of Pb and the microtomed samples used in this study. They would also like to thank G. S. Hartman, Administrative Assistant, for editorial help and C. G. Grimes, Director of Research of the Electric Storage Battery Co., for permission to publish this paper.

Manuscript received Nov. 29, 1956. This paper was prepared for delivery before the Cleveland Meeting, Sept. 29 to Oct. 3, 1956.

Any discussion of this paper will appear in a Discussion Section to be published in the June 1958 JOURNAL.

REFERENCES

1. J. J. Lander, *This Journal*, **98**, 213 (1951).
2. J. J. Lander, *ibid.*, **103**, 1 (1956).
3. E. Wolf and C. Bonilla, *Trans. Electrochem. Soc.*, **79**, 307 (1941).
4. J. Burbank, *This Journal*, **103**, 87 (1956).
5. W. W. Beck, R. Lind, and W. F. K. Wynne-Jones, *Trans. Faraday Soc.*, **50**, 147 (1954).
6. E. V. Krivolapova and B. N. Kabanov, *Trudy Sov. Elektrokhimii. Akad. Nauk. SSSR*, **1950**, 539 (1953).
7. P. Rüetschi and P. Delahay, *J. Chem. Phys.*, **23**, 195 (1955).
8. P. Rüetschi and P. Delahay, *ibid.*, **23**, 556 (1955).
9. W. P. Davey, "A Study of Crystal Structure and Its Applications," p. 369, McGraw Hill Book Co., New York (1934).
10. C. S. Barrett, "Structure of Metals," p. 175, McGraw Hill Book Co., New York (1943).
11. W. J. Hamer, *J. Am. Chem. Soc.*, **57**, 9 (1935).
12. W. M. Latimer, "Oxidation Potentials," p. 155, Prentice Hall Inc., New York (1953).
13. P. Jones, R. Lind, and W. F. K. Wynne-Jones, *Trans. Faraday Soc.*, **50**, 972 (1954).
14. W. Hofman, "Blei und Bleilegierungen," p. 15, Springer, Berlin (1941).
15. E. Kure, E. Yeager, and F. Hovorka, Enlarged Abstracts of Papers Presented at the Sessions of The Theoretical Division, The Electrochemical Society, San Francisco Meeting (1956).
16. J. Van Muydler and M. Pourbaix, "Proceedings of the 6th meeting of the International Committee for Electrochemical Thermodynamics and Kinetics," p. 342, Poitiers (1954).
17. Y. M. Kolotyrkin and N. Y. Bune, *Zhur. fiz. Khim.*, **29**, 435 (1955).
18. B. Kabanov and Z. Iofa, *Acta Physicochim. USSR.*, **10**, 617 (1939).
19. H. Hunt, J. Chittum, and H. W. Ritchey, *Trans. Electrochem. Soc.*, **73**, 299 (1938).
20. A. Hickling and F. Salt, *Trans. Faraday Soc.*, **36**, 1226 (1940).
21. J. O'M. Bockris, *ibid.*, **43**, 417 (1947).
22. Y. Kolotyrkin and L. Medredera, *Zhur. fiz. Khim.*, **25**, 1355 (1951).
23. J. O'M. Bockris, "Modern Aspects of Electrochemistry," p. 199, Academic Press Inc., New York (1954).
24. P. Delahay, M. Pourbaix, and P. Van Rysselberghe, *This Journal*, **98**, 57 (1951).
25. H. S. Harned and W. J. Hamer, *J. Am. Chem. Soc.*, **57**, 27 (1935).
26. A. I. Zaslavsky, Y. D. Kondrashov, and S. S. Tolkachev, *Doklady Akad. Nauk. SSSR.*, **75**, 559 (1950).
27. J. J. Lander, *This Journal*, **98**, 220 (1951).
28. A. C. Simon and E. L. Jones, Enlarged Abstracts of Papers Presented at The Electrochemical Society Fall Meeting, Cleveland (1956).
29. P. Rüetschi and R. T. Angstadt, Abstracts of Papers Presented at a Joint Symposium of the Battery and Theoretical Divisions of the ECS, Cleveland Meeting (1956).
30. J. F. McGivern, Private communication.

Oxidation of Iron-Nickel Alloys

II. Electron Diffraction at High Temperature

R. T. Foley, C. J. Guare, and H. R. Schmidt

General Engineering Laboratory, General Electric Company, Schenectady, New York

ABSTRACT

The oxidation of iron-nickel alloys of 30%, 41%, and 78% Ni content has been studied at temperatures of 600°, 700°, 800°, and 900°C by the electron diffraction technique. A special furnace was developed for the electron diffraction instrument for these experiments.

Usually more than one oxide was present on the alloy at these elevated temperatures. Unlike the conclusion drawn from exclusively room temperature observations, the predominant oxide on the 30% and 41% Ni alloys was the ferrite (Fe_3O_4 or $NiFe_2O_4$) rather than alpha-Fe_2O_3. At 700° and 900° both NiO and MoO_3 exist on the 78% alloy. (This alloy contains 3.8% Mo.) The presence of MoO_3 above its melting point and where it exerts considerable vapor pressure is difficult to explain.

In some cases the lattice spacings of the alloy structure are carried over into the first formed oxide film. With subsequent growth the spacings achieve the normal (x-ray) values for the oxide.

Iron and nickel form a continuous series of solid solution alloys, both components of which are oxidizable. Such alloys, often with the addition of other elements, provide materials of considerable engineering usefulness because of their magnetic characteristics, thermal expansion coefficients, ability to form glass-to-metal seals, or general corrosion resistance. The study of the oxidation of Fe-Ni alloys is thus of practical as well as theoretical interest.

The examination of oxide films by the electron diffraction technique is of particular value in oxidation work because the electron beam penetrates to a depth of less than 50Å. As has been pointed out before (1, 2) maximum information is obtained when the measurement is made at the temperature

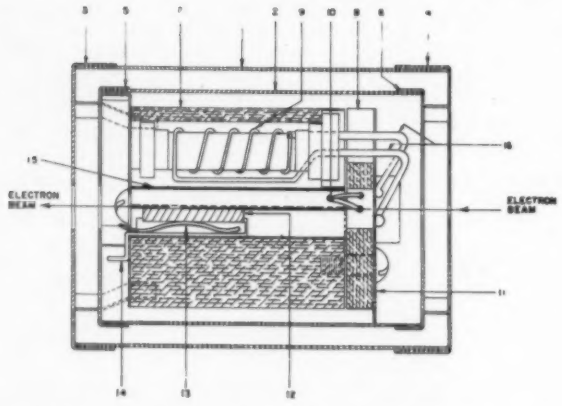

Fig. 1. High temperature electron diffraction furnace; 1, outer radiation shield—stainless steel; 2, inner radiation shield—Pt; 3-4, outer radiation shield end caps with apertures—stainless steel; 5-6, inner radiation shield end caps with apertures—Pt; 7, furnace body—ceramic; 8, insulator—ceramic; 9, heater solenoid wound on ceramic spool—Pt; 10, thermocouple—chromel—alumel; 11, locator and shield—Pt; 12, sample; 13, spring for positioning sample—stainless steel; 14, sample tray—Pt; 15, screen—Pt; 16, leads—Pt.

of reaction. The transformations and decompositions that take place upon cooling from the reaction temperature to room temperature may mislead one in the interpretation of the reaction mechanism.

This paper reports an electron diffraction study of the oxidation of three commercial Fe-Ni alloys at 600°, 700°, 800°, and 900°C. The purpose of the study was to achieve a better understanding of the structure of the oxide films formed on these alloys to add to the over-all knowledge of the mechanism of the oxidation of alloys.

Experimental

Electron diffraction equipment.—For the oxidation studies, a furnace originally designed for use in vacuum up to 1000°C was modified. W and Ta parts were replaced by Pt in regions of highest temperature and by stainless steel in the cooler areas to insure resistance to oxidation. This unit has produced a sample temperature of 900°C for a number of hours and 1000°C for a short time with no evidence of deterioration. The furnace construction is shown in Fig. 1.

Alloys.—The Fe-Ni alloys were nominally 30, 41, and 78% Ni in composition. Since they all contained more than 29% Ni, they were assumed to be austenitic. All three alloys are manufactured commercially and used because of their special physical properties. They were obtained in the form of cold-rolled sheet stock, thickness 0.051 cm (0.020 in.) for the 30 and 78% Ni alloys, and 0.080 cm (0.031 in.) for the 41% Ni alloy. Small sections, 0.80 x 1.60 cm (5/16 x 5/8 in.), were sheared from the stock for oxidation in the furnace. Careful shearing was necessary to insure flatness of the samples, and all edges were deburred to prevent obstruction of the electron beam by edge particles.

After shearing, samples were heat treated for 2-3 hr in H_2, dew point 30°F, at 1100°-1125°C. They were then cooled in H_2 to room temperature.

Surface preparation.—The chemically cleaned surface was prepared by pickling at 80°-90°C for 2 min in a bath of nine parts water and one part each of concentrated H_2SO_4, HNO_3, and HCl. This was followed by a water rinse and a bright dip in a solution of two parts concentrated H_2SO_4 and one part HNO_3. A second rinse was followed by immersion in NaCN solution (5 g/100 ml) for about 1 hr. Samples were then washed in running water, dried, and stored in dry acetone or benzene. At this point, the surface possessed a matte appearance. Composition of the alloys in the chemically cleaned condition is shown in Table I.

Electron diffraction studies.—Patterns were first taken at room temperature and a pressure of 0.01 -0.1 μ Hg. The sample was brought up to 600°C and a pattern obtained before oxidation. The alloy was then oxidized at 600°C by introducing air to bring the system to atmospheric pressure and maintaining at temperature and pressure for 2 min. The system was then evacuated and a pattern obtained. This was repeated to effect oxidations for additional 10- and 20-min periods, patterns being recorded for each time interval. (Total oxidation time at the end of each period was 2, 12, and 32 min.) The sample was then allowed to cool in vacuum and a pattern obtained when room temperature was reached. A similar procedure was used for studies at 700°, 800°, and 900°C.

The approximate times for the various operations in the electron diffraction unit were: 25 min to bring the sample to temperature in vacuum, 5 min to evacuate from atmospheric pressure after an oxidation period to obtain a pattern and 4 hr to cool the sample to room temperature in vacuum after oxidation. Heating and cooling periods varied somewhat depending on the temperatures.

Results

Oxides Found on 30% Ni-Fe *Alloy*

Observations made on oxide films developed during the oxidation of the 30% Ni alloy are given schematically in Table II. The "before oxidation" column refers to the situation wherein the sample was heated to temperature in the vacuum of the instrument, and any oxidation at this stage was not deliberate but occurred as the result of oxygen pressure in the vacuum. The "first formed oxide" refers to the 2-min oxidation only. Usually the 12- and 32-min diffraction patterns supplemented each other, and the "thicker oxide" column in the table then was based on the composite data for these two

Table I. Composition of alloys studied

Alloy	A	B	C
Nominal Ni content	30%	41%	78%
Ni	29.6	40.9	78.0
Fe	balance	balance	17.4
Mn	0.57	0.49	0.73
C	0.010	0.012	0.010
Mo	—	—	3.80
S	0.012	—	0.009
Si	0.17	0.14	0.13
P	0.02	0.02	0.02

Table II. Patterns found on 30% Ni-Fe alloy

Temp, °C	Before oxidation	First formed oxide	Estimated* thickness, A	Thicker oxide	Estimated thickness, A
600	Alloy pattern —Fe_2O_3 or Fe_3O_4	Distorted Fe_3O_4 or Fe_2O_3	Less than 500	Fe_3O_4 and Fe_2O_3	1000
700	Distorted alloy pattern	Distorted Fe_2O_3	1000	Distorted Fe_3O_4	2000-3000
800	Alloy pattern (trace Fe_2O_3 or Fe_3O_4)	Fe_2O_3 (possibly Fe_3O_4)	2000	Fe_3O_4	4000-8000
900	Alloy pattern (trace Fe_3O_4)	Fe_3O_4	5000	Fe_3O_4 (possibly Fe_2O_3)	10,000-20,000

* This was based on the kinetic equation developed in a parallel investigation.

time periods. On a few occasions, however, one or the other of these two time periods produced a very poor pattern, and in those cases "thicker oxide" refers to the good pattern only.

When the alloy was heated to 600°C, the diffraction pattern was that of the alloy plus a few lines corresponding to Fe_2O_3 or Fe_3O_4. (In this paper, Fe_2O_3 refers to the alpha form only.) The pattern obtained after the 2-min oxidation was quite distorted and could be assigned to Fe_2O_3 or Fe_3O_4. As used here, "distorted" means the spacings of the lines were shifted from those found in the corresponding x-ray pattern probably because of altered lattice parameters. Upon oxidation for longer times, a very good pattern for Fe_2O_3 developed, and there was strong evidence for Fe_3O_4.

All patterns at 700°C were distorted although distortion lessened with increasing thickness. The best pattern fit for the thicker films was Fe_3O_4. This film showed Fe_2O_3 as well as Fe_3O_4 at room temperature. Generally patterns were not obtained at room temperature.

At 800°C the alloy pattern and a few oxide lines were apparent. After 2-min oxidation, the preferred oxide was Fe_2O_3. The thicker film was Fe_3O_4.

At 900°C the preferred oxide was Fe_3O_4. The alloy pattern was observable at temperature "before oxidation." The presence of Fe_2O_3 was also indicated.

41% Ni-Fe *Alloy*

When this alloy was heated to 600°C in the instrument vacuum, the alloy pattern as well as a few lines for Fe_2O_3 were obtained as shown in Table III. With continued oxidation, both oxides $NiFe_2O_4$ and Fe_2O_3 appeared. From the electron diffraction patterns it was not possible to distinguish between Fe_3O_4 and $NiFe_2O_4$. However, previous investigation (3) had shown that the composition of the ferrite was $NiFe_2O_4$. Both Fe_2O_3 and the ferrite existed even in the first formed oxide films.

A pattern was obtained on the alloy before heating to 700°C. In addition to the alloy pattern, oxide lines were seen. It was interesting to note that heating to 700°C caused a distortion of the spacings. At 700°C the predominant oxide was the ferrite. In several incidents, the lines for the ferrite were distorted. As the oxidation progressed, a given spacing was seen to increase or decrease to approximate more closely the spacing reported from x-ray data.

At 800°C both oxides $NiFe_2O_4$ and Fe_2O_3 were in evidence.

When the sample was heated to 900°C in the instrument vacuum the alloy structure was covered by $NiFe_2O_4$. The ferrite was produced first at low oxygen pressure. Certain strong lines observed in the first formed films were carried through on oxidation and continually distorted. In the thicker films both $NiFe_2O_4$ and Fe_2O_3 were present as shown by "unique" lines.

A general observation appears to be that both oxides, $NiFe_2O_4$ and Fe_2O_3, grow on the 41% Ni-Fe when oxidized at these temperatures.

78% Ni-Fe *Alloy*

In addition to Ni and Fe, this alloy contained 3.8% Mo which entered into the reaction. Electron diffraction results are listed in Table IV.

A very good pattern for the alloy was obtained when the strip was examined at 600°C before oxidation. As oxidation proceeded, the alloy pattern distorted toward that of Fe_3O_4 and additional lines began to fill in the pattern. The distortion and addition of lines continued until the pattern from the thickest film gave excellent agreement with Fe_3O_4. This Fe_3O_4 probably contained considerable Ni.

Table III. Patterns found on 41% Ni-Fe alloy

Temp, °C	Before oxidation	First formed film	Estimated thickness, A	Thicker film	Estimated thickness, A
600	Alloy pattern (Fe_2O_3)	$NiFe_2O_4$, Fe_2O_3	Less than 500	$NiFe_2O_4$, Fe_2O_3	Less than 1000
700	Alloy pattern (Fe_2O_3)	$NiFe_2O_4$, (Fe_2O_3)	Less than 1000	$NiFe_2O_4$	1000-2000
800	Alloy pattern (Fe_2O_3, $NiFe_2O_4$)	$NiFe_2O_4$, Fe_2O_3	1500	$NiFe_2O_4$, Fe_2O_3	3000-6000
900	$NiFe_2O_4$	$NiFe_2O_4$, Fe_2O_3	4000	$NiFe_2O_4$, Fe_2O_3	10,000-20,000

Table IV. Patterns found on 78% Ni-Fe alloy

Temp, °C	Before oxidation	First formed film	Estimated thickness, A	Thicker film	Estimated thickness, A
600	Alloy pattern	Distorted alloy pattern	Less than 500	Fe_3O_4	Less than 500
700	Distorted alloy pattern, MoO_2	Distorted NiO, (MoO_2)	Less than 500	NiO, MoO_2	1000-2000
900	Alloy pattern, MoO_2	MoO_2, (NiO)	1000-2000	NiO, (MoO_2)	3000-10,000

At 700°C before oxidation, the pattern showed lines from the alloy and from MoO_2. In the first formed film a distorted NiO was observed along with lines for MoO_2. There was good evidence that the $NiFe_2O_4$ characteristic of oxidation on the 41% Ni alloy was also present. The thicker film appeared to be a mixture of MoO_2 and NiO, the lattices of which were distorted.

At 900°C "before oxidation" the lines for the alloy were observed. The alloy appeared to be covered with a thin layer of MoO_2 which was distorted. In the first formed film a very good pattern for MoO_2 was obtained. Upon further oxidation NiO predominated. The thickest film appeared to be composed of NiO with a trace of MoO_2.

Discussion of Results

Generally the electron diffraction patterns were of fair quality with respect to number and intensity of lines. Agreement with ASTM x-ray standards was almost always within 2-3% which is good considering the possibility of compounded deviations resulting from the inherent inaccuracy of the electron diffraction technique, the elevated temperatures, and distortion of oxide layers by substrates. The best patterns were obtained at 600° and 700°C, the room temperature, 800° and 900°C, patterns being less definite. There were no unidentified lines. Because of the shallow penetration of the electron beam, these patterns identified the surface structure only.

The ASTM x-ray standards used for comparison were those for Ni, NiO, $NiFe_2O_4$, Fe, FeO, α-Fe_2O_3, γ-Fe_2O_3, Fe_3O_4, MoO_2, MoO_3, and $NiMoO_4$. Alloy pattern standards were obtained from an examination of the alloys with a G-E XRD-3 unit and a SPG-2 spectrogoniometer head.

The studies demonstrated quite well that at these elevated temperatures more than one oxide layer was present even on fairly simple binary alloys. Unlike the conclusion to be drawn from exclusively room temperature observations (3), the predominant oxide on the 30% and 41% Ni alloy was not the α-Fe_2O_3 species, but rather the ferrite structure. Other chemical analyses (3) have shown the ferrite on the 41% Ni alloy to be $NiFe_2O_4$ rather than Fe_3O_4, and it might be inferred that the oxide produced on the 30% Ni alloy contained appreciable Ni.

The oxide layer produced on the 78% Ni alloy was complex. At 600°C the growth of the thin film was influenced by the structure of the alloy and the thick film by the ferrite structure. The ferrite probably contained considerable Ni. At 700°C there was evidence for MoO_2 along with NiO. Thus, the mechanism of oxidation must certainly change between 600°C and 700°C. More surprising, excellent agreement with the MoO_2 pattern was found for thin films at 900°C. The melting point of MoO_2 is 795°C and present thought (4) suggests that the formation of MoO_2 at temperatures above its melting point should lead to catastrophic oxidation of alloys containing Mo, whereas a stable compound such as $NiMoO_4$ must be produced to prevent catastrophic attack (5). In our case the nickel molybdate was definitely absent, but the 78% Ni alloy was the most resistant to oxidation of the three alloys studied as shown by kinetic data. The thick film showed less positive evidence for MoO_2 so the volatile oxide was eliminated as oxidation continued. This elimination could result by evaporation of MoO_2 from the surface followed by more rapid diffusion of Fe or Ni through the remaining oxide layer to give an oxide containing one or both of those atoms rather than Mo.

Although agreement of some electron diffraction patterns of the 78% Ni alloy was excellent with respect to MoO_2, almost equally good agreement was obtained for those same patterns with γ-Fe_2O_3. However, γ-Fe_2O_3 is not stable at 500°C or higher (6, 7).

It is encouraging that the pattern for the basis metal was obtained at these elevated temperatures in the oxygen pressure characteristic of the instrument. While less than 0.1 μ, this pressure would be termed high in terms of oxidizing potential (7). Even so, usually good patterns for the alloy itself were obtained. In many cases a few lines of an oxide were obtained in addition. It is possible that some reduction of the oxides by the carbon in the alloy was taking place (8).

Many patterns were distorted. This distortion could be accounted for in different ways. In at least one instance the distortion was produced by heating the sample from room temperature to 700°C. Very often the "d" spacings for the alloy were carried over to influence the "d" spacings of the oxide and a trend in distortion occurred. The termination of this trend in spacings was the x-ray spacing for the oxide. An excellent example is shown in Fig. 2 for the 78% alloy at 600°C.

The evidence in Fig. 2 indicates that in the growth of an oxide film, there is formed on the surface a series of structures with continuously varying parameters which change from those of the alloy when the film is thin to those of the oxide when the film is thick. Apparently this transformation can be completed at a thickness less than 500A, and the intermediate values of parameters would cause an error in the estimated values of film thickness based on the assumption that the film was entirely oxide of normal density. As the film increases in thickness,

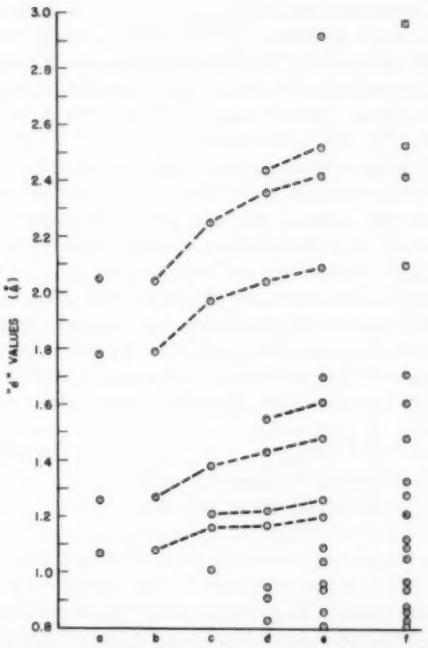

Fig. 2. Change in surface structure with oxidation on 78% Ni-Fe alloy at 600°C; (a) x-ray diffraction, alloy, chemically clean, 25°C; (b) electron diffraction, alloy, chemically clean, 600°C; (c) electron diffraction, alloy, 2 min in air, 600°C; (d) electron diffraction, alloy, 12 min in air, 600°C; (e) electron diffraction, alloy, 32 min in air, 600°C; (f) x-ray diffraction, Fe_3O_4, 25°C.

these intermediate parameter values are probably retained by that portion of the film near the alloy-oxide interface.

It would be of interest to know what alloy spacings were being distorted to the new oxide spacings. In a majority of the cases the trend in distortion could not be followed over the entire range because of multiple oxides or incomplete patterns. In the case of Fig. 2, the alloy planes 111, 200, 220, and 311, respectively, went to oxide planes 222, 400, 440, and 444 if the dotted lines are correct. Further work on orientation influences will be carried out in this laboratory.

In these studies it was difficult to distinguish between Fe_2O_3 and $NiFe_2O_4$ (or Fe_3O_4). Certain characteristic or "unique" lines were used to establish the presence of one or the other of these compounds. These lines were usually quite strong and were not ambiguous. For the nickel ferrite, a spacing at about 1.95 was significant. For Fe_2O_3, a "d" spacing at 1.84 was used. These varied from sample to sample; for example, the characteristic "d" spacing for the $NiFe_2O_4$ compound occurred at 1.97, 1.96, 1.91, 1.92, and 1.93 in various samples.

Observations reported at the present time are being used along with kinetic studies to establish the mechanism of oxidation of these alloys.

Acknowledgment

The authors would like to acknowledge the considerable contribution made by M.J. Columbe in the construction of the furnace and operation of the electron diffraction apparatus.

Manuscript received August 3, 1956. Some of the material in this paper was given at the American Chemical Society Meeting at Dallas, Texas, April 8-13, 1956.

Any discussion of this paper will appear in a Discussion Section to be published in the June 1958 JOURNAL.

REFERENCES

1. E. A. Gulbransen, *J. Appl. Phys.*, **16**, 718 (1945).
2. R. Jackson and A. G. Quarrell, *Proc. Phys. Soc., London*, **51**, 237 (1939).
3. R. T. Foley, J. U. Druck, and R. E. Fryxell, *This Journal*, **102**, 440 (1955).
4. O. Kubachewski and B. E. Hopkins, "Oxidation of Metals and Alloys," p. 3, 13, 88, Butterworths Scientific Publications, London (1953).
5. S. S. Brenner, *This Journal*, **102**, 7 (1955).
6. Z. G. Pinsker, "Electron Diffraction," p. 257, Butterworths Scientific Publications, London (1953).
7. E. A. Gulbransen and J. W. Hickman, *Trans Am. Inst. Mining Met. Engrs.*, **171**, 306 (1947).
8. Private communication.

Dissolution of Iron in Acidified Chromic Chloride Solutions

Robert Skomoroski and Cecil V. King

Department of Chemistry, New York University, New York, New York

ABSTRACT

The rate of dissolution of iron from rotating cylinders was studied in 4M HCl containing purple and green $CrCl_3$, also $AlCl_3$ and NaCl up to 0.2M. These salts affect the rate of dissolution somewhat, but chromic ion does not undergo reduction. While the standard potentials predict that reduction is possible, the actual potential of iron in acid solutions is not sufficiently negative. Cathodic polarization did not accomplish direct or indirect reduction of chromic ion, but only cathodic protection of the iron. It was also shown that metallic iron catalyzes the oxidation of chromous ion by hydrogen ion.

The dissolution of Fe in HCl-$CrCl_3$ solutions was studied in order to compare the reaction with that of Zn and Cd under similar conditions (1,2). From the published "standard" potentials, the equilibrium constant of the reaction

$$Fe + 2Cr^{+++} \rightleftharpoons Fe^{++} + 2Cr^{++} \qquad (I)$$

is found to be about 10, indicating nearly complete reduction of chromic ion by Fe to be thermodynamically possible. However, the actual potential

of Fe in acid solutions is always polarized cathodically by the H_2 evolution reaction, and is insensitive to ferrous ion. Reaction (I) then cannot take place unless the measured potential is not a determining factor, or the chromic ion acts as a depolarizer.

Chromous ion is thermodynamically unstable in acid solutions, the potential of the reaction

$$Cr^{++} + H^+ \rightleftharpoons Cr^{+++} + \tfrac{1}{2} H_2 \qquad (II)$$

being given in volts at 25°C by the equation

$$E = 0.40 - 0.059\ pH - 0.059\ \log\ (a_{Cr^{+++}}/a_{Cr^{++}}) \qquad (III)$$

At pH <6, essentially no chromous ion is present at equilibrium ($E = 0$). Reaction (II) is slow or negligible in many solutions and is not catalyzed by Zn or Cd, so that it may be neglected in studies with these metals (1,2). It is catalyzed by some metals, especially Pt (3,4), and, as shown below, by Fe. Nevertheless, if reactions (I) and (II) were to take place in succession, rates of Fe dissolution and H_2 evolution would be greater than in the absence of chromic ion. This research was designed to clarify the actual behavior of the system.

Experimental

Cylinders of high-purity Fe (SVEA Metal), about 1.9 x 2.5 cm in dimensions and 15 cm^2 in area, were rotated in 100 ml of acid solution, deaerated with N, as described before (2). The reaction cell was thermostatted at 25°C. A small saturated KCl-calomel cell was inserted for potential measurements, *IR* drop between the Fe cylinder and calomel cell being negligible in all cases. The experiments were done in 4M HCl to avoid *p*H changes or surface oxide complications. The Fe was polished lightly with No. 600 SiC paper before each third or fourth run since this gave the best reproducibility. Weight loss was determined after 1-hr immersions; it is linear with time in similar experiments with HCl alone (5).

Reproducibility was tested by repeating runs 6 or 7 times in some of the solutions. The average deviation from the mean varied from 4 to 9%, with a maximum single deviation of 17%. Results in other solutions are the average of 2 or 3 determinations. The rates and the average deviations are similar to results reported by Makrides, Komodromos, and Hackerman for Fe in HCl (5).

Table I gives the weight loss in deaerated 4M HCl solutions containing green and purple forms of $CrCl_3$, also $AlCl_3$ and NaCl for comparison.

Several solutions were tested for reduction of Cr^{+++} by introducing excess deaerated $K_2Cr_2O_7$ solution into the reaction cell at the end of the runs.

Table I. Average weight loss of iron cylinders, mg/cm^2/hr; peripheral speed 15,000 cm/min; 4M HCl; 25°C

C_{salt}, M	$CrCl_3$ Purple	$CrCl_3$ Green	$AlCl_3$	NaCl
0	4.3	4.3	4.3	4.3
0.05	4.3	3.6	4.6	4.8
0.10	4.6	3.6	4.4	4.6
0.15	4.7	3.1	4.7	4.8
0.20	5.1	2.9	5.0	4.5

The excess dichromate was then titrated with standard ferrous solution with diphenylamine sulfonic acid as indicator. The reducing power of the solutions averaged 2.9% less than calculated from the weight losses (40-50 mg), indicating that only Fe^{++} and no Cr^{++} had been formed.

To test the effect of $CrCl_3$ on H_2 evolution directly, strips of Fe sheet of 70 cm^2 area were rolled into spirals and inserted into a reaction flask which was connected to a manometer through a flexible glass capillary. The solution was introduced, the apparatus evacuated with shaking, and, after sealing from the pump, the pressure rise was followed. Initial rates were erratic, but after several periods of reading and re-evacuating, reasonably reproducible values were obtained. Averages were as follows:

4M HCl alone	5.55 cm Hg/5 min
+ 0.2M $CrCl_3$ (green)	4.35
+ 0.2M $CrCl_3$ (purple)	5.70

While these experiments cannot be compared directly with those of Table I, the green $CrCl_3$ evidently decreases H_2 evolution as well as weight loss; the effect of purple $CrCl_3$ is within the experimental error.

Potentials and polarization.—The potential of the rotating Fe cylinder was measured in deaerated solutions much as described by Makrides, Komodromos, and Hackerman (5). It drifted with time as these authors describe, in 4M HCl alone and with 0.2M $CrCl_3$, $AlCl_3$, or NaCl present. After 1 hr the value was −0.38 to −0.40 v vs. the SCE in all cases.

Since a more negative potential should be required to reduce Cr^{+++}, potential and weight loss studies were made with the Fe polarized cathodically. A vessel containing 1M KCl and a sheet Ag anode was connected to the reaction cell through an agar bridge (large enough to avoid overheating), and current was supplied from dry cells. Since the potentials did not change rapidly after 5 min, readings were taken after holding the current constant for that time. Polarization curves are shown in Fig. 1.

Weight losses were determined at small increments of polarizing current, over 1-hr periods as be-

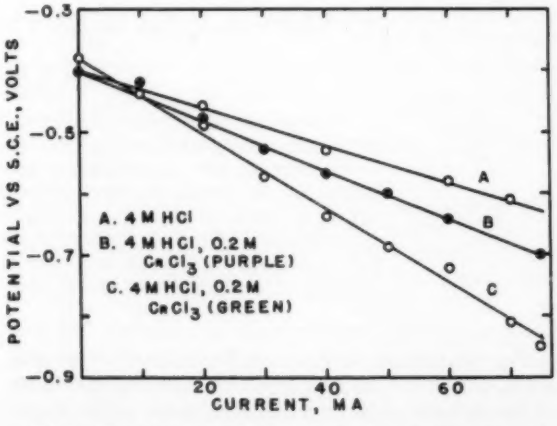

Fig. 1. Change in potential for rotating Fe cylinder with polarizing current.

fore. The Fe is protected in HCl alone and with both forms of $CrCl_3$ at 0.2M with any current from 10 to 75 ma (on 15 cm^2), weight losses falling to the order of 0.01-0.1 mg/cm^2/hr. Runs up to 8 hr at 75 ma showed no visual change in color of the solutions.

Other experiments.—To test the catalytic effect of Fe on reaction (II), 50 ml of 0.2M $CrCl_2$, prepared by reduction of $CrCl_3$ with amalgamated Zn and containing about 2M HCl, was brought into contact with an Fe cylinder in a Jones reductor tube, and stirred with purified N. In 30 min the bright blue color had changed to dark green, indicating oxidation to Cr^{+++}. An Fe cylinder was also rotated in 100 ml of 0.2M $CrCl_2$ containing about 4M HCl, in the reaction cell, the Fe being polarized cathodically with a current of 75 ma. The blue color changed to green in the course of 20 min.

Since the polarographic reduction of Cr^{+++} in 4M HCl has not been reported, polarization curves were run with 0.002M green and purple forms in 4M HCl at 25°C.[1] The green ion showed a rather poor wave starting at about −0.55 v (vs. SCE), with no clearly defined reduction plateau or half-wave potential. The purple form showed some reduction starting at about −1.0 v. Apparently reduction of both forms at the Hg surface is slow and the purple form shows considerable overvoltage.

Discussion

Since Fe catalyzes reaction (II) one cannot expect permanent reduction of Cr^{+++} unless the potential is in the region of stability of Cr^{++} according to Eq. (III). Alternate reduction by unpolarized Fe, reoxidation by H^+ does not take place. Cathodic reduction followed by reoxidation cannot be tested directly, since the amount of H_2 evolved depends only on the number of coulombs passed.

The potential of the chromic-chromous couple is somewhat uncertain, and the values of −0.40 to −0.41 given in the literature (6,7) are not strictly standard potentials, since activity coefficients in the solutions used are not reliably known. If Eq. (III) is correct, then in 4M HCl (pH = −0.9) a mixture of Cr^{+++} and Cr^{++} at equal activities should be stable at −0.71 v vs. the SCE.

The best work on polarographic reduction of Cr^{+++}, for comparison in the present connection, appears to have been done by Hamm and Shull (8). This was with very dilute $CrCl_3$ in 0.1-0.4M KCl and dilute HCl. With freshly prepared green solutions, a half-wave potential was found at −0.61 v vs. SCE. This wave disappeared with time, while another appeared at −0.89 v in the aged solutions (the hexaaquo ion). The violet ion thus displays an overvoltage on Hg even in dilute HCl. Some investigators have noted another wave at −1.06 v in purple solutions (9).

[1] Experiments by John Gorman, whom the authors wish to thank.

No plateaus appear in the curves of Fig. 1, which indicates that even in the region of supposed stability of Cr^{++} the reduction overvoltage on Fe is greater than any overpotential which was imposed. However, the oxidation of Cr^{++} at the Fe surface, even with 75 ma of current and a potential near −0.85 v, indicates that Cr^{++} is not stable at this potential under the given conditions.

It is significant that while $AlCl_3$ and purple $CrCl_3$ increase the dissolution rate somewhat, green $CrCl_3$ decreases it up to 30%. This probably indicates that the green ion is strongly adsorbed on Fe, decreasing the number of sites at which H^+ can be reduced (polarization of cathodes). While both forms of $CrCl_3$ react with Cd in HCl solution, the rate of H_2 evolution is diminished (2). Also, while ferric ion is reduced by Fe in H_2SO_4, H_2 evolution is decreased during this reaction (10). This has been ascribed by Gatos to competition for adsorption sites (10). Both the dichlorochromic ion and the sulfatoferric ion should be more strongly adsorbed than the symmetrical hexaaquo ions.

This view is supported at least partly by the polarization curves of Fig. 1. The green ion increases the H_2 overvoltage more than twice as much as the purple ion does. The question is raised, how can the purple ion be adsorbed to some extent, increase the H_2 overvoltage, and still increase the dissolution rate? Probably the purple ion is not adsorbed with no applied potential, and the green is adsorbed to a greater extent when the Fe is polarized.

It should be possible to investigate the adsorption of both chromic ions on Fe by classical or radiotracer methods. It has been shown that chromate and dichromate ions are retained on a steel surface (11), with the possibility that reduction to Cr^{+++} is involved.

Manuscript received September 18, 1956. This paper was prepared for presentation before the Cleveland Meeting, Sept. 29 to Oct. 3, 1956.

Any discussion of this paper will appear in a Discussion Section to be published in the June 1958 JOURNAL.

REFERENCES

1. C. V. King and N. Mayer, *This Journal*, **100**, 473 (1953).
2. C. V. King and E. Hillner, *ibid.*, **103**, 261 (1956).
3. K. Jablczynski, *Z. physik. Chem.*, **64**, 748 (1908).
4. A. Asmanov, *Z. anorg. u. allgem. Chem.*, **160**, 209 (1927).
5. A. C. Makrides, N. M. Komodromos, and N. Hackerman, *This Journal*, **102**, 363 (1955).
6. G. S. Forbes and H. W. Richter, *J. Am. Chem Soc.*, **39**, 1140 (1917).
7. G. Grube and L. Schlecht, *Z. Elektrochem.*, **32**, 178 (1926).
8. R. E. Hamm and C. M. Shull, *J. Am. Chem. Soc.*, **73**, 1240 (1951).
9. G. F. Reynolds, H. I. Shalgosky, and T. J. Webber, *Anal. Chim. Acta*, **8**, 564 (1953).
10. H. C. Gatos, *This Journal*, **103**, 286 (1956).
11. R. A. Powers and N. Hackerman, *ibid.*, **100**, 314 (1953).

The Activation and Passivation of Stainless Steel in Aerated Sulfuric Acid

G. H. Cartledge

Chemistry Division, Oak Ridge National Laboratory, Oak Ridge, Tennessee

ABSTRACT

Potential-time curves have been determined at 85°C for a niobium-stabilized stainless steel during its transition to the state that is essentially stable in aerated 0.1*N* sulfuric acid. Experiments were conducted both with pre-oxidized specimens and with others that were previously saturated with hydrogen by electrolysis. It was found that the potential passes through characteristic inflections, and an attempt was made to relate these to the processes with which they are associated. In particular, it was found that, for the conditions used, there is a "critical recovery potential" above which spontaneous passivation occurs, and this potential was shown to be approximately equal to the hydrogen potential for the same conditions. The corrosion rate was shown to be characteristically related to the changes in potential.

When certain types of stainless steel are superficially oxidized by exposure to hot air and then placed in aerated H_2SO_4 under suitable conditions, the initially noble system may first become active and subsequently return to an essentially stable passive state (1). Bonhoeffer and Vetter (2), who have studied the analogous phenomenon manifested by carbon steel in HNO_3, found that radical and characteristic changes in potential occur over an interval of about 0.5 sec. Berwick and Evans (3) studied the ennobling of the electrode potential of 18-8 stainless steel in aerated H_2SO_4 at 25°C and showed that a certain minimum amount of oxygen was required to produce passivity. Copper(II) ions and iron(III) ions also raise the potential of stainless steel and modify corrosion rates (4). The present work was undertaken as an introduction to an investigation of the mechanism of the action of a variety of substances on the electrochemical behavior of stainless steel in acidic solutions. To understand the possible effects of ions or molecules on the potential of a composite surface like that of a real metal, it was desirable to study in detail the processes involved in the transition between noble and active states of the system in the absence of ions other than corrosion products. Preliminary experiments disclosed conditions under which the activation and subsequent passivation by oxygen could be followed over much longer time intervals than were involved in the carbon-steel HNO_3 system, thus permitting a more thorough investigation of the several processes involved. It was found that the potential-time curves obtained by continuous recording showed smooth transitions or inflections that were very similar to the familiar titration curves of analytical chemistry. The problem, therefore, was to correlate these potential changes with the chemical processes with which they are associated.

Experimental Procedure

The metal used in most of the experiments was a Nb-stabilized stainless steel (type 347) having the following analysis: C, 0.05; Ni, 9.75; Cr, 18.10; Mn, 0.71; Si, 0.59; Nb, 0.57. The metal was in the form of cold-rolled, annealed, and pickled sheet 0.010 in. thick. In some cases the surface was the original mill finish; in others it was either abraded with 2/0 emery or else electropolished in a mixture of H_2SO_4, H_3PO_4, and water. The electrodes were, in most cases, 1 cm square and had an integral lead which was insulated by a coat of glyptal varnish dried at 110°C. In preliminary experiments at temperatures between 25° and 95°C, it was found that when such electrodes were placed in 0.1*N* H_2SO_4 the time required for a stable potential to be attained diminished with rising temperature. The potential became less noble with rise of temperature in the aerated acid and became progressively more noble when the electrode was repeatedly heated and cooled in the acid. The temperature of 85°C was selected for most of the experiments as a matter of convenience, since this is near the temperature of maximum corrosion rate in dilute H_2SO_4 exposed to the air and is far enough below the boiling point so that excessive evaporation is avoided. At this temperature the potentials were reestablished quickly after any displacement by polarization.

In those experiments in which an oxide film was artificially produced, the electrodes were heated in a muffle furnace for times varying between 15 min and 40 hr, and at temperatures between 300° and 450°C. For most of the experiments, the standard heating procedure was 2 hr at 445°C. This treatment produced a brown film on specimens having the mill finish, and pure, brilliant gold on electropolished specimens. Evidence that the results obtained were not influenced by any possible altera-

tion of the metal structure by the oxidation was found in the fact that similar results were obtained in the ultimate spontaneous passivation of specimens which received no prior oxidation, although the behavior at the beginning of an experiment was, of course, different.

The well-lacquered electrode stems passed through rubber stoppers into 150 ml of H_2SO_4 contained in a 250-ml, round-bottom flask having three or four necks. Through the central neck a glass stirrer was passed which operated at approximately 600 rpm. The stirring rate was just insufficient to draw bubbles of air into the solution. A bridge containing 0.1*N* H_2SO_4 made connection to a reference electrode of Ag-Ag_2SO_4 in 0.1*N* H_2SO_4 maintained at room temperature. This half-cell was frequently calibrated against a saturated calomel electrode (S.C.E.). Potentials were measured and continuously recorded by use of a vibrating-reed electrometer and Brown recorder. Pt electrodes (smooth or platinized for different purposes) were also inserted in the H_2SO_4. It was shown by tests that there was insufficient leakage between electrodes to give detectable polarization. Because of the experimental arrangement employed, all potentials given include a small but unknown potential due to the temperature gradient in the bridge. When desired, dissolved Fe was determined spectrophotometrically by use of thioglycolic acid (5).

All potentials are expressed by reference to the saturated calomel electrode. Nobility therefore is indicated by potentials that are positive to this electrode by 100 mv or more. Ennobling and debasing are frequently referred to as opposite processes, since the meaning of these terms is clear without regard to conventions as to signs. Under the conditions of these experiments the system may be reasonably stable only in the noble, or passive, region (more positive than +100 mv S.C.E.) or in the base, or active, region (more negative than −300 mv S.C.E.). In the intervening region of potentials rapid transitions of state are occurring.

General Results

The different types of potential-time curves obtained in aerated solutions are summarized in Fig. 1. Curve 1 represents the behavior of an electropolished and oxidized specimen which passed from the air-stable state to the acid-stable state with only a slight dip in its electrode potential and with only a minimum amount of corrosion. Curve 2 represents the other extreme, in which the initially noble electrode after a time underwent an abrupt activation to a potential at which H_2 was liberated, and after a slight rise in potential continued at an active potential with rapid corrosion. After some time, passivation was artificially induced in this experiment by passing a stream of O_2 through the flask. Curve 3 represents a case in which the dE/dt value in the base region was slightly positive until an abrupt ennobling began which was followed by ultimate passivation. Curve 4 represents the behavior of an electrode which was connected to a platinized electrode in the same solution throughout most of the experiment. In this case the potential

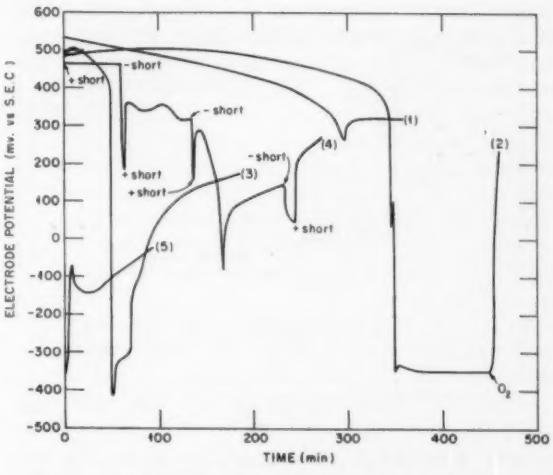

Fig. 1. Types of potential-time curves at 85°C, referred to the saturated calomel half-cell.

never reached the region of active potentials and there was only a small amount of corrosion. Finally, curve 5 shows the behavior of an electrode which was saturated with H_2 by cathodic treatment in very dilute NaOH before being inserted into the aerated H_2SO_4 solution. Here there was rapid ennobling from the initially active potential, with very little corrosion.

Potential-Time Curve for Initially Oxidized Electrodes

As indicated in Fig. 1, curves 2 and 3 represent the contrast between conditions which resulted in continuous corrosion, in the one case, and in spontaneous recovery with essentially complete stability in the other case. Which of the two curves was followed proved to be highly dependent on temperature, acidity, concentration of oxygen, and specific corrosion resistance of the metallic specimen. Thus,

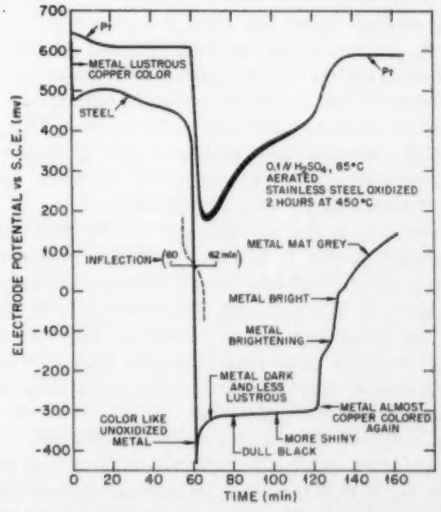

Fig. 2. Potential-time curves for oxidized stainless steel and smooth Pt in aerated 0.1*N* H_2SO_4 at 85°C. The brief inflection recorded on the chart at 61 min is indicated on an expanded time scale by the dashed curve.

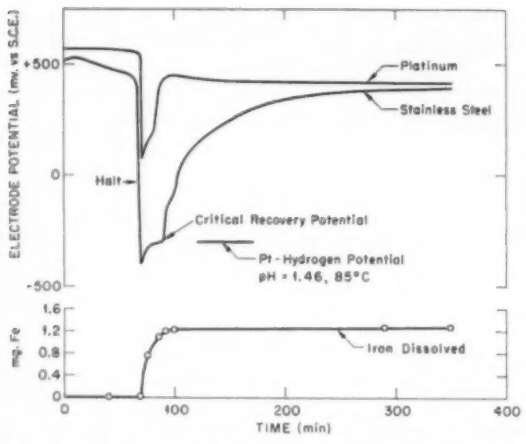

Fig. 3. Potential-time and corrosion curves at pH 1.46, 85°C, aerated.

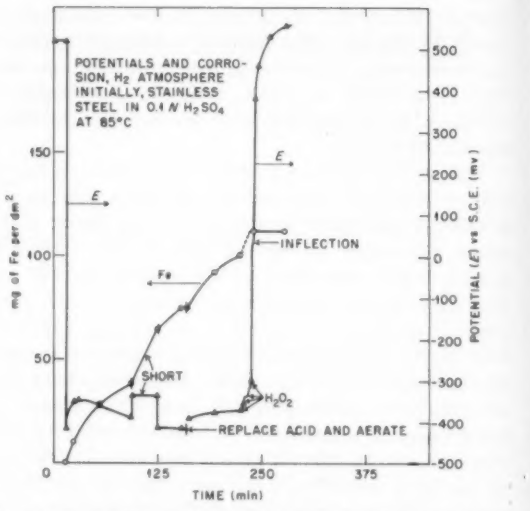

Fig. 4. Potential-time and corrosion curves in a hydrogen atmosphere initially: pre-oxidized electrode.

when the temperature was 85°C and the electrolyte was 0.1*N* H_2SO_4, one specimen of stainless steel (type 347) almost invariably followed curve 3, whereas electrodes cut from a different batch of metal having approximately the same analysis invariably followed curve 2 under the same conditions. It was found that the dE/dt slope in the active region could be changed from zero or negative to positive, as a rule, by lowering the temperature by 5-10 degrees, or by raising the pH by a few tenths of a unit. Other means of producing the ennobling artificially are discussed later.

Fig. 2 shows the potential-time curve of a specimen which was abraded with 2/0 emery, oxidized for 2 hr at 450°C, and then placed in 0.1*N* H_2SO_4 at 85°C, together with a smooth Pt electrode. The behavior shown is typical of numerous experiments made under these conditions. The figure indicates also the consistently observed visual changes. The disappearance of film coloration, particularly on specimens that were not abraded, was often spectacularly abrupt when the brief halt around 0 mv was passed. In the numerous experiments of this type, the fairly sudden change from a slow to a very rapid ennobling of the potential occurred uniformly when the rising potential reached -295 ± 5 mv. This characteristic potential is called here the "critical recovery potential". It was observed to vary slightly with changes in pH and temperature.

Variations in the potential of the Pt electrode are also shown in Fig. 2. During the noble period of the stainless steel electrode the Pt remained nearly constant after a few minutes. Its potential fell sharply with the activation of the stainless steel electrode and underwent subsequent changes that were clearly correlated with the processes occurring at the surface of the stainless steel.

Fig. 3 shows the results of an experiment of similar character except that the electrolyte was a mixture of 0.1*N* H_2SO_4 with 0.1*N* sodium sulfate in such proportions (3:1) that the mixture had a pH of 1.46. In this case careful spectrophotometric determinations were made on the Fe which passed into solution during the experiment. As long as the potential remained noble, the dissolved Fe was barely detectable. The break in potential was accompanied by the onset of an extremely high rate of corrosion and the subsequent diminution in corrosion rate coincided precisely with the passage through the critical recovery potential. Chromium and Ni were determined in only a few instances, since it is known (6) that stainless steel dissolves essentially in the proportions present in the metal. The relation between the drop in potential and increase in corrosion rate is similar to that observed by Schwartz (7) in the activation of passive iron.

In Fig. 4, which is considered more fully later, an experiment is shown which was conducted in a current of purified H_2 with an electrode that was initially oxidized. The curve shows that the stainless steel held its noble potential with no immediate response whatever to the molecular H_2. After 15 min, the electrode was activated by momentarily short circuiting it to a platinized electrode in the same solution. This electrode was about 800 mv negative to the stainless steel and the treatment instantaneously destroyed the nobility. Thereafter, corrosion proceeded rapidly.

Experiments in an Atmosphere of H_2

When the oxide film on the stainless steel electrode broke down, the potential fell to a sufficiently low value for H_2 to be liberated. It was suspected that the inflections or halts observed in the recovery of nobility were somehow associated with the presence of hydrogen in the metal and with processes connected with its displacement by oxygen. For this reason experiments were conducted to determine the electromotive behavior of electrodes which were initially saturated with hydrogen. Such electrodes were measured in an atmosphere of purified H_2, in a stream of an inert gas, and also when the solution was stirred in contact with air according to the standard procedure.

Cylinder H_2 was purified by passage through a catalytic oxygen remover followed by a solution of

Table I. Empirical potential of the hydrogen electrode, 85°C

Electrolyte	pH	E (mv vs. S.C.E.)
0.1N H_2SO_4	1.25	−284
0.1N H_2SO_4 + 0.1N Na_2SO_4 (2:1)	1.50	−303

chromous chloride in HCl. Abraded electrodes of stainless steel type 347 of 2.0 cm^2 area were used. The electrodes were made cathodes in very dilute NaOH solution in a porous cup. A Pt anode was used outside the cup and current of approximately 10 ma/cm^2 was passed for various periods of time from 15 min to 48 hr. For the potential measurements, the electrode was quickly transferred to the solution of H_2SO_4 or sulfate mixture which had already been brought to temperature and equilibrated with the appropriate gas.

For comparative purposes the potential of a platinized coil was measured simultaneously to obtain an empirical reversible hydrogen potential appropriate to the experimental conditions. Table I gives the values obtained, the potential being referred to a saturated calomel half-cell dipping into the specified acid solution at 25°C. It is to be understood that hydrogen bubbled over the Pt electrode in the acid solution at 85°C and escaped at a barometric pressure of approximately 740 mm, and that the potential difference was measured between this hydrogen half-cell and a reference half-cell of Ag-Ag_2SO_4 in 0.1N H_2SO_4 at 25°C. The Ag half-cell was then measured against a calomel half-cell which dipped into a 0.1N sulfate solution of the indicated pH value. Over the narrow range of acidities involved, the variation of potential with pH corresponds to that calculated from the Nernst equation within 1 mv, although pH was measured at 25°C.

Fig. 4 and 5 show results that are typical of experiments done in an atmosphere of hydrogen with subsequent aeration, Fig. 4 referring to a preoxidized electrode and Fig. 5 to one that was first treated cathodically to saturate it with hydrogen. For these experiments the apparatus was equipped with a sampling device for transferring electrolyte to or from the flask without admission of air. The significant observations in these experiments were as follows. (*A*) The initially oxidized electrode remained noble until it was momentarily short-circuited to the platinized hydrogen electrode. (*B*) On being activated, the preoxidized electrode went to a more negative potential than that initially exhibited by the cathodized electrode. (*C*) The potentials of the stainless steel electrodes were negative to the platinized electrode and became essentially constant during the period of active corrosion in hydrogen. (*D*) The corrosion rate of the oxidized electrode immediately after its activation exceeded that of the cathodized electrode. (*E*) The corrosion rate increased during periods when the stainless steel was short-circuited to the platinized electrode; the rate decreased when the circuit was opened. (*F*) The current passing between the stainless steel and Pt electrodes was measured by a microammeter in one experiment. This current accounted for 75-82% of the total corrosion occurring during the short. [The calculation was based on the analysis for Fe and on the assumption that the metallic constituents of the alloy dissolved in the proportions in which they were present to give Fe(II), Ni(II), and Mn(II) ions. The two percentages shown are for the alternative assumptions that Cr(III) and Cr(II), respectively, were the immediate products of the electrode reaction.] (*G*) The corrosion rate increased temporarily when air displaced the hydrogen atmosphere or when very small amounts of H_2O_2 were added. (*H*) The corrosion rate fell nearly to zero after the potential ennobled past the critical recovery potential (Fig. 4). (*I*) The potentials showed the characteristic brief halts during the ennobling process in air. (*J*) When a cathodized electrode was transferred directly to aerated electrolyte, ennobling began at once and was quite rapid (curve 5 of Fig. 1). (*K*) In one experiment, after the electrode had reached a nearly constant active potential in hydrogen, the hydrogen was replaced by an indifferent gas that was freed of oxygen.[1] The potential of the stainless steel electrode continued its slow drift to more negative potentials.

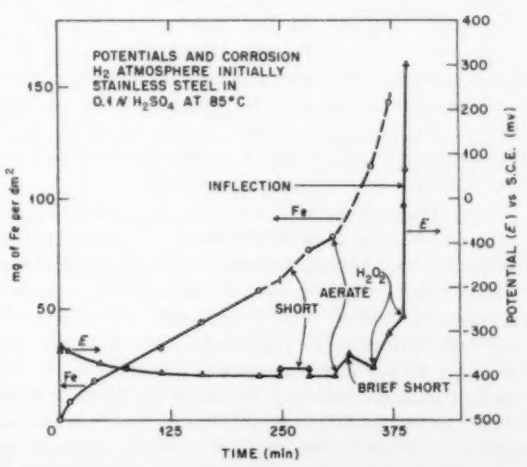

Fig. 5. Potential-time and corrosion curves in a hydrogen atmosphere initially: cathodized electrode.

Experiments with Composite Electrodes

When pre-oxidized electrodes were first introduced into aerated 0.1N H_2SO_4 at 85°C, the potential was unsteady, irregular fluctuations of 50 mv or so being generally observed for a time. This behavior would be expected if the film were heterogeneous, so that currents could flow between local cathodes and anodes. It was consistently observed that specimens that were electropolished prior to oxidation had potentials 50-150 mv more noble than specimens that were not so treated before formation of the oxide film. This observation made it possible to separate anodic and cathodic processes to a very considerable degree by studying the potential of a composite electrode made by connecting an electro-

[1] The gas is believed to have been N_2 but owing to the erroneous labeling of a cylinder that was discovered after completion of the experiment it is possible that the gas was A.

polished electrode through a microammeter to a specimen having the mill finish, both electrodes having been oxidized 2 hr at 445°C. The electrodes were of 3.74 cm^2 area each.

Because the actual extent of the functioning areas is unknown, the polarizations measured can have no quantitative significance. It was found, however, that, when the potentials of the separate components were measured while both were in the noble region, the mixed potential of the composite electrode was almost that of the unpolished component. The polarization of the cathodic process therefore greatly exceeds that of the anodic process, even though the effective anodic area was doubtless very much smaller than the cathodic film of the electropolished member.

A composite pair was observed through the fall to an active potential, both the potential and the interelectrode current being measured. It was observed that the current increased rapidly when the potential of the anode began to fall, then dropped to zero as the electropolished component debased, and briefly reversed its direction when the activation approached completion. Correspondingly, the electropolished component, although normally the more stable, lost its golden color while some brown film was still visible on the unpolished member. It is clear that the loss of nobility is associated with a "reductive-dissolution" of the oxide, as demonstrated by Pryor and Evans (8) for the case of carbon-steel films. As shown by repeated analysis, however, a barely detectable amount of Fe passed into solution until activation was complete (Fig. 3 and 4).

Experiments on the Ennobling Process

One of the most striking results of the experiments was the abrupt ennobling that occurred whenever the potential reached the critical recovery potential. The complexity of the ensuing processes is indicated by the two inflections that were generally observed before the ultimate passive potential was reached. The relation of hydrogen to the persistence of active potentials is clearly indicated by the approximate coincidence of the empirical hydrogen potential with the critical recovery potential in the same environment. For these reasons, further experiments were devoted to an attempt to explore the factors operative in the ennobling process.

As indicated previously, not all samples of type 347 stainless steel ennobled spontaneously after debasing into the region of active potentials. The selected experimental conditions of temperature, acidity, and oxygen concentration were definitely marginal in this regard for specimens of the alloy employed. Thus, in the experiment illustrated in curve 2 of Fig. 1, the corrosion potential was essentially constant at −350 mv, a steady state of some kind having been reached. Upon replacing the air with a stream of O_2, immediate passivation was induced. Addition of small amounts of other oxidizing agents acted in like manner; thus, less than 1 mg of Fe^{3+} or of Cu^{2+} in 150 ml was found to cause immediate recovery. Addition of 1 mg of Cr^{3+} as sulfate had no influence on the potential. When the potential of a specimen persisted in the active region, passivation could also be induced by lowering the temperature 5 or 10 degrees, raising the pH value from 1.25 to perhaps 1.50, or, usually, by shorting the stainless steel to a platinized electrode in the same aerated solution. It is clear that all these ennobling procedures affected the relative polarizations of the cathodic and anodic processes in such a way that the mixed potential became more noble.

In many experiments a smooth Pt wire was used to serve as a ferric-ferrous indicator electrode after an appreciable concentration of Fe had built up. As may be seen in Fig. 3, such an electrode ennobled rapidly once the stainless steel electrode passed the critical recovery potential and hydrogen ceased to be evolved. The Pt soon reached a maximum positive potential and then slowly debased until the two electrode potentials in time became essentially equal. The declining Pt potential indicated that the Fe^{3+}/Fe^{2+} ratio was decreasing as ennobling of the stainless steel proceeded, hence the following experiment was done with radioactive Fe to determine whether dissolved Fe ions and the passivating film were interacting.[2]

The electrolyte was aerated 0.1*N* H_2SO_4 and the temperature 85°C. In one experiment four abraded electrodes of 2 cm^2 area each were placed in the acid together with a smooth Pt electrode. All four electrodes were cathodized directly in the solution from an external source of current, using the Pt as anode. The four electrodes had potentials in the neighborhood of −310 mv when the current was stopped. One pair of electrodes was then held at −324 mv by continuing the passage of 0.6-0.8 ma; the other pair was allowed to begin the ennobling process while stirring of the solution in contact with air was maintained. At this point radioactive Fe (Fe^{55}, Fe^{59}) in 0.1*N* H_2SO_4 was added. This Fe had been electrolytically reduced to Fe(II) before addition. After the addition (1 mg Fe), the two electrodes which were not being cathodized ennobled by about 600 mv in the next 10 min, while the first pair of electrodes was held at the base potential. Fifteen minutes after addition of the radioactive Fe all four electrodes were removed, thoroughly washed in water and acetone, and counted on a beta proportional counter. As may be seen in Table II, electrodes 77a, b had a small count; a considerably greater count was obtained on the specimens which had been allowed to ennoble (77c, d).

Table II gives also the results of a second experiment which was done in similar manner except that electrodes 77e, f were kept at the base potential only 6 min before addition of 1 mg of Fe containing radioactive tracer. An additional electrode, 77g, was first ennobled by heating it in 0.1*N* H_2SO_4 containing 1.68 mg of ordinary Fe(III) until its potential had passed +350 mv. It was then quickly transferred to the acid containing the radioactive Fe and held for 15 min at 85°C to determine whether the

[2] The assistance of Dr. Franz A. Posey in this experiment is gladly acknowledged.

Table II. Exchange of $Fe^{55,59}$ between film and solution

Specimen	Condition	Total cpm
77-a	—324 mv	91
77-b	—324 mv	100
77-c	Ennobled	415
77-d	Ennobled	270
77-e	—320 mv	61
77-f	Ennobled	314
77-g	Pre-ennobled	304
77-g	Overnight	466*
77-g	—330 mv, 48 min	82†

* Kept overnight in $Fe^{55,59}$ at 60°C, then 1 hr at 85°C.
† Same electrode cathodically reduced in radioactive solution.

surface state of the already ennobled metal was in dynamic exchange with the Fe in solution. As seen from the table, this electrode also gained radioactive Fe amounting to 304 cpm (counts per minute). This activity was increased to 466 cpm after the sample had stood overnight in the same radioactive Fe solution at about 60°C.

The following experiment demonstrated that the radioactive Fe measured in these experiments is associated with the noble potential. The same specimen, 77g, was returned to the radioactive Fe solution and current of about 1 ma was passed between it and the Pt electrode, the stainless steel being the cathode. Meanwhile, the solution was stirred in contact with air in the usual manner. After the potential had been maintained at about —330 mv for 48 min the sample was withdrawn, washed, and again counted. The activity had reduced to 82 cpm, showing that about 83% of the activity previously present had gone back into solution. Measurement of the potential of a smooth Pt electrode in the same solution showed that the Fe was still approximately 85% in the form of Fe(III).

The counts of the radioactivity deposited on the electrodes cannot be considered precise, but a count on the H_2SO_4 solution at the time specimens a-d were removed, coupled with an Fe analysis at the same time, indicated that the total amount of Fe associated with the radioactivity on the metal surface was of the order of $2\text{-}4 \times 10^{18}$ at./cm^2, which would represent only a small fraction of a monatomic layer.

Experiments with numerous other ions such as Cu^{2+} and $Cr_2O_7^{2-}$ showed that many of them also enter into the ennobling process by a reaction that deposits some form of the added species almost irreversibly in the oxide film. These results will be reported in a subsequent paper.

Discussion

As shown in Fig. 3, the initial potential of abraded and oxidized electrodes was almost as noble as that of smooth Pt. This potential very generally became less noble for a time until its value was in the neighborhood of +350 mv, when the rate of debasing increased greatly. During this rapid fall of potential a brief, but definite, halt or inflection was usually observable, its mid-point averaging 0 mv in 33 experiments in which it was measurable (Fig. 2). During this halt the last traces of film coloration disappeared. The visual effect was most noticeable with specimens having the original mill finish when oxidized, since the irregular disappearance of the film left spots of color which flashed off abruptly at the end of the halt. One of the inflections observed during the subsequent reennobling occurred at approximately the same potential (cf. Fig. 2, 4, and 5). This behavior closely resembles that observed by Flade (9) and by Bonhoeffer and Vetter (2) in connection with the activation and passivation of Fe. With electropolished electrodes, in most instances the golden color gradually faded into the bright, silvery appearance of the unoxidized metal without activation and, hence, with very little corrosion (curve 1, Fig. 1). As previously indicated, the activation process is doubtless to be ascribed to reductive-dissolution of the film by local action.

While the metal was actively corroding at around —330 mv the corrosion rate was shown to be limited by the hydrogen polarization, since the rate increased when the stainless steel was short-circuited to Pt or when oxygen or other oxidizing agent was added. The fact that the corrosion rate was highest just after activation and higher for the preoxidized specimen than for a cathodized specimen (Fig. 4 and 5) can be accounted for by two considerations. Immediately after activation the H polarization has not built up; in this condition the electrode was shown to have a much higher anodic polarization resistance (dE/di) than it had later when fully charged with hydrogen. Secondly, it has been shown that oxidation of stainless steels causes Cr (10) and Si and Nb (11) to pass into the film in considerable excess over the proportions in which they are present in the metal. The outer metallic layer is therefore depleted of these stabilizing elements and of higher chemical activity than normal metal. This enhanced activity was observed also by Vernon, Wormwell, and Nurse (10).

The corrosion rate decreased as the most active metal was dissolved (Fig. 3 and 4) and the potential slowly became less negative under conditions of aeration (Fig. 3). During this period, hydrogen was being removed from the surface (*a*) by reaction with oxygen; (*b*) by reduction of ferric ions present in only minute concentration; or (*c*) by formation of molecular H_2. (At more positive potentials the hydrogen may also pass back into solution by ionization.) Since ultimate passivation is accomplished by reduction of oxygen (3), it is obvious that spontaneous passivation depends on the relative rates of the two chief cathodic processes, namely, reduction of oxygen and reduction of hydrogen ions. The experimental results indicate that, for the present conditions, the oxygen reaction becomes preponderant at the critical recovery potential of —295 mv, or just slightly below the reversible hydrogen potential.

For passivation to result, it is necessary that the metal be polarized above this potential for a sufficient time to remove the hydrogen. The extremely rapid ennobling that results when the critical recovery potential is reached is believed to be associated with reaction of oxygen with the active hydrogen on or in the metal to form a peroxy com-

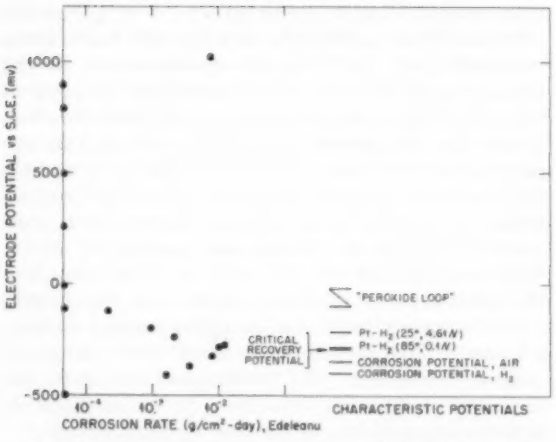

Fig. 6. Corrosion rate at fixed potentials (Edeleanu) in relation to characteristic potentials observed in the present work.

pound. The formation of H_2O_2 by reduction of oxygen at the cathode in electrolysis of dilute H_2SO_4 is well established, the yield being very high when the current density is low, as it is in the corrosion process (12, 13). Such an effect was seen in the present experiments in the following way: a Pt electrode in aerated H_2SO_4 was at a stable potential a few hundred millivolts more noble than a corroding stainless steel electrode in the same solution. When the electrodes were connected, the Pt was the cathode of the cell so formed and its potential became less noble. When the circuit was opened, the potential of the Pt rose at once to a more noble value than it had before being short-circuited, and in a few minutes returned to the initial stable value.[5] On the basis of this interpretation, the first halt observed after the rapid ennobling above the critical recovery potential most probably represents the time required for the residual hydrogen to diffuse from the interior of the metal. The second halt usually observed is most likely associated with the building of the acid-stable film, in which Fe(III) ions were shown to be involved.

There would seem to be no qualitative or fundamental difference between stainless steel and Fe with respect to the essential condition for passivation to occur. As has been pointed out elsewhere (14), the passivation of Fe can be achieved by atmospheric oxygen provided an efficient inhibitor such as the XO_4^{n-} ions or molecules is present. It was suggested (15, 16) that these particles are adsorbed and exert electrostatic forces at the interface such as to diminish the chemical activity of the electrons in the metal sufficiently to prevent the reduction of hydrogen ions.[6] The difference between Fe and stainless steel, therefore, is a quantitative one, in that stainless steel may be raised above the hydrogen potential by oxygen without benefit of a cathodic inhibitor, as if its electrons already had a somewhat diminished chemical activity. To this extent there is merit in the electron theory of passivity developed by Uhlig and Wulff (17) and by Uhlig (18). That the difference is not very large, however, is shown by the fact that electrolytic Fe corroded under the conditions of these experiments at a potential only about 200 mv below that of stainless steel.

The present experiments shed light on the results of Edeleanu (19), who studied the corrosion rate of an 18-8 stainless steel held at constant potentials in 20% H_2SO_4 (4.61*N*) at 25°C. For comparison with his results, the empirical hydrogen potential under his conditions was determined and found to be −217 mv. The corrosion rates of Edeleanu are shown by the points at the left of Fig. 6. The characteristic potentials found in the present work are indicated at the right. It is clear that the maximum corrosion rate occurred just slightly below the empirical hydrogen potential for 4.61*N* acid at 25°C. As was shown previously, the corroding metal in 0.1*N* acid at 85°C has a potential somewhat more negative than the hydrogen potential for the same conditions. A potential just under the hydrogen potential would then represent the highest anodic polarization that could be applied to the metal without going to the potential for passivation.

Manuscript received August 13, 1956. The work on this paper was done for the A.E.C. under contract with the Union Carbide Nuclear Co.

Any discussion of this paper will appear in a Discussion Section to be published in the June 1958 JOURNAL.

REFERENCES

1. G. H. Cartledge, *Nature*, **177**, 181 (1956).
2. K. F. Bonhoeffer and K. J. Vetter, *Z. physik. Chem.*, **196**, 127 (1950).
3. I. D. G. Berwick and U. R. Evans, *J. Applied Chem., London*, **2**, 576 (1952).
4. *See*, for example, H. H. Uhlig and A. Geary, *This Journal*, **101**, 215 (1954).
5. H. W. Swank and M. G. Mellon, *Ind. Eng. Chem., Anal. Ed.*, **10**, 7 (1938).
6. S. A. Burke, *Trans. Faraday Soc.*, **33**, 309 (1937).
7. W. Schwartz, *Z. Elektrochem.*, **55**, 170 (1951).
8. M. J. Pryor and U. R. Evans, *J. Chem. Soc.*, **1950** 1259.
9. F. Flade, *Z. physik. Chem.*, **76**, 513 (1911).
10. W. H. J. Vernon, F. Wormwell, and T. J. Nurse, *J. Iron and Steel Inst.*, **150**, 81P (1944).
11. T. N. Rhodin, *Corrosion*, **12**, 123t (1956).
12. M. Traube, *Ber. König. Akad. Wiss. Berlin*, 1041 (1887).
13. F. Fischer and O. Priess, *Ber.*, **46**, 698 (1913).
14. R. F. Sympson and G. H. Cartledge, *J. Phys. Chem.*, **60**, 1037 (1956).
15. G. H. Cartledge, *ibid.*, **60**, 32 (1956).
16. G. H. Cartledge, *ibid.*, **60**, 1571 (1956).
17. H. H. Uhlig and J. Wulff, *Am. Inst. Mining Met. Engrs.*, **135**, 494 (1939).
18. H. H. Uhlig, *Trans. Electrochem. Soc.*, **85**, 307 (1944).
19. C. Edeleanu, *Nature*, **173**, 739 (1954).

[5] Similar activation of oxygen by hydrogen in Pt was observed in the slower conversion of cathodically deposited TcO_2 into $HTcO_4$ by aerated water when the hydrogen was removed from the electrode before exposure to oxygen. H_2O_2 rapidly effects the oxidation.

[6] It is to be noted that, in the kinetics of irreversible electrode processes, the cathodic consumption of electrons as a reactant may be affected by factors that do not appear in the chemical equation expressing the electrode process. Such effects may conceivably alter the pre-exponential factor as they surely change the activation energy in the exponential term. It is in this sense that the term "activity" of electrons is used, without assuming any specific mechanism for the effects in question.

Ionic Conductivity of Anodic Films at High Field Strengths: Transient Behavior

D. A. Vermilyea

Research Laboratory, General Electric Company, Schenectady, New York

ABSTRACT

Studies of the changes in ionic conductivity of anodic Ta_2O_5 films following rapid changes of applied voltage or following a heat treatment of the film have shown that the activation energy and activation distance for ionic motion vary with changes in electric field and temperature. A consideration of these results along with other information obtained from the corrosion behavior of the films and from x-ray diffraction by the films shows that a mechanism proposed earlier to account for ionic conduction in these films requires modification. It is suggested that a change of the applied field changes not only the number of conducting ions, as proposed earlier, but also changes the average local configuration in the glass-like film and, hence, changes the mobility of the ions as well. Transient behavior similar to that shown by the Ta_2O_5 films is also shown by anodic films of Al_2O_3 and Nb_2O_5, but not by anodic ZrO_2.

According to a recent theory (1) of high field ionic conduction in Ta_2O_5, the current is carried by interstitial Ta ions which are created when a Ta ion leaves its normal position. The Ta ion vacancies left behind act as traps for interstitials, and an equilibrium is established when the rates of formation and capture of interstitials become equal. The equilibrium interstitial Ta ion concentration is field dependent. If the field in the Ta_2O_5 is suddenly changed, a transient current should be observed because of the finite time required to establish the new equilibrium. If, for example, the field was suddenly increased, the initial current would be lower than the steady value corresponding to the new field, and there would be a measurable increase in the current while the new equilibrium was being established. Such transients have been known to exist for many years (2); this paper is a report of a study of these transients. The data obtained considered together with results of x-ray diffraction and corrosion studies (3) make it appear unlikely that the proposed theory is adequate for the description of ionic conduction in Ta_2O_5 films, and a modification which takes account of the glass-like structure of the films is discussed. Preliminary experiments using other anodic films are also discussed briefly.

Theory

Two types of experiments can provide useful information. In one type transient currents are observed at constant voltage and in the other voltage transients are observed at constant current. The theory for the voltage transient at constant current is discussed first.

Transients at constant current.—According to the theory of high field ionic conduction (1), the rate of creation of interstitials is given by

$$\frac{dn_+}{dt} = (N - n)\ \exp\ \nu\ [-(Q_i - q\lambda_i E)/kT] \qquad (I)$$

where n is the concentration of interstitials, N is the concentration of Ta ions in the film, ν is a frequency, Q_i is the activation energy for creation of an interstitial, q is the charge on the ion, λ_i is the distance from the normal position of the ion to the top of the activation barrier, and E is the magnitude of the electric field. Q_i and λ_i have different values in different ranges of field strengths. The rate of capture of interstitials is

$$\frac{dn_-}{dt} = \frac{n^2}{N}\,\nu \exp\,[-(Q - q\lambda E)kT] \qquad (II)$$

where Q is the activation energy for migration of an interstitial far from a vacancy and λ is the corresponding activation distance. The equilibrium concentration can be found by equating Eqs. (I) and (II) and solving for n.

Now consider an anodic Ta_2O_5 film through which a current is passing so that there are n_0 interstitial Ta ions per cubic centimeter. If the field is interrupted and the specimen is held at a temperature T, these ions will move about in the film by diffusion and eventually will all recombine with vacancies. The rate of recombination will be given by an equation similar to Eq. (II) with $E = 0$. For zero field, however, the capture cross section should be considerably larger than for high fields. This can be allowed for formally by multiplying the right hand side of Eq. (II) by b, where $b >> 1$. The number of ions left at any time t, n_t, is found by integration to be

$$n_t = \frac{n_0}{1 + n_0 \gamma t} \qquad (III)$$

where $\gamma = b\nu/N \exp(-Q/kT_s)$. If a constant ion currently density, j, is now passed through the film the initial field, E_i, can be found from

$$j = 2\lambda\nu\, n_i \exp -(Q - q\lambda E_i)/kT \qquad \text{(IV)}$$

where T is the temperature at which the transient is observed. Solving for E_i gives

$$E_i = \frac{kT}{q\lambda}\left[\ln\frac{j}{2\lambda\,\nu\,n_o} + \frac{Q}{kT} + \ln(1 + n_o\gamma t)\right] \qquad \text{(V)}$$

which shows that when $n_o\gamma t >> 1$ a plot of the initial field required to give a particular current vs. the logarithm of the annealing time should give a straight line of slope $kT/q\lambda$. If the temperature at which the transients are observed is constant and the annealing temperature variable, a plot of the logarithm of the annealing time required to cause a given initial field vs. the reciprocal of the absolute temperature should give a straight line of slope Q/k. It should therefore be possible to determine both the activation energy Q and activation distance λ for the diffusion of Ta ions when they are far from any vacancies. From the data on the kinetics of growth of the film (4), it would then be possible to determine the activation energy Q_i and activation distance λ_i for the creation of interstitial ions and hence their number at any particular field strength.

It is not easy to obtain an expression for the voltage as a function of time during a constant current transient. However, the order of magnitude of the duration of the transient can be estimated in the following manner. Upon application of a constant current to an annealed Ta_2O_5 film the voltage increases rapidly to a maximum and then decreases as new interstitial Ta ions are formed. The time required for the complete disappearance of the transient depends primarily on the steady field in tne oxide when the transient has disappeared. The time for the voltage transient to disappear at a constant current is therefore the same as the corresponding time for a current transient at the final steady field. Rewriting Eqs. (I) and (II) for a constant field experiment and assuming $n << N$ gives

$$\frac{dn_+}{dt} = \alpha \qquad \text{(I')}$$

$$\frac{dn_-}{dt} = \beta n^2 \qquad \text{(II')}$$

where α and β are constants. Adding Eqs. (I') and (II') to obtain dn/dt and integrating gives

$$\frac{\alpha - n\sqrt{\alpha\beta}}{\alpha + n\sqrt{\alpha\beta}} = \frac{\alpha - n_o\sqrt{\alpha\beta}}{\alpha + n_o\sqrt{\alpha\beta}} \exp(-2t\sqrt{\alpha\beta}) \qquad \text{(VI)}$$

where n_o is the number of interstitial ions present initially and t is the time. Eq. (VI) shows that the transient will have disappeared almost completely when

$$t \cong \frac{3}{\sqrt{\alpha\beta}} \qquad \text{(VII)}$$

at which time $n = \sqrt{\alpha\beta}$. From Eqs. (I), (I'), (II), and (II')

$$\sqrt{\alpha\beta} = \nu \exp\{-[Q_i + Q - q(\lambda_i + \lambda)E]/kT\} \qquad \text{(VIII)}$$

where E is the steady field after the disappearance of the transient. With Eq. 6 of Ref. (1) Eq. (VIII) becomes

$$\sqrt{\alpha\beta} = 2\lambda N j \qquad \text{(VIII')}$$

Transients at constant voltage.—Analysis of data from constant voltage experiments is much simpler than with that of the constant current experiments. Consider an anodic Ta_2O_5 film which is held at a constant voltage. If a current j_1 is passing through the film, a sudden change of voltage will cause a sudden change of current to j_2. The value of $q\lambda$ is now found from Eq. (IV) to be

$$q\lambda = \frac{kT}{E_1 - E_2}\ln\frac{j_1}{j_2} \qquad \text{(IX)}$$

where E_1 and E_2 are the initial and final field strengths.

Once the value of $q\lambda$ has been determined from Eq. (IX), the activation energy Q can be determined by taking several specimens all in the same initial condition and recording the initial current upon sudden application of a convenient field strength. The currents at the same field strength at several temperatures can then be determined with the use of Eq. (IV), and the activation energy determined from a plot of log current vs. $1/T$.

Experimental Methods

Anodic Ta_2O_5 films were formed on chemically polished Ta sheet obtained from Fansteel Metallurgical Company. This material was the same type as that used previously (5). All of the films used in the constant current experiments were formed at 1.56 ma/cm^2 (specimen area 6.4 cm^2) to 120 v at 29°C using 2% Na_2SO_4 solution in water, and were 1760Å thick.[1] As soon as the required thickness was reached the cell was short circuited to eliminate any changes in the film due to a slow discharge of the applied potential. After formation the films were annealed at various temperatures using heating baths of water or silicone oil depending on the annealing temperature. After the anneal a current of 0.1 ma/cm^2 was impressed on the specimen again using 2% Na_2SO_4 solution at 29°C, and the voltage recorded as a function of time on a Brush Recording Oscillograph. The zero point of the recorder was suppressed so that only about 40 v appeared on the scale, and the voltage could be read with an estimated uncertainty of ±0.4 v.

Constant voltage experiments were conducted using the same material and electrolytic solution. Sudden changes in the applied voltage were made with the apparatus shown in Fig. 1. By operating switch S the voltage set on the potentiometer could be added to or subtracted from that of the constant voltage supply.

Results

Experiments using constant current.—Fig. 2 shows typical voltage-time traces at constant current. Each horizontal division represents 0.2 sec, and each

[1] Thickness measured by comparison with optical step gauge (5).

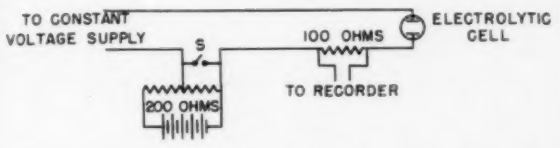

Fig. 1. Apparatus used for producing sudden changes in the voltage applied across a specimen.

small vertical division is 1.0 v. The voltage rises fairly rapidly, reaches a maximum, and then decreases. The voltage rises slowly because of the necessity for charging the condenser formed by the system Ta-Ta_2O_5-solution which has a capacitance of 0.8 mfd and requires 0.15 sec to reach 120 v at 0.64 ma. As the voltage approaches the maximum some conduction in the film occurs, so that the voltage rises more slowly and the maximum is reached in all cases at about 0.35 sec. As the conductivity of the film increases due to the process responsible for the transient the voltage falls, reaches a minimum in about 10 sec, and then increases slowly as the film continues to grow at a steady rate. The increase in film thickness during the transient is only about 5Å, so no appreciable error is made in calculating the field if it is assumed that the thickness is constant.

The duration of the voltage transients at constant current, 10 sec, was the same for all specimens as it should be according to the theory. With $\lambda \approx 2 \times 10^{-8}$, $N = 2.3 \times 10^{22}$, Eq. (VIII′) gives $t \sim 8$ sec, in very good agreement with the experimental value.

Fig. 3 shows the maximum field reached during the transient at constant current against the logarithm of the time. An approximation to the initial field [Eq. (V)] can be obtained by extrapolating the voltage time curve back until it meets the voltage time curve for charging the condenser. Data obtained in this way are shown in Fig. 4, and linear field vs. log time plots are obtained. This extrapolation method is probably fairly good when the maximum field is small so that the voltage changes slowly with time, but is very inaccurate when the maximum field is large.

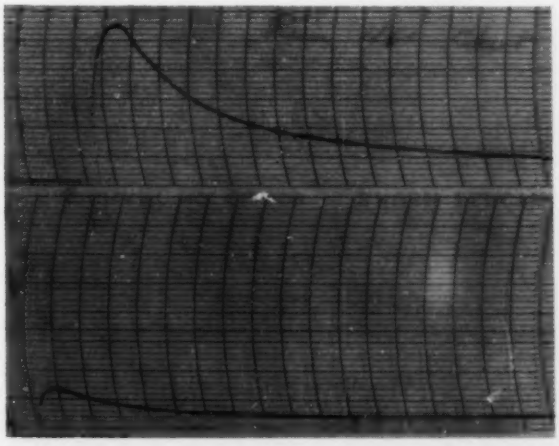

Fig. 2. Voltage vs. time at constant current. Upper curve, specimen annealed 1.5×10^5 sec at 100°C; lower curve, specimen annealed 4 sec at 100°C. Each small division in the vertical direction is 1.0 v, and each division in the horizontal direction is 0.2 sec.

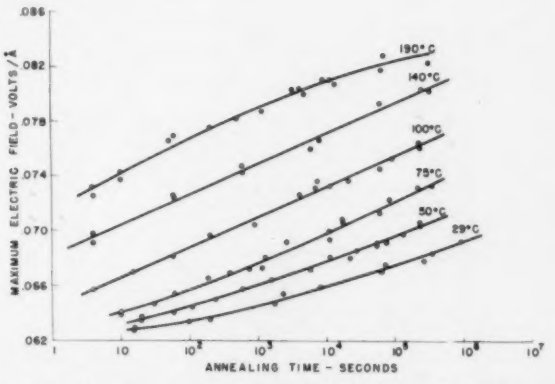

Fig. 3. Maximum field reached during formation of films at constant current after annealing for various times at different temperatures.

Fig. 5 shows the logarithm of the annealing time required to reach a given maximum field against the reciprocal of the absolute annealing temperature. Since all of the curves which have a given maximum field also have approximately the same shape, each maximum field corresponds to a given initial field and hence a given state of the oxide. The slopes of the curves of Fig. 5 thus are equal to Q/k, and activation energies calculated from the slopes are plotted vs. maximum field in Fig. 6. It may be seen that the activation energy increases with increasing extent of annealing from about 0.8 ev to 1.35 ev.

The activation distance λ times the charge q can be estimated from the slopes of the curves of Fig. 4 using Eq. (V). Values of $q\lambda$ thus obtained increase from 12 at 190°C to 21 at 29°C, in units of electron charges times angstrom units. While these values are clearly of the right order of magnitude, they are probably considerably too large because of the fact that the activation energy increases as annealing progresses.

Dependence of transient on the history of the film. —Several experiments were performed using the constant current method to determine whether the

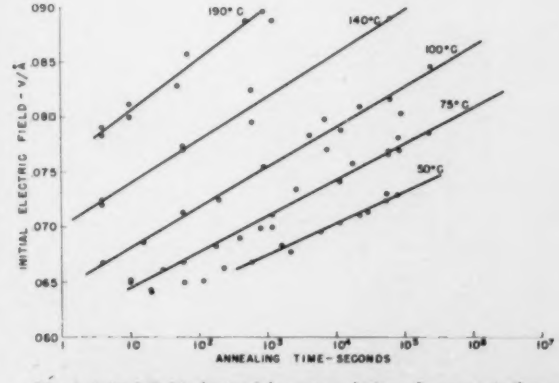

Fig. 4. Initial field obtained by extrapolation of curves similar to those of Fig. 2 vs. annealing time.

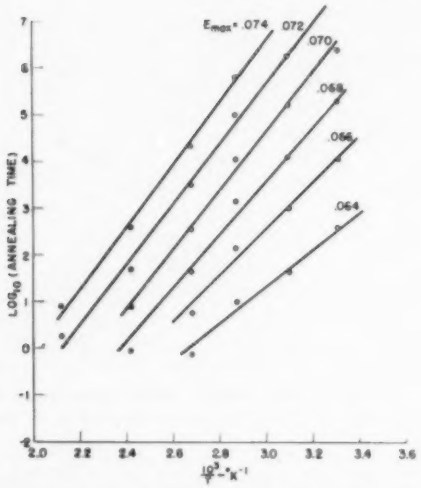

Fig. 5. Logarithm of the annealing time required to reach a given value of maximum field (see Fig. 3) vs. $1/T$.

curve of E_{max} vs. time was sensitive to the previous history of the film. Fig. 7 shows typical results. Curve 1 is the curve for 140°C from Fig. 3. Curve 2 is for specimens first held at 190°C for 10 sec to give an E_{max} of 0736. Since this E_{max} would have been produced in 250 sec at 140°C, E_{max} was plotted against log (time + 250). There is some indication of a more rapid initial rate and a slower final rate. When the specimens were first held at 80°C until the current was 0.5 ma (curve 3) the value of E_{max} was about the same (0.0734) corresponding to 200 sec at 140°C. Upon annealing these specimens at 140°C, however, there is a marked deviation from the previous results. Thus, a given value of E_{max} is not associated only with a certain number of interstitials and vacancies, since the behavior of the film on subsequent annealing is a function of the manner in which the given E_{max} was achieved. The presence of history effects makes it possible that the activation energies shown in Fig. 6 might be in error.

Experiments at constant voltage.—Fig. 8 shows typical current transients at constant voltage. Each hoizontal division is 0.04 sec, and each small vertical

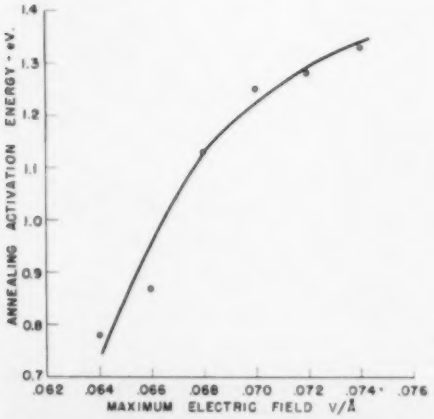

Fig. 6. Activation energy obtained from Fig. 5 vs. maximum field

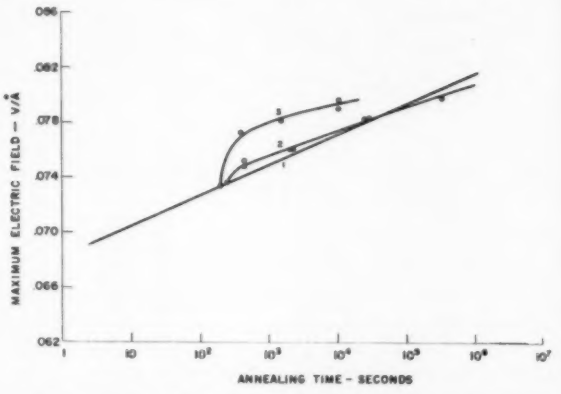

Fig. 7. History effects. Annealing at 140°C alone (curve 1) and after annealing 10 sec at 190°C (curve 2) or forming at 0.5 ma, 80°C (curve 3).

division 0.05 ma on the upper trace, 0.4 ma on the lower trace. There is some oscillation of the oscillograph pen after the sudden voltage change, but the oscillation is damped out in about 0.02 sec and causes no difficulty in determining the current immediately after the voltage change. The major advantage of the constant voltage method is that the time required to charge the condenser is now only about 10^{-4} sec.

Values of $q\lambda$ were obtained for many different ratios of initial and final currents using different temperatures. At any one temperature the value of $q\lambda$ was approximately constant, independent of the field or film thickness, although there was some indication that $q\lambda$ was larger when the field before the voltage change was smaller. Increasing the temperature caused an increase in $q\lambda$ from 4.5 e.Å at 19°C to 6.1 e.Å at 100°C as shown in Fig. 9. Other experiments designed to detect a dependence on specimen history used specimens formed at 29°C, 10 ma to 1750Å, then annealed at 100°C for 5 and 15 min. Values of $q\lambda$ observed initially in these history

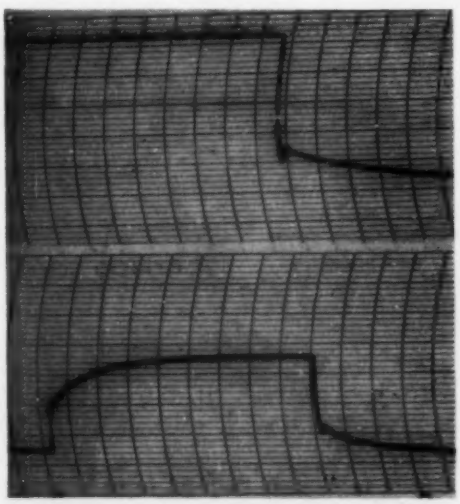

Fig. 8. Current vs. time at constant voltage. Upper trace, 91°C, small vertical division = 0.05 ma, field changed from 0.056 to 0.0515 v/Å. Lower trace, 81°C, small vertical division = 0.4 ma, field changed from 0.062 to 0.0575 v/Å. Both curves, one horizontal division = 0.04 sec.

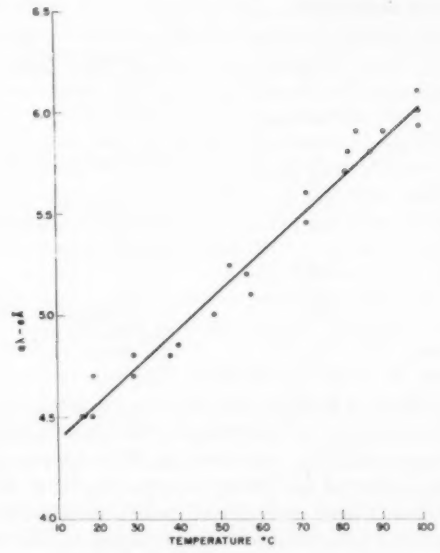

Fig. 9. Variation of $q\lambda$ with temperature

experiments were 6.3 and 6.5, respectively. As current flowed, however, the values of $q\lambda$ decreased to 4.7. Thus the value of $q\lambda$ is not a single valued function of the temperature but depends on the previous history of the specimen.

To determine the activation energy for ionic conduction several specimens were formed at 1.56 ma/cm² to 1759Å at 29°C in 2% Na_2SO_4, annealed at 100°C in boiling water for 5 min, and the initial current measured when a suitable field was applied at different temperatures. Currents which would be produced by a field of 0.058 v/Å were then calculated using Eq. (IV) with $q\lambda = 6.3$ as obtained above for specimens annealed in this manner. The slope of a plot of the logarithm of the current at $E = 0.058$ v/Å vs. $1/T$ (Fig. 10) gives an activation energy for ionic conduction of 0.7 ev. The zero field activation energy would be $0.7 + 0.058 \times 6.3 = 1.06$ ev. Annealing for 5 min at 100°C would result in an E_{max} of about 0.07 v/Å (Fig. 3), and from Fig. 6 the activation energy would be about 1.2 ev. Thus, considering the uncertainty in the annealing activation energies caused by history effects, activation energies for annealing and for ion conduction appear to be the same. The activation energy for ion conduction is therefore probably variable, and the value of 1.06 ev would be found only for specimens treated in exactly the same manner as those used above.

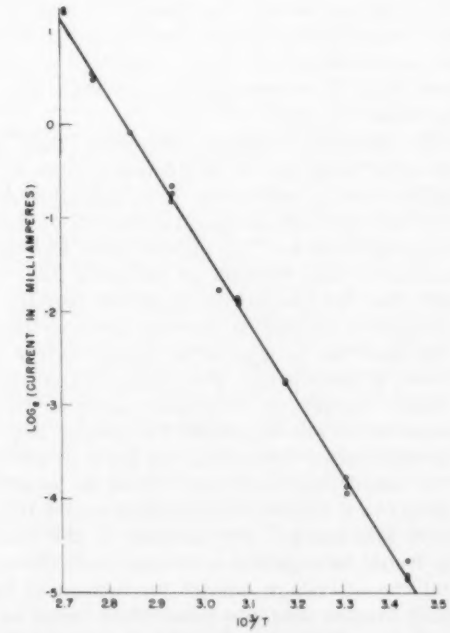

Fig. 10. Logarithm of the current produced by a field of 0.058 v/Å on specimens annealed 5 min at 100°C vs. $1/T$.

Transient studies using other metals.—It might be expected that the kinds of changes which occur in anodic Ta_2O_5 films might also occur in other amorphous anodic films such as Al_2O_3, Nb_2O_5, and ZrO_2. The constant voltage method has been used to determine the values of $q\lambda$ for films formed on chemically polished Zr, Nb, and Al. For these tests a solution of 5% $NH_4HB_4O_7 \cdot 3H_2O$ in water, with sufficient H_3BO_3 to give a *p*H of 7, was used; all tests were conducted at room temperature (26°C). The thickness of the ZrO_2 and Al_2O_3 films was estimated from capacitance measurements using values for the dielectric constant of 20 and 10,[2] respectively, and are fairly reliable. The thicknesses of the Nb_2O_5 films were estimated by comparison with the optical step gauge for Ta_2O_5 films, and may be in error because of differences in the refractive indices for the two materials. Results are given in Table I, along with the results obtained for Ta. The "effective $q\lambda$" in the table is found by allowing the transient to decay completely, using the ratio of initial to final current in Eq. (IX). Values of effective $q\lambda$ agree fairly well with those reported earlier by various authors as shown in the table.

The results show that Nb_2O_5 behaves in a manner similar to that of Ta_2O_5, having a small value of $q\lambda$ which does not vary with the current density. Al and Zr show somewhat different behavior, the values of $q\lambda$ increasing with decreasing current density. For Zr this increase is probably the result of the increasing electronic component of the current at small currents; probably only the results at high currents are reliable. For Al, on the other hand, the current is almost all ionic at all of the current densities used (12), and the change in $q\lambda$ may be a result of an actual change of structure with changing current.

The most interesting part of these data is the difference between Zr and the other metals. There is almost no transient with Zr, the current immediately after the change of voltage being nearly the steady value. Attempts to increase any possible transient by intermediate annealing were not successful. Also, the value of $q\lambda$ found for Zr is much larger than that for the other metals. It may be that

[2] This value for the dielectric constant of anodic aluminum oxide was chosen so that the thickness for formation at room temperature, 3 ma/cm², would be about 13.5Å/v, in agreement with the results of Hass (7).

Table I. Results of transient studies using several metals

Material	Oxide film thickness, A	Current density range, ma/cm²	Initial qλ e.A	Effective qλ e.A	Values of effective qλ from the literature
ZrO_2	1500	0.007-0.003	4.0	——	
		0.3-0.15	5.0	——	
		1.5-1.0	10.8	11.3	11.2 Charlesby (8)
Al_2O_3	1200	3.0-1.5	3.3	10.6	
		0.3-0.15	4.1	——	7.5 Charlesby (9)
		0.03-0.015	4.5	12.1	10.5 Guntherschulze and Betz (10)
Nb_2O_5	1800	0.5-0.2	5.8	12.2	
		0.005-0.02	5.8	——	
Ta_2O_5	1600	3-1.5	4.6	12.1	11.7 Vermilyea (4)
		0.5-0.2	4.6		12.5 Young (11)
		0.1-0.05	4.8		

the ionic current in the ZrO_2 film is controlled at an interface rather than in the bulk of the material.

Except for Zr, however, results show that slow changes in the film follow changes in the applied field, as for tantalum oxide films. Values of qλ for all except ZrO_2 are all very reasonable, giving values of λ ranging from 1 to 1.5A if the full ionic charges are assumed. In view of the lack of transients in ZrO_2 films and the very large value of qλ it would be interesting to make a more thorough study of ionic conduction in these films.

Discussion

Results obtained from constant current and constant voltage tests are summarized in Table II.

Values of qλ obtained in constant voltage experiments are believed to be more reliable.

The points of agreement between the results and theory are that transients which are qualitatively of the type predicted are observed, and that the duration of the transients agrees with the predicted value. There are, however, several serious points of disagreement. In the first place, qλ varies with the temperatures at which it is measured and also with the history of the film. Second, the constant current transients also depend on the history of the film. Third, the activation energy for annealing depends on the extent of annealing, while, if the only process occurring were the recombination of defects, it should be constant. Finally, the numbers of defects, calculated with the values given in Table I and using Eq. (5) of Ref. (1), approach the number of lattice ions in some ranges of field and temperature. The theory should apply only to very low concentrations of defects, of the order of 10^{-4} or less of the number of lattice ions.

Further evidence which appears to contradict the theory has been obtained in tests to determine the solution rate of the films in HF (3). It was found that the solution rate decreased linearly with log time at annealing temperatures from room temperature to 330°C. Since the theory predicts that the change which is occurring is simply a decrease in the number of defects, and that the number of defects is inversely proportional to the time, these results imply that the corrosion rate is proportional to the logarithm of the defect concentration. It would be expected that for small defect concentrations the solution rate would be proportional to the number of defects rather than to the logarithm of the number, and it is therefore difficult to account for this behavior unless it is postulated that changes in solution rate and rate of ion transport are completely unrelated. However, the magnitudes of the activation energies for the process responsible for the change in corrosion rate are the same as those for the change in the constant current transient, which indicates that the processes are probably the same.

Table II. Summary of activation energies and values of qλ

Method	Activation energy ev	q-e.A
Constant current	0.8-1.35	12-21
Constant voltage	1.06	4.5-6.5

In addition to the changes in solution rate which occur upon annealing the films, it was also found (3) that x-ray diffraction patterns from the film become somewhat less diffuse upon annealing at temperatures between 200° and 600°C. A decrease in the diffuseness of the pattern might conceivably occur if the concentration of interstitial Ta ions decreased as predicted by the theory. It is probable, however, that such a change would have to involve defect concentrations of about a tenth of a percent or more, that is, a concentration so high that the theory would not apply.

All the evidence suggests, therefore, that some change other than that of the concentration of defects alone must be occurring. A modification of the theory which can explain qualitatively all of the observed results follows. The anodic oxide film on Ta is amorphous, and appears to be glass like. It is assumed that the passage of a current through the film produces a change in the local ionic configuration and that the change is of such a nature that conduction is made easier. For example, the current flow might change an originally uniform Ta ion concentration to one in which the spacing between ions varied slightly from place to place in the film, with the result that some ions would be located so that jumps to a neighboring position would require relatively less energy. An increase in the current density would be expected to change both the number and the activation energy for motion of these favorably located ions, the total effect being to increase the conductivity. This mechanism bears a strong resemblance to that originally proposed, since

here there are a field dependent number of mobile ions which correspond to the "interstitial ions" of the earlier theory. The differences are, first, that all ions are now supposed to be lattice ions, some of which are in favorable configurations for motion and, second, that both the number and the activation energy for motion of these ions changes with the passage of current instead of just the number as previously assumed. Support for the reasonableness of changes in local configuration is found in the fact that changes in local configuration in ordinary glasses accompany heat treatments such as rapid cooling from high temperature or annealing in the transition range of temperatures (6), and the changes are believed to be responsible for the observed variations in density, refractive index, conductivity, and other properties.

No quantitative predictions are attempted, but qualitatively the explanations of the experimental results are as follows. First, consider a constant voltage transient experiment such as those described above. When the field is suddenly changed there is an instantaneous change in current because the effect of the smaller field on the activation barrier is less. Following the instantaneous change there is a slow change in both the number of conducting ions and in the barriers to their motion which makes ionic motion more difficult. The net result is that the field has produced a much larger effect than that due solely to changing the field on the barrier which existed before the voltage change. In other words, the effective value of $q\lambda$, defined by an equation similar to Eq. (IX) but measuring the final current after the decay of the transient, is much larger than the ionic charge times half the distance between successive minima in the energy of an ion. The change of $q\lambda$ with temperature and the history dependence of $q\lambda$ are, according to this mechanism, a result of an actual change of activation distance with changes in local configuration. The range of values of $q\lambda$, $4.5 - 6.5$ e.Å, is reasonable, particularly since it is possible that the ionic charge would be less than five. The value of the pre-exponential factor calculated from the data shown in Fig. 10 is about 2×10^{24}, while the value of $2\lambda\nu N$ is about 4×10^{27} if $\nu = 5.10^{13}$. Thus it appears that for Ta_2O_5 films treated in this one particular manner only about one Ta ion in a thousand is in a favorable local configuration for motion. The values of preexponential factors found in the earlier work (0.2×10^{27} to 2×10^{27}) are difficult to interpret since they represent the intercepts of log rate vs. $1/T$ plots for specimens with different local configurations held at the same electric field.

When a film is annealed the structure would tend to change toward a more stable configuration, so that upon re-application of a field the current would be smaller. The activation energy for annealing is that observed above, 0.8-1.35 ev, and increases as annealing progresses. Annealing and conduction may both involve the same sort of atomic movements, since the activation energies are similar. The effect of the history of the film on the annealing process is the result of the fact that different methods of reaching a state measured by the transient behavior result in different local configurations, and hence films brought to such a state by different methods behave differently on subsequent annealing by the same method.

In addition to producing changes in the rate of ionic transport, such changes of local configuration would be expected to change the x-ray scattering by the film and also the chemical properties of the film. Furthermore, there is no reason to suppose that such changes would be restricted to annealing in any particular small range of temperatures. The results of measurements of the solution rate in HF and of x-ray scattering by the films are thus in good qualitative agreement with this mechanism, since it would be expected that the most stable state would be one of minimum lattice distortion and would show greater chemical stability and give less diffuse x-ray patterns.

If it is accepted that changes in local configuration do occur, it is clear that the only experiments which can supply easily interpreted information about the values of activation distance and activation energy are those in which measurements are made on specimens having the same history and in a time short enough so that no changes in local configuration can occur. Measurements such as those reported earlier (4) for Ta_2O_5 are very difficult to interpret in terms of the activation energies and distance actually existing at any instant in the film.

Acknowledgement

Discussions with C. P. Bean were of great value in arriving at an interpretation of these experimental results. Helpful criticisms of the manuscript by D. Turnbull are gratefully acknowledged.

Manuscript received October 2, 1956.

Any discussion of this paper will appear in a Discussion Section to be published in the June 1958 JOURNAL.

REFERENCES

1. C. P. Bean, J. C. Fisher, and D. A. Vermilyea, *Phys. Rev.*, **101**, 551 (1956).
2. A. Guntherschulze and H. Betz, "Elektrolytkondensatoren," p. 69, Berlin (1937).
3. D. A. Vermilyea, *This Journal*, to be published.
4. D. A. Vermilyea, *ibid.*, **102**, 655 (1955).
5. D. A. Vermilyea, *Acta Met.*, **1**, 282 (1953).
6. R. O. Davies and G. O. Jones, *Adv. in Physics*, **2**, 370 (1953).
7. G. Hass, *J. Opt. Soc. Amer.*, **39**, 532 (1949).
8. A. Charlesby, *Acta Met.*, **1**, 340 (1955).
9. A. Charlesby, *Proc. Phys. Soc.*, **66B**, 317 (1953).
10. A. Guntherschulze and H. Betz, *Z. Phys.*, **92**, 367 (1934).
11. L. Young, *Trans. Faraday Soc.*, **50**, 153 (1954).
12. A. Charlesby, *Proc. Phys. Soc.*, **66B**, 533 (1953).

Metal-Water Reactions

V. Kinetics of the Reaction between Magnesium and Water Vapor

Harry J. Svec and Dale S. Gibbs

Institute for Atomic Research and Department of Chemistry, Iowa State College, Ames, Iowa

ABSTRACT

The rate of reaction between magnesium and water vapor was studied in the temperature range between 425° and 575°C and in the water vapor pressure range between 31 and 208 mm Hg. The reaction took place according to the linear rate law. Rate constants were found to be linearly dependent on the water vapor pressure. The activation energy for the reaction was found to vary with both temperature and water vapor pressure, increasing as the temperature was increased and the water vapor pressure was decreased. This type of variation is explained on the basis of a change from a surface to a vapor phase reaction due to the very large increase in the vapor pressure of Mg metal in the temperature range between 500° and 600°C.

The kinetics of the oxidation of Mg metal by oxygen gas have been studied by many workers (1-5). The effect of the presence of water vapor on the rate of reaction was also examined in some of these researches. The work reported here includes the study of the surface oxidation of Mg metal by water vapor in the absence of other gases. Reaction temperature and water vapor pressure are varied independently to determine their influence on the rate of reaction. The results of these studies are correlated with the results of the oxidation of Mg by oxygen and other metal-gas reactions.

In the temperature range covered by this work, the products of the reaction between Mg and water vapor are MgO and H_2, according to the equation

$$Mg + H_2O \rightarrow MgO + H_2$$

Because of the nature of this stoichiometry, the rate was followed by measuring the pressure increases due to H evolution in a closed system.

Experimental

Apparatus

The apparatus for the study of the reaction of water vapor and Mg is depicted diagrammatically in Fig. 1. The vacuum apparatus was built around a 25 mm OD, Pyrex glass tube (A) which was suspended vertically in the center of a 12 gal, controlled-temperature water bath. A 10 mm, high-vacuum grade stopcock (S_1) at the top of the tube and at the water line of the bath isolated the thermostatted part of the apparatus from the outer vacuum pumping system. Apiezon T grease was used to lubricate this stopcock, and it was found to hold satisfactorily at all bath temperatures up to 72°C. The lower portion of the tube (A) was connected to an opening through the bottom of the bath by means of a kovar seal (B) and a stainless steel ball joint (C). The port was fitted with a thin disk which was sealed to the glass water bath jar with Apiezon W wax to give a water-tight seal. A 35/20 ball joint (T_1) was an integral part of the stainless steel port. The reaction tube (D) was constructed of 24 mm OD Vycor tubing and the socket was also made of Vycor. The metal sample (F) was suspended in the reaction tube by means of nichrome wire, A.W.G. 34. The sample was insulated from the nichrome wire by a small alumina tube placed in a hole drilled across one end of the specimen.

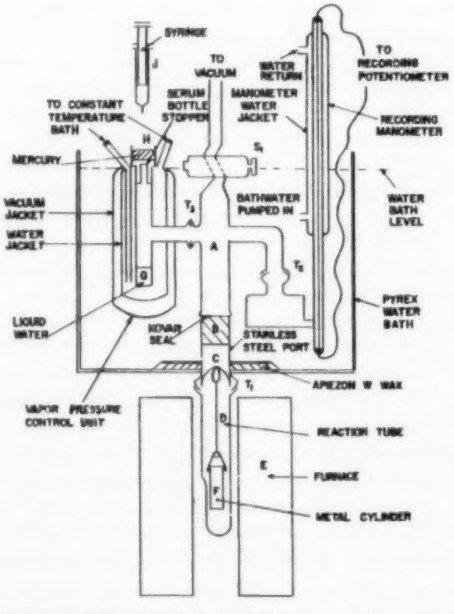

Fig. 1. Manometric apparatus for the study of the kinetics of the reaction of Mg and water vapor.

The reaction tube was heated by an electric furnace (E), the core of which consisted of an Inconel tube 18 in. long, with an ID of 1.0 in. The linear temperature variation was ±0.1°C for a section 4.0 in. long in the middle of the tube. The furnace had a Chromel A heating winding and a Pt temperature-sensing winding. An electronic proportioning furnace controller (6) was used, and the temperature in the region of the sample was controlled to better than ±0.05°C in the temperature range between 400° and 600°C.

A recording mercurial manometer (7) was connected to the vacuum apparatus through a 35/20 ball joint (T_2) using Apiezon W wax. At high bath temperatures, breaks occurred in the calibration curves when the Hg in the manometer emerged above the water line of the bath. A glass jacket through which bath water was circulated was placed over the manometer tube as shown in Fig. 1. The calibration curves were then linear at all bath temperatures up to 72°C, the highest employed in this work.

A water vapor pressure control unit, following the design of Apel (8), was connected to the vacuum apparatus through a 35/20 ball joint at (T_3). Water was pumped from a second controlled temperature bath through the jacket enclosing the tube containing liquid water (G), thus controlling the temperature of the liquid water and, therefore, the water vapor pressure. An evacuated jacket was placed around the water jacket to insulate the water jacket from the surrounding bath. The surrounding bath and the reaction tube were always maintained at sufficiently high temperatures to prevent condensation of water in areas outside the vapor pressure control unit. Only the ball joint (T_1) was in an unthermostatted region, but convection of heat upward from the furnace was sufficient to prevent condensation in this area. The top of the vapor pressure control unit was fitted with a rubber serum bottle stopper (H) and covered with Hg to give a vacuum tight seal. Water was introduced into the vapor pressure control unit through the stopper, using a hypodermic syringe (J). The water vapor pressure control unit was calibrated for several temperatures of the second controlled temperature bath. The vapor pressures were reproducible to within ±1.5 mm for successive runs at all temperatures employed in this work. The limiting water vapor pressure for this apparatus was approximately 250 mm Hg. The greases and waxes used in assembling the apparatus and the pumps used for circulating the water would not withstand the temperatures necessary to produce higher water vapor pressures. Also, the increment of change of water vapor pressure for small temperature changes became increasingly large at higher temperatures, to the extent that above 70°C close control with the present apparatus was virtually impossible.

Procedure

Mg metal, in the form of blocks with the approximate dimensions 1 x 1 x 8 in., was obtained from the Dow Chemical Company, Midland, Mich. Spectrographic analysis for impurities, furnished with the metal, was as follows: Al, 0.0047%; Ca, 0.01%; Cu, 0.009%; Fe, 0.031%; Mn, 0.058%; Ni, 0.003%; Pb, 0.005%; Si, 0.001%; Sn, 0.001%; Zn, 0.001%. The blocks of Mg were cut lengthwise into four pieces and turned into rods. The rods were cut into cylinders approximately 4.5 cm long. These specimens were then finished on a lathe under carefully controlled and duplicated machining conditions. After this treatment the cylinders averaged 4.1 cm in length and 1.1 cm in diameter. They were washed in dry, thiophene-free benzene to remove traces of surface oil, and were allowed to stand in air until needed for an experiment.

In preparation for a run, the dimensions of the cylinders were measured with machinist's calipers, and a ⅛ in. hole was drilled across one end of the sample to accommodate an alumina tube. The cylinders were handled with polyethylene covered forceps to eliminate finger prints on the surface. They were etched for 5 min in a solution containing 2% HNO_3 in absolute ethanol, followed by two rinses of dry, 1:1 acetone-methanol; then the cylinders were placed in a beaker of dry, thiophene-free benzene. The alumina tube was positioned in the hole in the end of the cylinders, and a nichrome hook, connected to the nichrome suspension wire, was positioned into the ends of the tube. Samples were protected from the atmosphere in the benzene bath during these operations.

After the etching and rinsing procedure had been completed, the ball joint on the stainless steel port (T_1) (*see* Fig. 1) was heated and de Khotinsky-hard cement was applied. After the socket on the reaction tube had been heated, the sample was taken out of the benzene rinse and suspended on a nichrome wire clip inside the ball joint (C). The reaction tube was placed over the sample and sealed to the apparatus immediately. After being evacuated for about 1 min with an auxiliary pump, and with a cold trap to catch the benzene, the apparatus was opened to a high vacuum pumping system. Pumping was continued for 5 min at 200°C in order to outgas the system. Then the system was brought to the reaction temperature (425° to 575°C) by sliding the furnace up over the reaction tube. By continuing the pumping for 5 min more, the pressure was reduced to less than 10^{-4} mm Hg. The apparatus was isolated from the vacuum pumps by closing stopcock (S_1) (*see* Fig. 1) and 1 ml of degassed water was introduced into the vapor pressure control unit. The water vapor pressure corresponding to the temperature of the vapor pressure control unit was attained in less than 3 min, even at the highest water vapor pressures. The reactions were generally allowed to proceed for 10 hr or longer. At the lowest reaction temperatures, the induction periods approached 8 hr, and it was necessary to increase the length of a run to get suitable rate data. At the end of each run, the water vapor, the excess liquid water, and the H_2 were pumped out of the apparatus by the auxiliary pumping system. The samples were cooled to room temperature in a vacuum, air was admitted to the apparatus, and the specimens and products were stored under argon

gas for x-ray analysis. The reaction was studied at 31, 55, 92, 153, and 208 mm water vapor pressures and 425°, 450°, 475°, 500°, 525°, 550°, and 575°C.

At the beginning of each reaction there was an induction period. The length of the induction periods was a function of the reaction temperature and ranged from approximately 8 hr at 425°C to 15 min at 575°C. During this time the increases in pressure were so small that the apparatus was not sensitive enough to furnish data for the determination of the rate law. Toward the end of the induction periods, the rate increased sharply and then became constant with time.

At the end of each run, as the cylinders cooled to room temperature, the reaction product on the surface of the metal broke away from the cylinders spontaneously, exposing etched metal surfaces. The coatings were identified by x-ray powder photographs for the highest and lowest water vapor pressures at each reaction temperature. In every case the only product was MgO. The gas evolved during the reaction was analyzed mass spectrometrically, and only H_2 and water vapor appeared in the samples.

Reactions of Mg and water vapor of different character than described above occurred under conditions of high temperature and low water vapor pressure. These reactions began with the usual induction period, followed by a sharp increase in the rate and the leveling off to a constant rate. However, after proceeding normally for periods of 1-4 hr, depending on the temperature, a second sharp rise in the reaction rate was observed. MgO was deposited on the walls of the reaction tube following each reaction of this type. When the Mg cylinders were cooled, most of the oxide coating peeled off spontaneously, leaving a sheath surrounding the metal cylinders. The metal cylinders could be easily lifted out of these sheaths, and the insides of the sheaths were found to be lined with Mg crystals. The reaction rate always decreased after recrystallization of Mg began. Due to limitations of the apparatus and method used in this work, it was not possible to determine the rate law governing the vapor phase reactions. Rate law determinations in this work were limited to reactions in which the oxide product was confined to the metal surface.

Because of the formation of the MgO coating on the metal surface, the reaction of Mg and water vapor was expected to follow one of the four principle rate laws (4, 9, 10) governing gas-solid reactions. A plot comparing these laws for the data of a typical run is shown in Fig. 2. Water vapor-weight values were obtained readily from the knowledge of the H_2 pressure, the volume of the apparatus, the area of the Mg cylinders, and the stoichiometry of the reaction. It was assumed that the measured areas of the cylinders were minimum values and that these values were proportional to the true surface areas by a fairly constant factor. Reproducibility of the data corroborated this assumption.

For each run the amount of water vapor reacted per cm^2 was plotted against the time in hours. Examples of these plots for each reaction temperature of this study, at a constant water vapor pressure of 208 mm Hg, are shown in Fig. 3. Rate constants were calculated from the slopes of these curves. Three or more reactions were carried out for each set of reaction conditions. Rate constants for each run are listed in Table I with average rates for each temperature and water vapor pressure indicated. It may be noted that the rate constants at 31 mm water vapor were greater than for 55 mm water vapor at both 525° and 550°C. This was attributed to the vapor phase character of these reactions which is explained in the discussion which follows. Above 500°C, the lower limiting water vapor pressures for this work were determined by the appearance of the vapor phase type of reaction. The lower

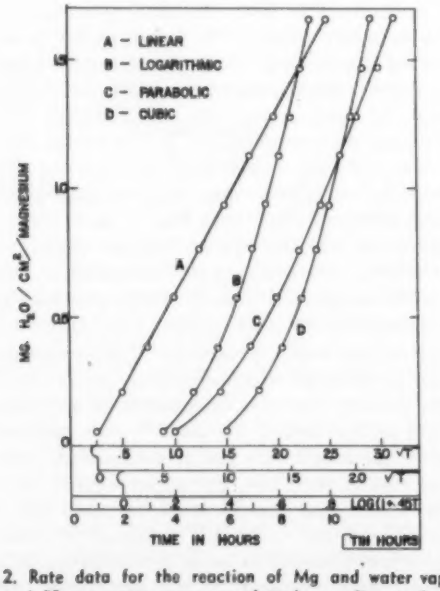

Fig. 2. Rate data for the reaction of Mg and water vapor at 525°C and 55 mm water vapor are plotted according to four rate laws.

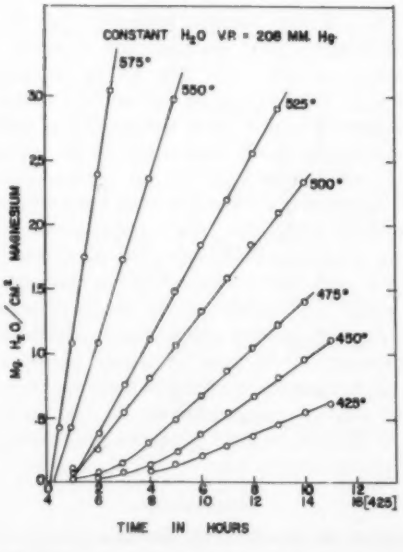

Fig. 3. Examples of the plots of mg water vapor reacted per cm^2 Mg surface against time for each reaction temperature of this study. Rate constants were calculated from the slopes of these curves.

Table I. Results of rate studies of the reaction of Mg and water vapor in the temperature range between 425° and 575°C in the water vapor pressure range between 31 and 208 mm Hg

Reaction temp, °C	Water vapor Press, mm Hg	Rate constants Runs 1	2	3	Mean	Avg. dev.
425	153	0.075	0.097	0.084	0.082	0.007
425	208	0.067	0.078	0.101	0.085	0.013
450	153	0.103	0.103	0.086	0.097	0.008
450	208	0.131	0.141	0.153	0.141	0.007
475	31	0.041	0.039	0.039	0.039	0.002
475	55	0.055	0.055	0.050	0.053	0.002
475	92	0.095	0.097	0.086	0.092	0.004
475	153	0.141	0.138	0.143	0.140	0.002
475	208	0.182	0.187	0.189	0.186	0.002
500	31	0.068	0.067	0.066	0.067	0.001
500	55	0.100	0.080	0.109	0.096	0.011
500	92	0.128	0.125	0.133	0.128	0.002
500	153	0.197	0.190	0.190	0.192	0.003
500	208	0.261	0.253	0.253	0.255	0.003
525	31	0.225	0.174	0.122	0.174	0.034
525	55	0.168	0.165	0.157	0.163	0.004
525	92	0.212	0.205	0.211	0.209	0.003
525	153	0.277	0.284	0.283	0.281	0.002
525	208	0.350	0.365	0.362	0.359	0.006
550	31	0.337	0.400	0.400	0.379	0.028
550	55	0.288	0.316	0.337	0.313	0.017
550	92	0.394	0.390	0.408	0.397	0.007
550	153	0.507	0.480	0.514	0.500	0.013
550	208	0.612	0.623	0.620	0.618	0.004
575	208	1.273	1.200	1.323	1.265	0.058

limit was 55 mm water vapor at 525° and 550°C and was 208 mm at 575°C. Because the apparatus was not capable of attaining higher water vapor pressures, only one water vapor pressure was examined at 575°C. Plots of rate constant against water vapor pressure show a linear dependence in the temperature range covered.

Plots of log k against $1/T$ for water vapor pressures of 55, 92, 153, and 208 mm Hg are shown in Fig. 4. Two straight lines were obtained for each water vapor pressure. One of the straight lines covers the temperature range between 425° and 500°C, and the other covers the range between 525° and 575°C. Activation energies at the various water vapor pressures for the two temperature ranges are shown in Table II.

Activation energies for the water vapor pressures below 208 mm were not calculated for the temperature range between 525° and 575°C because only two points were available for these curves. There was a gradual decrease in activation energy with increase in water vapor pressure in the lower temperature range, and there was a sharp increase in activation energy above 500°C at all water vapor pressures investigated. The trend of all plots in Fig. 4 indicates that all activation energies above 500°C are the same.

Table II. Activation energies for the reaction of Mg with water vapor

Water vapor pressure, mm Hg	Activation energy, kcal/mole 425°-500°C	525°-575°C
55	31.7 ± 7.6	—
92	21.8 ± 3.9	—
153	15.2 ± 2.7	—
208	11.1 ± 2.7	33.7 ± 1.5

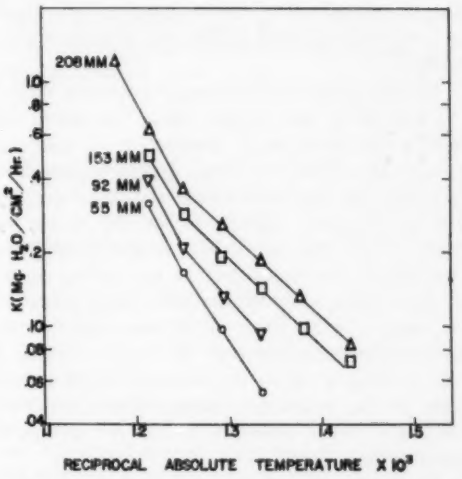

Fig. 4. Log k is plotted against the reciprocal of the absolute temperature for four water vapor pressures to demonstrate the variation of the rate constants with temperature in the Arrhenius equation.

In the early part of this work, difficulty was encountered in the development of a method of preparation and handling Mg so that the reaction with water vapor would take place. The Mg cylinders were etched for 2 min in a solution of 2% HCl in ethanol, washed in two baths of acetone-methanol, and rinsed in dry, thiophene-free benzene. The cylinders were supported in the bottom of the reaction tube by a small, U-shaped, stainless-steel clip. Screws at each end of the clip were used to hold the cylinders in place. The cylinders were insulated from the clip by ceramic tips on the ends of the screws, and the clip served to support the cylinders concentrically in the reaction tube. Even with this preparation and with the temperature at 525°C for periods as long as 20 hr there was no visible evidence of reaction in over 80% of the trials. In some instances the reaction took place only at isolated spots on the Mg surface. The metal around the spots appeared bright and shiny. Each variable in the procedure of preparing for a run was changed independently in an effort to determine the important factors involved. None of the variables investigated made significant differences as to whether or not the reaction took place. When the use of the nichrome wire method of suspension of the sample was adopted and the HNO_3 etch was used to replace the HCl etch, only about 5% of the specimens failed to undergo reaction. This phase of the surface oxidation of Mg by water vapor warrants further investigation. The apparent passivation of the metal under certain conditions offers an opportunity for future study.

Discussion

The oxidation of Mg by water vapor in the temperature range between 425° and 575°C and the water vapor pressure range between 31 and 208 mm

Hg can be explained by three different mechanisms, all of which are related to the vapor pressure of the Mg metal.

1. In the temperature range between 425° and 500°C and over the entire range of water vapor pressures, the reaction is confined to or takes place very near the metal surface. Water vapor diffuses readily through the loose oxide structure and reacts at the metal-oxide interface. As the water vapor pressure is reduced, some Mg atoms actually leave the surface of the metal before encountering water vapor molecules, and the reaction takes place either in the vapor phase within the porous oxide structure or on the internal surface of the oxide sheath. This concept is supported by the occurrence of a gradual increase in the activation energy which is observed as the water vapor pressure is reduced in this temperature range.

2. In the temperature range between 500° and 575°C and at water vapor pressures sufficiently high to confine the MgO product to the surface of the metal cylinders, the reaction takes place interstitially in the loose oxide coat. The rate of vaporization of the Mg atoms is so great that few water vapor molecules ever reach the solid metal surface before reaction takes place, and a large water vapor concentration gradient exists between the metal-oxide and the gas-oxide interfaces. The reaction takes place either on the internal surfaces of the oxide sheath or in the vapor phase within the loose oxide structure. This mechanism explains the sharp increase in the activation energy at all water vapor pressures above 525°C.

3. When the water vapor pressure is reduced below 55 mm at 525° and 550°C and below 208 mm at 575°C, there is no longer sufficient water vapor within the oxide coat to react with all of the vaporized Mg atoms, and these atoms escape from the oxide coat. MgO is deposited on the walls of the reaction tube, and the reaction takes place either in the vapor phase or on the walls of the reaction tube. Leontis and Rhines (2) observed a vapor phase reaction above 575°C in the oxidation of Mg by oxygen.

The most important factor affecting the reaction mechanism in the temperature range of this work is the vapor pressure of the Mg metal. The rapid rise in the vapor pressure between 500° and 600°C is shown by the values given in Table III (11).

It was interesting to observe that the amount of vaporization in these experiments increased after the oxidation had taken place for some time. This increase in the amount of vaporization was due presumably to an increase in the surface area of the metal during the oxidation process. The surface of the metal under the oxide coat was always roughly etched. Gulbransen (1), by using a vacuum microbalance technique, clearly showed a similar increase in the amount of vaporization, after a period of oxidation.

Table III. Vapor pressure of Mg

Temp, °C	Vapor pressure of Mg, mm Hg
500	0.053
550	0.190
600	0.684

The concept of increase in vaporization with reaction on the metal surface serves to explain the steps leading to the vapor phase reactions. In these reactions the normal induction period is always observed and the reaction starts off at a constant rate. However, as the reaction proceeds, the amount of vaporization increases as the surface becomes etched by the oxidation process and there is no longer sufficient water vapor traversing the oxide coat to confine the reaction to the surface of the metal. When this occurs another sharp rise in reaction rate is observed. As recrystallization of Mg on the inside of the oxide sheath takes place, the rate of reaction decreases, presumably because the Mg-lined sheath is less permeable to Mg vapor than is the oxide coat.

These conclusions are corroborated by correlation of the activation energy data as determined in this study with other thermodynamic data. Reactions occurring at high temperatures and/or low water vapor pressures have been explained on the basis of the high vapor pressure of Mg. Activation energies obtained for these reactions in this work are 31.7-33.7 k/cal. These results agree well with the heat of sublimation of Mg, which is 34.4 kcal (12). At lower temperatures and at the highest water vapor pressure used in this study, the activation energy was found to be 11.1 kcal. This value compares favorably with energies determined in other water vapor-metal studies (8, 13, 14) in which adsorption on or diffusion of some species through the solid product coating was the rate-controlling step. Inasmuch as activation energies intermediate to these values have been found for some reaction conditions, the conclusion is tenable that a combination of both vaporization and diffusion through the coating determines the over-all reaction rate.

Manuscript received August 6, 1956. Contribution No. 529. Work on this paper was performed in the Ames Laboratory of A.E.C.

Any discussion of this paper will appear in a Discussion Section to be published in the June 1958 JOURNAL.

REFERENCES

1. E. A. Gulbransen, *Trans. Electrochem. Soc.*, **87**, 589 (1945).
2. T. E. Leontis and F. N. Rhines, *Metals Technol.*, **13** (4), 1 (1946).
3. I. A. Makolkin, *J. Appl. Chem. (USSR)*, **24**, 505 (1951).
4. N. B. Pilling and R. E. Bedworth, *J. Inst. Metals*, **29**, 529 (1923).
5. H. N. Terem, *Compt. rend.*, **226**, 905 (1948).
6. H. J. Svec, A. A. Read, and D. Hilker, Atomic Energy Commission A.E.C. Rept. ISC-585, 1955.
7. H. J. Svec and D. S. Gibbs, *Rev. Sci. Instr.*, **24**, 202 (1953).
8. C. T. Apel, Unpublished M. S. Thesis, Iowa State College Library, Ames, Iowa (1956).
9. U. R. Evans, *Trans. Electrochem. Soc.*, **83**, 335 (1943).
10. O. Kubaschewski and B. E. Hopkins, "Oxidation of Metals and Alloys," p. 37, Academic Press, New York (1953).

11. American Society for Metals, "Metals Handbook," p. 28 (1948).
12. F. F. Coleman and E. Egerton, *Trans. Roy Soc. London*, **234A**, 177 (1935).
13. B. E. Deal, Unpublished Ph.D. Thesis, Iowa State College Library, Ames, Iowa (1955).
14. B. E. Deal and H. J. Svec, *J. Am. Chem. Soc.*, **75**, 6173 (1953).

Enhanced Surface Reactions

Manfred J. D. Low and H. Austin Taylor

Nichols Laboratory, New York University, New York, New York

ABSTRACT

The influence of an electrodeless gaseous discharge on the rates of adsorption of hydrogen on Pd·Al_2O_3, ZnO and Ni-kieselguhr and of carbon monoxide on ZnO was investigated. Enhanced adsorption rates and extent were found. A mechanism for the observed effect has been suggested which should have general applicability in chemisorption, oxidation of metals, and other similar phenomena.

An interesting experiment on the influence of a high-frequency induced gaseous discharge on the rate of chemisorption of oxygen on NiO has been reported by Engell and Hauffe (1). The application of a Tesla coil to the system after 150 min when adsorption had almost ceased caused a marked increase in adsorption, the amount adsorbed almost doubling in 30 min. Lack of an explanation for this large effect caused by such a minor discharge prompted a repetition of the experiment.

Experimental

A Tesla coil of the type frequently used for leak detection was applied to a standard constant volume adsorption system so that a discharge could be caused and maintained in a region 40 cm from the adsorbent chamber in an 8 mm O.D. tube leading from the chamber to the adsorption measuring apparatus. A plug of Pyrex-glass wool was located in this tube, 20 cm from the point of discharge and between the latter and the adsorbent. The coil was adjusted to give a continuous discharge which was barely visible in a darkened room. Preliminary experiments under the conditions prevailing in actual runs but in the absence of the adsorbent showed that the discharge had no noticeable effect on the pressure in the system.

Experiments using three different adsorbents are described: (*a*) 15.53 g of a commercial Pd hydrogenation catalyst made by Baker and Co. of 0.5% Pd on 1/16 in. extruded Al_2O_3 pellets; (*b*) 18.76 g ZnO from oxalate, prepared according to the method of Taylor and Sickman (2); (*c*) 10 g Ni-kieselguhr containing 11.5% Ni (3).

Gases used were H_2 and CO. Pure H_2 was prepared by diffusion of tank H through heated Pd thimbles. CO was obtained from the reaction of CH_2O_2 and H_2SO_4 and was purified by suitable washing and drying.

Results and Discussion

The statement made earlier that the discharge was without effect unless adsorbent was present is illustrated by the data of two such runs at different gas pressures shown in Table I. Pressures were measured on a dibutyl phthalate (DBP) manometer.

The small pressure changes in run II are attributable to the changes in room temperature and, as seen from run I, when this is constant, so also is the pressure before, during, and after the discharge. Pressure changes observed during discharge when adsorbent is present are exemplified by Table II showing the pressure readings for the enhanced adsorption of H_2 on ZnO shown later in Fig. 4.

It may be seen that the rate of pressure change, just before the discharge was applied, fell to about 3 mm DBP in 25 min. During the first 5 min of discharge the pressure fell 5 mm and more than 20 mm during the half hour the discharge was applied. It is seen, therefore, that the effect of the discharge is real; it is far from being a small, delicate effect and is comparable with the normal adsorption rates on the same adsorbent. It is the more startling, since this enhanced adsorption occurs on surfaces, which, from the classical point of view, are almost fully saturated at the prevailing pressure.

Fig. 1 is a plot of the data of a typical experiment on the adsorption of H_2 on Pd · Al_2O_3 at 257°C. The

Table I. Effect of discharge in absence of adsorbent

Time, min	Run I Room temp, °C	Press. H_2 cm DBP	Time, min	Run II Room temp, °C	Press. H_2 cm DBP
5	26.4	68.20	5	27.0	30.09
10	26.4	68.20	10	27.0	30.09
15	26.4	68.20	15	27.0	30.09
20	26.4	68.20	20	27.0	30.09
Discharge on			Discharge on		
25	26.4	68.20	25	27.0	30.09
30	26.4	68.20	30	27.0	30.09
40	26.4	68.20	35	27.0	30.09
50	26.4	68.20	40	27.1	30.8
Discharge off			42	27.1	30.10
55	26.4	68.20	45	27.1	30.10
60	26.4	68.20	50	27.2	30.13
70	26.4	68.20	60	27.3	30.20
			65	27.0	30.05

Table II. Enhanced adsorption of H_2 on ZnO at 100°C. $P_0 = 66.9$ cm DBP

Time, min	Room temp	Press. cm DBP
975	30.6	27.32
1115	32.2	26.98
1190	31.2	26.65
	Discharge on	
1195	31.2	26.10
1200	31.2	25.58
1205	31.2	25.08
1215	31.2	24.38
1220	31.2	24.10
1225	31.4	23.88
1230	31.4	23.76

run having continued for 3 hr and the pressure of the H_2 having fallen from 77.23 to 56.75 cm DBP, the Tesla coil was turned on. The rate of disappearance of the gas is markedly increased under the influence of the discharge. After 70 min the Tesla coil was turned off. The rate of gas uptake is seen to decline rapidly, although the enhancing effect of the discharge is still apparent 10 min later. The insert in Fig. 1 is an Elovich plot (4) of the data and shows the return of the rate to its initial value after cessation of the discharge by the constancy of slope of the first and third parts of the curve. A similar continuation of the enhancement after the discharge is to be found in the experiment by Engell and Hauffe.

In Fig. 2 the effect of a discharge on the rate of CO adsorption on ZnO at 257°C and 55 cm DBP is shown. Again the rate of gas uptake is markedly enhanced by the discharge but decreases again when the discharge ceases, falling almost to the same rate as that before the discharge was applied.

A similar effect was observed in the influence of the discharge on the rate of adsorption of H_2 at an initial pressure of 71.3 cm DBP on a Ni-kieselguhr catalyst at 322°C as shown in Fig. 3.

The most pronounced effect was found on studying the adsorption of H_2 on ZnO. Fig. 4 and 5 again show the marked enhancement of the adsorption caused by the discharge. The enhancement is apparent not only during the course of a run while

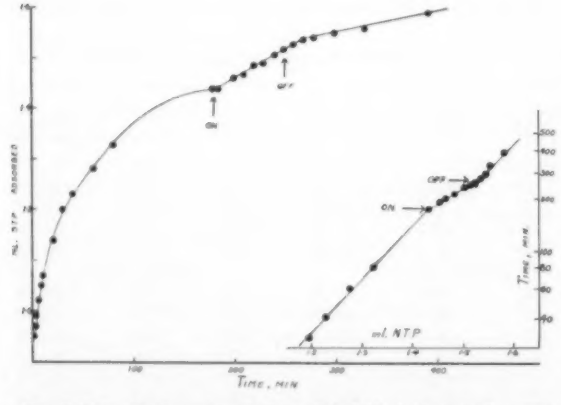

Fig. 1. Rate of adsorption of H_2 on Pd. Al_2O_3 before, during, and after application of discharge. Insert is a plot of amount adsorbed against the logarithm of time. Temp, 257°C; $P_0 = 77.23$ cm DBP.

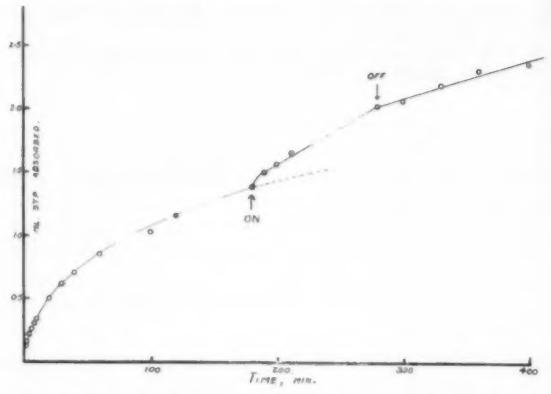

Fig. 2. Effect of discharge on adsorption of CO on ZnO. Temp, 257°C; $P_0 = 55.0$ cm DBP.

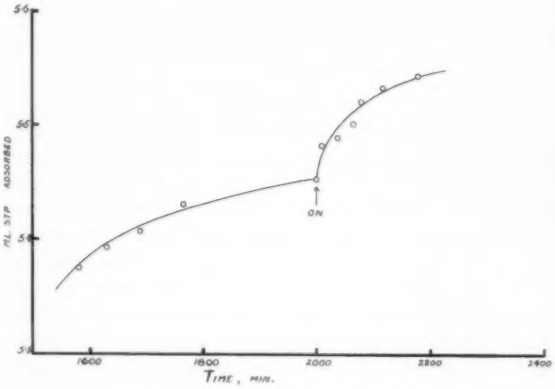

Fig. 3. Effect of discharge on adsorption of H_2 on Ni-kieselguhr. Temp, 322°C; $P_0 = 71.3$ cm DBP.

spontaneous gas uptake is occurring (Fig. 4) but also the adsorbent, seemingly saturated after seven days' exposure, may be made to take up more gas (Fig. 5).

As pointed out by Engell and Hauffe the increase in adsorption shown in their experiment, and in these many experiments, cannot be related to a saturation of adsorbent surface by adsorbate, since in such a case a discharge would be ineffectual. It is also unlikely that, in the case of H_2 adsorption, the effect is due to a direct and massive production of H atoms, since, in the first place, the conditions of the Tesla coil discharge are so feeble in comparison with those necessary for effective atom production in a Wood's discharge tube and, in the second place, experience shows how effective is a plug of dry glass wool, such as used here as a protection for the catalyst, in causing atom recombination. The similarity of the enhancement of adsorption of CO indicates that the effect of the discharge can at best be but a feeble excitation or activation of molecules. The concentration of such species, atoms, or molecules reaching the catalyst surface must be extremely small and the marked increase in adsorption would suggest some form of a chain process. Engell and Hauffe have attempted to explain the effect in terms of their Barrier Layer theory, suggesting that the observed increase in gas uptake is due to an increased electron-affinity of the oxygen. Gray and

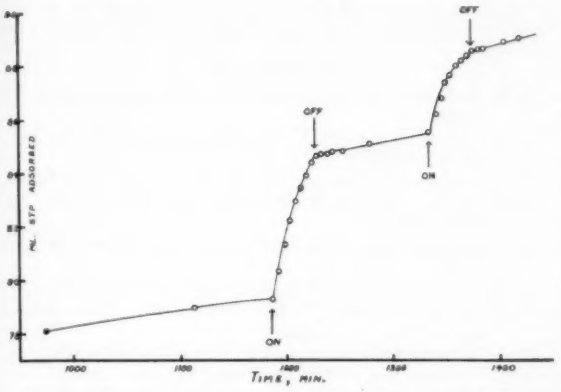

Fig. 4. Effect of discharge on adsorption of H_2 on ZnO before saturation of the surface. Temp, 100°C; P_0 = 66.9 cm DBP.

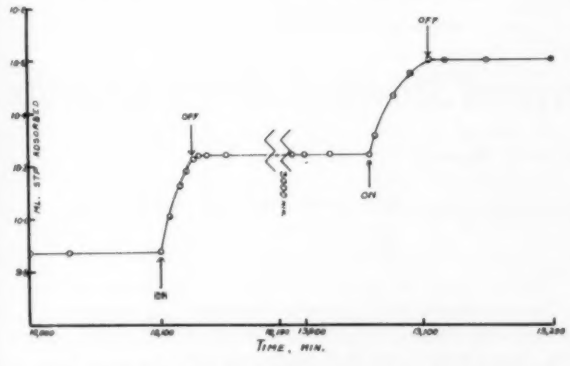

Fig. 5. Effect of discharge on adsorption of H_2 on ZnO after saturation during 7 and 9 days. Temp, 100°C; P_0 = 64.6 cm DBP.

Darby (5) suggest that the effect, in the case of oxygen on NiO, may be due to oxygen being built into the lattice of the adsorbent.

An alternative, more attractive, and more general theory, not applicable alone to semiconductor surfaces, may be deduced from the theory of Taylor and Thon (4) which Taylor (6,7) has extended. It has been amply demonstrated in the vast majority of such studies to which the Elovich equation is applicable that the rate of slow chemisorption is independent of the changing pressure in the gas phase. Therefore, the observed deceleration can be attributed only to the other reactant, the surface. Taylor and Thon (4) suggested that this effect can result from a spontaneous bimolecular disappearance of sites which are created initially through the contact of the gas and the surface. It has been shown (6,7) that this site creation can occur by a branching chain mechanism initiated by the reaction of an active particle, G, with a surface atom, S, causing a "dissociation" of the atom into two adsorption sites, V. The over-all reaction for the branched chain may be represented:

$$G + nS \rightarrow GV + (2n-1)V$$

The remaining $(2n-1)$ sites can be active for adsorption, or alternatively, suffer bimolecular recombination and decay. It is therefore suggested that during the discharge, a new site creation process is induced and sites are produced to an extent which is enormous in comparison with the number of exciting particles. Chemisorption of normal molecules then proceeds on the newly created sites resulting in an enhanced rate of adsorption.

Confirmation of the proposed mechanism is to be found in the continuation of the enhanced adsorption even after cessation of the discharge. Gray and Darby (5) measured the adsorption of oxygen on a NiO film by a conductimetric method and found that an R.F. discharge, momentarily applied, yielded immeasurably high values for the conductivity and that the conductivity decreased only gradually to the normal value after the cessation of the discharge. Gray and Darby offer no explanation for this observation. In terms of the above mechanism, the gradual change on cessation of the discharge is to be attributed to spontaneous site decay accompanied by site disappearance through occupancy, processes in their experiments extending over some 20 min. After the surface has returned to the "normal" state, that is, its state immediately before the discharge was applied, adsorption also continues at the "normal" rate, although somewhat decreased because of the larger concentration of material now on the surface. Gray and Darby observe this "permanent" alteration in the value of the surface conductivity.

When the discharge is applied over an extended period rather than momentarily, site production can be a continuing process. Site decay as a bimolecular process must eventually equal or exceed site production. The former leads to a constant site density, with adsorption linear in time. This was observed by Engell and Hauffe and appears in Fig. 1. Other data of the authors confirm the second case.

Confirmation of the proposed mechanism should be available also in all processes which involve any form of surface energizing. The oxidation of metals under the influence of a gaseous discharge has been studied by Dravnieks (8). In this study, although perhaps less conclusively because electrodes were used, enhanced oxidation was occasionally detected. A more precise study by Fryburg (9) on the oxidation of Pt showed that oxygen atoms are at least 400 times more effective than oxygen molecules. The proposal made here offers a mechanism for this enhancement as a branched chain length of around 400.

In like manner, photo-excited adsorptions observed by Kobayashi and Kawaji (10) of oxygen on ZnS under the influence of 3650Å radiation similarly point to site creation induced by the absorbed energy. Similar effects have found their way into the patent literature. It has been claimed (11) that the coal consumption of a vertical lime kiln was decreased from 180 to 126 kg/ton of limestone by the application of a silent electrical discharge to the kiln.

The above and other examples of abnormal reaction have the common criteria that they are (*a*) heterogeneous and (*b*) show enhancement of rate, or of extent of reaction, or both, by the application of a relatively minute stimulus. The amount of en-

ergy supplied to the system is extremely small yet its effects are large. This is precisely the situation which originally prompted the suggestion of a chain mechanism for homogeneous chemical reactions. The absence of a chain mechanism in current proposals suggested to account for heterogeneous reaction, including chemisorption, infers that none is able to account for the peculiarities described in this work. The general applicability of the site-creation mechanism to chemisorption (4), heterogeneous chemical reactions (7, 12), and to the enhancements described herein would infer a high degree of plausibility. Further quantitative data are required for its confirmation.

Manuscript received Nov. 1, 1956. It was abstracted from a dissertation by M. J. D. Law submitted to the faculty of the Graduate School of Arts and Science, New York University in partial fulfillment of the requirements for the Ph.D. degree, June 1956.

Any discussion of this paper will appear in a Discussion Section to be published in the June 1958 JOURNAL.

REFERENCES

1. H. J. Engell and K. Hauffe, *Z. Elektrochem.*, **57**, 762 (1953).
2. H. S. Taylor and D. V. Sickman, *J. Am. Chem. Soc.*, **54**, 602 (1932).
3. L. Leibowitz, Thesis, New York University (1956).
4. H. A. Taylor and N. Thon, *J. Am. Chem. Soc.*, **74**, 4169 (1952).
5. T. J. Gray and P. W. Darby, *J. Phys. Chem.*, **60**, 209 (1956).
6. H. A. Taylor, Ann. N.Y. Acad. Sci., **58**, 798 (1954).
7. H. A. Taylor, Peter C. Reilly Lectures, Notre Dame University (in press).
8. A. Dravnieks, *J. Am. Chem. Soc.*, **72**, 3761 (1951).
9. G. C. Fryburg, *J. Chem. Phys.*, **24**, 175 (1956).
10. A. Kobayashi and S. Kawagi, *ibid.*, **24**, 907 (1956).
11. British Pat. 691, 476 May 1953; *C. A.* **47**, 9069 (1953).
12. N. Thon and H. A. Taylor, *J. Am. Chem. Soc.*, **75**, 2747 (1953).

Luminescence of Modified Tin-Activated Strontium Orthophosphate

H. Koelmans and A. P. M. Cox

Philips Research Laboratories, N. V. Philips' Gloeilampenfabrieken, Eindhoven, The Netherlands

ABSTRACT

The introduction of Al, Zn, Mg, Ca, or Cd in $Sr_3(PO_4)_2$ produces a new crystal phase which is probably isomorphous with $\beta Ca_3(PO_4)_2$. Activated with tin this Sr-orthophosphate gives a strong luminescence with a maximum at about 6300Å under excitation with 2537Å.

In the systems studied so far, Sn must be present in the lattice as Sn^{2+} in order to be an effective activator. Since Sn^{2+} is easily reduced to Sn metal and, on the other hand, is also readily oxidized to Sn^{4+}, a carefully controlled atmosphere is required in preparing efficient Sn-activated phosphors. Recently, Butler (1) prepared Sn-activated alkaline earth orthophosphates. He found that a firing atmosphere of N_2 containing a small percentage of H_2 is very effective in keeping Sn in the divalent state.

$\beta Ca_3(PO_4)_2$—Sn, whose emission has a maximum at 6300Å and a secondary maximum at 4950Å, proved to be an excellent phosphor. $Sr_3(PO_4)_2$—Sn has an emission at 3700Å. On introducing Al, Zn, Mg, Ca, or Cd into the Sr-orthophosphate lattice the rather weak u.v. emission of the pure Sn-activated Sr-orthophosphate is replaced by a strong emission at 6300-6500Å.

Preparation

The raw materials used were reagent grade $SrCO_3$, $(NH_4)_2HPO_4$, SnO, $Al(NO_3)_3 \cdot 9H_2O$, ZnO, $MgCO_3$, $CaCO_3$, and $CdCO_3$. The required amounts of dry base materials were mixed in a runner mill for 10 min. The blends were preheated at 500°-600°C for 1 hr in order to eliminate NH_3, H_2O, and occasionally NO_2 in preparations containing Al. After this the mixture was milled again for 20 min.

In order to form the matrix, the powders were then heated in air for 2 hr at temperatures ranging from 1000°-1100°C. After this firing the powders are white and nonluminescent. Following Butler (1), the final firing was done in N_2 containing some H_2.

In the authors' experiments, samples were fired for 30 min at 1000°-1100°C in N_2 with 0.5-1% H_2 in alundum crucibles. The furnace tube was sintered alundum (5 cm diameter) and in all preparations the gas flow was 5 l/min. Samples were allowed to cool to about 400°C in the same reducing atmosphere by moving the crucibles from the hot zone to a cooler portion of the alundum tube.

Structure

X-ray diagrams showed that the strong luminescence at about 6300Å occurring when part of the Sr in $Sr_3(PO_4)_2$—Sn is substituted by Al, Mg, Zn, Ca, or Cd is associated with a change in crystal structure. This new crystal structure is the same, irrespective of which of the elements mentioned above is substituted for Sr. The modified $Sr_3(PO_4)_2$ is probably isomorphous with $\beta Ca_3(PO_4)_2$ as shown in Fig. 1. It appears from this figure that, starting with $\beta Ca_3(PO_4)_2$, a gradual replacement of Ca by Sr, apart from other minor differences, results in a widening of the $\beta Ca_3(PO_4)_2$ lattice until a Ca/Sr ratio of about 0.2 is reached. With more Sr added there is a rather sharp transition to the normal Sr-orthophosphate structure. This transition is accompanied by a change in emission from 6200 to

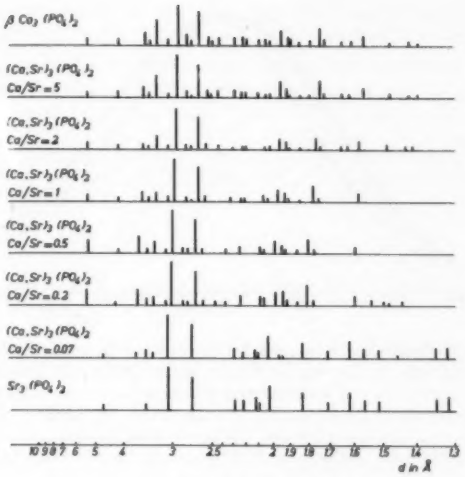

Fig. 1. X-ray diagrams of Ca,Sr-orthophosphates

3700Å. This result is different from that of Butler (1), who states that at a Ca/Sr ratio of 2.3 a new crystal phase appears without a marked change in emission and also that samples with a high Sr content, which show the long wave-length fluorescence, may have the normal Sr-orthophosphate structure.

The $\beta Ca_3(PO_4)_2$ structure as a single phase is retained between much narrower limits in the case of substitution of Sr by Mg, Zn, Cd, or Al (*see* section on Composition). With increasing substitution of Sr by Mg, Zn, or Cd there are strong indications that a new crystal phase appears of the composition $SrX_2(PO_4)_2$, where X = Mg, Zn, or Cd, with a weak greenish-bluish Sn emission. The substitution of Sr by Al is discussed later. The metal ions which produce the phase transition in $Sr_3(PO_4)_2$ are smaller than the Sr ion which they replace, so it is not surprising that their introduction results in a change to a structure like that of $\beta Ca_3(PO_4)_2$ with a smaller spacing of the metal ions. Moreover, x-ray work of Mackay (2) has shown that the structure of $\beta Ca_3(PO_4)_2$ is rather closely related to that of $Sr_3(PO_4)_2$ (3).

In agreement with this view, it was found that the smaller the metal ion substituting for the Sr ion, the less of it is required to cause the transition to the $\beta Ca_3(PO_4)_2$ structure. The minimum ratios of the cations at which the $\beta Ca_3(PO_4)_2$ structure strongly dominates, arranged in the order of increasing ionic radius of the substituting ion, are: Al/Sr = 0.08; Mg/Sr = 0.03; Zn/Sr = 0.07; Ca/Sr = 0.13; and Cd/Sr = 0.13. It is seen that Al does not fit into the series; this point is discussed later. The fact that partial substitution of the larger Ba ion for Sr does not produce the $\beta Ca_3(PO_4)_2$ structure is also consistent with the above theory.

Attempts to convert the modified Sr-orthophosphate into the normal one by varying firing conditions were quite unsuccessful. Firing at temperatures not much below the melting point resulted in highly distorted structures, x-ray diagrams showing no resemblance to either of the Sr-orthophosphate modifications. X-ray diagrams of powders fired at high temperatures and containing rather large amounts of Al showed in these structures the presence of Al_2O_3 as a second phase.

Composition

In all preparations except those containing Al an excess of 2 mole % phosphate was used. An excess of the alkaline constituents gave brownish or grayish products on firing in the reducing atmosphere due to insufficient incorporation of the Sn. Optimum ratios of the molar concentrations of the cations are: Al/Sr = 0.1 — 1; Mg/Sr = 0.07 — 0.4; Cd/Sr = 0.2; Zn/Sr = 0.1 — 0.15; Ca/Sr = ∞.

Kröger (4) suggested that the great solubility of Al_2O_3 in the Sr-orthophosphate matrix might be explained by assuming a distribution of Al over Ca and P sites in a proportion of 2 to 1, thus maintaining compensation of charge. The compositions $Sr_{6-2x}Al_{2x}P_{4-x}Al_xO_{16}$, corresponding to such a distribution of Al, are represented by the dotted line in the ternary diagram of Fig. 2a. Thus in the extreme case (x = 3) the hypothetical compound $9Al_2O_3 \cdot 1P_2O_5$ (point P in Fig. 2a) might have an orthophosphate structure without vacancies.

$$9Al_2O_3 \cdot 1P_2O_5 = 2Al_6(Al_2P)O_{16} \sim 2Sr_6P_4O_{16} = 4Sr_3(PO_4)_2$$

Since substitution of Sr ions by the smaller Al ions is accompanied by a substitution of P ions by the larger Al ions, it is clear that Al need not fit into the series (*see* section on Structure).

The symbols placed underneath each point in Fig. 2a denote the phases occurring in the phosphors in decreasing order of concentration, as found by x-ray analysis. It is seen from Fig 2a that samples with a composition corresponding to points above the dotted line (Sr + Al > 6 + x) all show the normal Sr-orthophosphate structure. Possibly more Al ions than indicated in the above formula may be incorporated at P sites; some Sr sites must then be vacant to maintain charge compensation.

Fig. 2b gives the quantum efficiency of the Al-containing phosphors as a function of their composition.

Efficient phosphors containing Cd are somewhat difficult to prepare since part of the Cd is volatilized

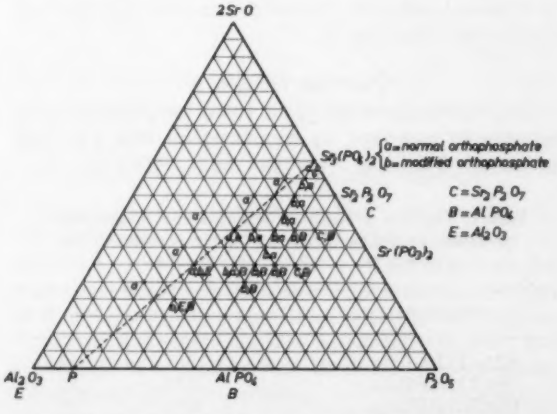

Fig. 2a. Partial composition phase diagram of the system SrO-Al_2O_3-P_2O_5. The symbols underneath each point give the various phases present in the order of their concentration.

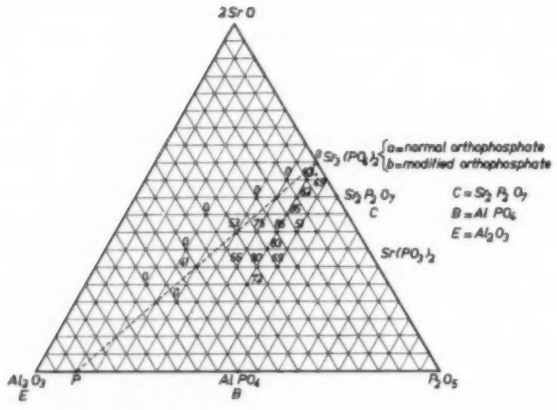

Fig. 2b. Partial composition phase diagram of the system SrO-Al_2O_3-P_2O_5. The figures give the quantum efficiency of the luminescence.

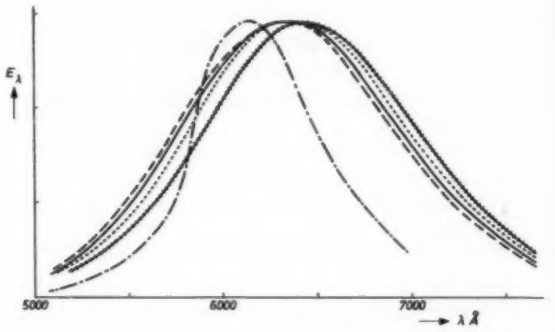

Fig. 3. Emmission of Sn- and Sn,Mn-activated Sr-orthophosphates modified with Al, Zn, Mg, or Cd. Excitation 2537Å. Sn concentration 0.4 mole %, Mn concentration 0.8 mole %. — — —(Sr,Mg)$_3$ (PO_4)$_2$-Sn; Mg/Sr = 0.16; . . . . . (Sr,Zn)$_3$(PO_4)$_2$-Sn; Zn/Sr = 0.16; |-|-|-|-|-|-|-|-|-(Sr,Cd)$_3$(PO_4)$_2$-Sn; Cd/Sr = 0.16; ——————— (Sr,Al)$_3$(PO_4)$_2$-Sn; Al/Sr = 0.33; -.-.-.-.-.-.-(Sr,Al)$_3$(PO_4)$_2$-Sn,Mn; Al/Sr = 0.33.

during firing in the final reducing atmosphere. Good results can be obtained by making the H_2 content of the final atmosphere as low as possible and by firing for short times.

The activator concentration can be varied between 0.1 and 1 mole % without much change in efficiency. In the authors' preparations, the Sn content was 0.4 mole %.

Emission Spectra

The emission of the modified Sn-activated Sr-orthophosphate, when excited with 2537Å, consists of a broad band at 6300-6500Å and a weak band at 4000Å. The emission energy in the blue band is about 5% of the total emission energy. The relative energies in the short wave and long wave emission bands do not change sensibly with activator concentration or the nature and amount of the substituents. The position of the main band depends slightly on the metal which is substituted for Sr, as shown in Fig. 3. In Fig. 3 all curves are normalized to the same maximum height. The emission spectra obtained when Ca is substituted for Sr are in accord with Butler's (1) results. The position of the maximum is not influenced by the Sn concentration nor by the amounts of Al, Zn, Mg, or Cd. With Mn as a second activator, the peak becomes sharper and shifts to 6100Å (Fig. 3).

Quantum Efficiency

The optimum efficiency at room temperature of a number of powders, as measured by Bril (5), are given in Table I, together with $\beta Ca_3(PO_4)_2$-Sn.

Table I. Quantum efficiency of Sn-activated orthophosphate phosphors; excitation 2537Å; activator concentration 0.4 mole %. x = Al, Zn, Mg, Ca, Cd

Phosphor	x/Sr	Q.E., %
$\beta Ca_3(PO_4)_2$		81
$(Sr,Al)_3(PO_4)_2$	0.33	85
$(Sr,Zn)_3(PO_4)_2$	0.16	87
$(Sr,Mg)_3(PO_4)_2$	0.12	87
$(Sr,Ca)_3(PO_4)_2$	0.16	75
$(Sr,Cd)_3(PO_4)_2$	0.20	70

It is seen from Table I that the quantum efficiency of the Sn-activated Sr,Al- the Sr,Zn-, and the Sr, Mg-orthophosphate is at least as good as that of $\beta Ca_3(PO_4)_2$-Sn. As the modified Sr-orthophosphates do not show the sub-band at 4950Å of $\beta Ca_3(PO_4)_2$-Sn and as the band at 4000Å corresponds to only about 5% of the total emission energy, this means that these phosphors give more light in the long wave emission band. The latter may be an advantage for applications in fluorescent lamps.

Resistance toward Oxidation

In fluorescent lamp manufacture the tubes are heated in air at about 540°C in order to remove the binder used in applying the coating. This heat treatment causes a reduction in light output of about 15% for $\beta Ca_3(PO_4)_2$-Sn due to partial oxidation of the Sn^{2+}. This decrease in light output is far less in the Sr,Mg-, Sr,Zn-, Sr,Cd-, and Sr,Al-orthophosphate phosphors as shown in Table II. The Sr,Ca-orthophosphate phosphor does not show a better resistance than the pure $\beta Ca_3(PO_4)_2$-Sn.

When samples are heated in air for longer periods, the light output decreases slowly but continuously until it is practically zero after 100 hr of heating in air at 700°C. Thus, it appears that the introduction of Mg, Zn, Al, or Cd does not affect the equilibrium between Sn^{2+} and Sn^{4+} in the lattice, but only the rate at which the equilibrium is reached.

The melting point of the Mg-, Zn-, Al-, or Cd-containing phosphors is much lower than that of Ca- or Ca,Sr-orthophosphate; therefore, they are prob-

Table II. Percentage reduction in light output on heating 200 mg samples in air for 15 min; firing 2 hr 1100° in air and ½ hr 1050° in N_2 — 0.4% H_2. Ratios of the cations are the same as in Table I. Sn concentration 0.4 mole %.

T, °C	500°	600°	700°
$\beta Ca_3(PO_4)_2$	5	27	92
$(Sr,Ca)_3(PO_4)_2$	6	39	90
$(Sr,Mg)_3(PO_4)_2$	0	0	8
$(Sr,Zn)_3(PO_4)_2$	3	10	12
$(Sr,Al)_3(PO_4)_2$	1	4	16
$(Sr,Cd)_3(PO_4)_2$	0	0	0

ably less reactive because they are better crystallized. This view is confirmed by the fact that, on lowering the firing temperature, the improved resistance toward oxidation on heating in air is gradually lost.

Manuscript received Oct. 10, 1956. This paper was prepared for delivery before the Washington Meeting, May 12-16, 1957.

Any discussion of this paper will appear in a Discussion Section to be published in the June 1958 JOURNAL.

REFERENCES

1. K. H. Butler, *This Journal*, **100**, 250 (1953).
2. A. L. Mackay, Thesis, University of London (1952).
3. W. H. Zachariasen, *Acta Cryst.*, **1**, 263 (1948).
4. F. A. Kröger, Unpublished work.
5. A. Bril, Unpublished work.

Energy Transport by Cascade and Resonance Processes in Doubly Activated Phosphors

Esther W. Claffy and Clifford C. Klick

U. S. Naval Research Laboratory, Washington, D. C.

ABSTRACT

A method, using quantum efficiency measurements, is described for obtaining the efficiency of energy transfer from sensitizer to activator centers in doubly activated phosphors when both centers have allowed transitions. From these measurements and applying the theory of resonant transfer it is concluded that, for NaCl: Ag, Cu, both cascade and resonant transfer mechanisms are important and that the resonant transfer process increases more rapidly with concentration than does the cascade process.

Processes by which energy is transferred from one activator to another in a phosphor have been of interest for a long time. Part of this interest stems from the widespread commercial use of doubly activated phosphors and part stems from interest in the mechanisms themselves. Materials such as the sulfides in which photoconductivity plays an important role are not considered here, but only materials where energy transport occurs without an accompanying transport of charge.

In inorganic phosphors a long series of experimental investigations (1-15) has shown that energy may be absorbed in one center, called the sensitizer, and transferred to another type of center, called the activator, which then emits. These investigations have been concerned with cases in which the sensitizer has allowed optical transitions, while those in the activator are largely forbidden. For this type of transfer the range of interaction between sensitizer and activator has also been determined (10, 13, 14).

In organic phosphors the field of interest has been primarily in the absorption of energy in the solvent molecules, followed by transfer from solvent molecule to solvent molecule until the energy reaches a solute molecule (16). Here the energy is transferred between identical centers with allowed transitions.

A quantum theory of resonant transfer between like molecules has been developed by Kallman and London (17), Perrin (18), and Förster (19) and applied to problems of organic phosphors. This theory has been adapted by Dexter (20) to the case of inorganic phosphors where the sensitizer and activator are different centers; the theory has also been extended to cover cases where the activator suffers forbidden transitions of various types.

In addition to a resonant type of transfer of energy from sensitizer to activator, another process may occur which is called the cascade process. This process occurs when the sensitizer actually emits light which is reabsorbed by the activator before the light has a chance to escape from the phosphor sample. For most sensitized inorganic materials previously investigated, the activator has forbidden transitions so that the direct absorption of light by the cascade process is negligibly small. However, this is not the case for phosphors where the activator has allowed transitions.

It is the purpose of this paper to describe methods for determining the efficiency of transfer of energy by resonance and cascade processes, and to investigate the relative importance of these processes in an inorganic phosphor having allowed transitions in both the sensitizer and activator. To achieve this end use is made of results both from experiment and from theory.

Determination of Transport Efficiencies

The method used here for the determination of transport efficiencies rests on measurements of quantum efficiencies. A detailed description of the experimental and mathematical techniques involved in such a measurement will be described elsewhere. The quantum efficiency for luminescence from the sensitizer in a doubly activated phosphor may be determined from the relation

$$S_D = \frac{\alpha_{sens}}{\alpha_{total}} (1 - \eta) S_S \qquad (I)$$

where (S_D) is the quantum efficiency for sensitizer emission in the doubly activated phosphor, and (S_s) is the quantum efficiency of the same phosphor with no activator present. The subscripts refer to singly or doubly activated phosphors. (α_{sens}) and (α_{total}) are, respectively, the absorption coefficients for the sensitizer centers alone and for the whole phosphor at the exciting wave length, and (η) is the efficiency of transfer from sensitizer to activator. Thus (η) may be determined from Eq. (I) if the absorption coefficients are known. For materials which can be prepared as transparent solids, coefficients of absorption may be obtained from transmission measurements; for materials obtainable only as powders the absorption coefficient may be obtained from reflection measurements (21).

In a similar way the quantum efficiency of the activator emission may be obtained. There are two contributions to the emission. One arises from the direct absorption of exciting light in the activator and the other arises from transfer of energy from sensitizer to activator. The total efficiency is given by

$$A_D = \frac{\alpha_{act}}{\alpha_{total}} Q + \frac{\alpha_{sens}}{\alpha_{total}} \eta A_s \qquad \text{(II)}$$

Here (A_D) is the observed efficiency of activator emission on irradiation in the sensitizer. Q is the efficiency of luminescence of the activator in the same phosphor sample with no sensitizer, but excited with light corresponding to the sensitizer's absorption band. A_s is the activator efficiency when excited in its main absorption band which must overlap the emission of the sensitizer for efficient transfer to occur. In many cases the first term on the right hand side of Eq. (II) may be neglected either because the absorption of the activator is small at the exciting wave length or because its efficiency is negligible. If this is the case, Eq. (II) simplifies and the ratio of Eqs. (I) and (II) becomes

$$\frac{S_D A_s}{S_s A_D} = \frac{1}{\eta} - 1 \qquad \text{(III)}$$

It should be noted that, where Eq. (III) can be used, the transfer efficiency may be obtained from quantum efficiency measurements alone without the necessity of determining absorption coefficients.

Once the total transfer efficiency has been obtained from experiment, it is necessary to separate it into its resonant transfer and cascade components. This is accomplished by the use of the results of theory. First, review the computation of resonant transfer for cases where the activator has an allowed transition. Dexter uses a reduced concentration, y, to relate experimental parameters to the resonance transfer efficiency; y is given by

$$y = 7.96 \times 10^{-10} X_a C' \frac{Q_a^{1/2}}{n^2} \left(\frac{\epsilon}{K^{1/2}\epsilon_c}\right)^2 \left[\int \frac{f_s(E) F_a(E)}{E^4} dE\right]^{1/2} \qquad \text{(IV)}$$

In this expression X_a is the concentration of activator centers given as a mole fraction; C' is the number of sites per cubic centimeter that can accommodate an activator center; n is the index of refraction. Dexter takes the term in round brackets to be unity; this is equivalent to assuming that the electric field at a center is the same as the average electric field in the medium. Q_a is the cross section of the activator for absorption of light and is defined by

$$Q_a = \int \frac{\alpha_{act}\, dE}{X_a C'} \qquad \text{(V)}$$

where E is in units of electron volts. $f_s(E)$ is the emission spectrum of the sensitizer in terms of the relative number of emitted photons as a function of the energy in electron volts. The curve is normalized so that

$$\int f_s(E) dE = 1 \qquad \text{(VI)}$$

Similarly $F_a(E)$ is the absorption spectrum of the activator normalized so that

$$\int F_a(E) dE = 1 \qquad \text{(VII)}$$

The reduced concentration, y, is related to the quantum yield for resonant transfer by Eq. (18) of Dexter's paper which is plotted there as Fig. 1. For y much less than unity this yield varies as

$$\eta = y(\pi/2 + y \ln y - 0.4228y)$$

For y much larger than unity the yield approaches unity; it is ½ for $y = 0.65$. With these equations, then, it is possible to calculate the resonance transfer efficiency.

An attempt has been made to calculate the efficiency of transfer by cascade processes in powders. The method developed by Johnson (21) for the reflectivity of powders was extended to this case which is complicated by the fact that the exciting light arises in the powder itself. Here, however, the approximations involved became increasingly troublesome so that this technique, which is also quite cumbersome, was discarded. Instead, the quantum yield for transfer by cascade is obtained by subtracting the calculated resonant transfer yield from the total transfer yield obtained from experiment.

Measurements on NaCl:Ag, Cu

The NaCl:Ag, Cu system was chosen for study because many of its optical properties are known and because it can be prepared as a single crystal for transmission measurements. The strong absorption bands introduced in NaCl by Ag and Cu indicate that optical transitions in these centers are not strongly forbidden.

Special precautions were necessary to prepare samples which were free of luminescent impurities and gave reproducible results. Reagent grade NaCl was specially purified with dithizone to remove traces of such heavy metal impurities as Pb, Tl, Cu, and Ag. Special high purity AgCl and reagent grade $CuCl_2$ were used (the cupric salt being converted to cuprous at the temperature needed for crystal growth). Single crystals were grown from the melt by the Kyropoulos method; just before measurement the samples were pulverized and sieved to a particle size of 179-149 μ diameter (No. 80-100 mesh fraction). The final grinding and sieving were

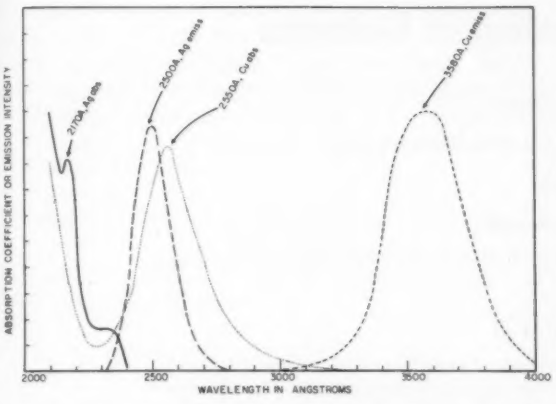

Fig. 1. Absorption and emission spectra of both Ag and Cu in NaCl plotted to arbitrary scales. The emission spectrum of Ag and the absorption spectrum of Cu overlap, giving rise to energy transfer from the Ag to Cu centers both by resonance transfer and by cascade processes.

done in a room with low humidity. Attempts to use polycrystalline melts were unsuccessful; these preparations had quantum efficiencies which were lower than the single-crystal preparations.

An attempt was made to keep the concentration of Ag constant at about 10^{-4} mole fraction while varying the Cu concentration. Analysis for Cu was made colorimetrically, for Ag, nephelometrically.

The absorption and emission spectra of both Ag and Cu luminescent centers in NaCl are shown in Fig. 1. In each case the scale of the ordinate is chosen arbitrarily. It is apparent from the figure that there is strong overlapping of the emission spectrum of Ag and the absorption spectrum of Cu. For measurements of the quantum efficiency of transfer from Ag to Cu, the exciting wave length was chosen as 2180Å which is at the peak of the Ag absorption band. At this wave length the quantum efficiency of a NaCl:Cu phosphor was measured to be only 4%. This indicates that the emission from the Cu centers due to direct absorption in the centers may be neglected although there is another Cu absorption band present which extends into the region of the exciting wave length.

It is interesting to note that both Ag and Cu alone in NaCl give rise to efficient phosphors with a measured quantum efficiency of 80%. It is apparent, then, that radiationless transitions are not an important complication in this problem.

Results of these measurements and computations are given in Table I. The transfer yield, η, is computed using Eq. (III); computations using the more exact expressions (I) and (II) indicated that the error introduced using Eq. (III) was less than the error of measurement. In all cases the resonant transfer yield is less than that due to cascade, but it increases with Cu concentration so that for sample 4 the two processes are roughly comparable. It was not possible to follow the processes to higher activator concentrations in this case because of the apparent onset of precipitation of Cu in the crystals.

Conclusions

From the measurements of this paper it may be expected that both resonant transfer and cascade processes are important in doubly activated inorganic phosphors with allowed transitions. While both processes increase with activator concentration, the resonant transfer process increases more rapidly in the case investigated here.

Acknowledgments

The authors wish to express their appreciation to Owen Gates for the silver analyses of these materials and to Robert J. Ginther and James H. Schulman for frequent discussions of this work.

Manuscript received December 26, 1956. This paper was prepared for delivery before the Cincinnati Meeting, May 1-5, 1955.

Any discussion of this paper will appear in a Discussion Section to be published in the June 1958 JOURNAL.

REFERENCES

1. S. Rothschild, *Physik. Z.*, **35**, 557 (1934); **37**, 757 (1936).
2. J. H. Schulman, L. W. Evans, R. J. Ginther, and K. J. Murata, *J. Appl. Phys.*, **18**, 732 (1947).
3. J. B. Merrill and J. H. Schulman, *J. Opt. Soc. Amer.*, **38**, 471 (1948).
4. H. C. Froelich, *This Journal*, **93**, 101 (1948).
5. F. A. Kröger, "Some Aspects of the Luminescence of Solids," Elsevier Publishing Co. Inc., Houston (1948).
6. Th. P. J. Botden and F. A. Kröger, *Physica*, **14**, 553 (1948).
7. F. A. Kröger, *ibid.*, **15**, 801 (1949).
8. H. G. Jenkins, A. H. McKeag, and P. W. Ranby, *This Journal*, **96**, 1 (1949).
9. R. Nagy, R. W. Wollentin, and C. K. Lui, *ibid.*, **96**, 183 (1949).
10. J. H. Schulman, R. J. Ginther, and C. C. Klick, *ibid.*, **97**, 123 (1950).
11. Th. P. J. Botden, *Philips Research Repts.*, **6**, 425 (1951).
12. R. J. Ginther, *This Journal*, **98**, 874 (1951).
13. Th. P. J. Botden, *Philips Research Repts.*, **7**, 197 (1952).
14. R. J. Ginther, *This Journal*, **101**, 248 (1954).
15. R. W. Wollentin, *ibid.*, **103**, 17 (1956).
16. For an introduction to this field *see* Th. Förster, "Fluoreszenz organischer Verbindungen," Vandenhoeck and Ruprecht, Göttingen (1951).
17. H. Kallman and F. London, *Z. physik. Chem.*, **B2**, 207 (1929).
18. F. Perrin, *J. Phys. et radium*, **7**, 1 (1936).
19. Th. Förster, *Ann. Physik*, **2**, 55 (1948).
20. D. L. Dexter, *J. Chem. Phys.*, **21**, 836 (1953).
21. P. D. Johnson, *J. Opt. Soc. Amer.*, **42**, 978 (1952).

Table I. Transfer efficiency values for NaCl:Ag,Cu

Sample	X_{Ag}	X_{Cu}	S_D	S_S	A_D	A_S	η	Efficiency of resonant transfer	Efficiency of cascade transfer
1	11×10^{-5}	3×10^{-6}	0.52	0.81	0.028	0.80	0.052	0.004	0.048
2	6×10^{-5}	6×10^{-5}	0.56	0.81	0.23	0.80	0.29	0.070	0.22
3	7×10^{-5}	8×10^{-5}	0.39	0.81	0.26	0.80	0.40	0.090	0.31
4	12×10^{-5}	16×10^{-5}	0.21	0.81	0.19	0.80	0.48	0.17	0.31

Electrolytic Production of Bromates

Takasi Osuga

Sanwa Pure Chemicals Co., Ltd., Tokyo, Japan

and

Kiichiro Sugino

Department of Chemical Engineering, Tokyo Institute of Technology, Tokyo, Japan

ABSTRACT

An electrolytic process for the production of potassium or sodium bromate using a pure lead peroxide anode has been operated successfully. A concentrated bromate solution was electrolyzed continuously at a cathode of stainless steel with an anodic current density of 20 amp/dm² at 70°C; current efficiency, about 90%; anode consumption about 50-60 mg/K amp-hr. Pure crystalline bromate could be obtained by cooling the cell effluent at room temperature.

Among alkali metal halogenates, only chlorates have been produced commercially in Japan by the electrolytic process. New uses for bromate brought about its electrolytic production, although in much smaller amounts than chlorate. A new electrolytic process using a lead peroxide anode is described here.

Anode for Electrolytic Production of Bromate

Electrolytic production of bromate is usually carried out at a graphite anode. However, the use of graphite has unfavorable effects. It spalls during electrolysis, forming a mud which makes continuous operation difficult. Also, the final product becomes slightly yellow[1] and can be decolorized only with difficulty. These two facts are the main reasons for the search for a better material.

A brief investigation showed that the lead peroxide electrode manufactured by a process reported earlier (2) was the most practical choice for an anode material.

A compact lead peroxide layer is deposited electrolytically from neutral lead nitrate solution upon the inner surface of an iron cylinder which acts as an anode. An example of the operating conditions is shown in Table I. Apparatus used is shown in Fig. 1.

During electrolysis, the acidity of the electrolyte gradually increased and the concentration of Pb^{++} decreased according to the following reaction.

$$2Pb(NO_3)_2 + 2H_2O \rightarrow PbO_2 + Pb + 4HNO_3$$

The change of these two was found to give a brittle deposit of lead peroxide which could not be cut for finishing or not used for an anode of the electrolysis. Moreover, sudden change of pH due to direct neutralization of acid in the electrolytic bath gave a deposit consisting of heterogeneous layers which was also brittle. Therefore, the pH and the concentration of Pb^{++} should be maintained as constant as possible during electrolysis. This was accomplished by flowing the electrolyte at constant rate and neutralizing the increasing acidity with $Pb(OH)_2$ by using the apparatus shown in Fig. 1.

The electrolysis was conducted until the thickness of the deposit reached about 8 mm. Each end of the mother cylinder 75 mm in length was cut off; then by cutting the iron part of the cylinder lengthwise, a lead peroxide cylinder of suitable strength and compactness as well as of a smooth outer surface was

Table I. Operating conditions

Electrolyte:	21-22% lead nitrate solution.
Anode:	iron cylinder with surface polished inside; length 500 mm, ID 204 mm, thickness 8 mm, weight 20.6 kg, available surface area 32 dm².
Cathode:	copper rod (diameter 25 mm)
Current:	172 amp
Current density, anodic:	5.4 amp/dm²
Voltage:	7.4 v
Temp:	50°C
Flow rate of electrolyte:	4 to 5 l/min
Time:	66 hr

[1] This coloration has been considered hitherto to be due to the presence of chromate added to the cell (1). By the use of a lead peroxide anode instead of graphite, colorless crystals were obtained as shown here.

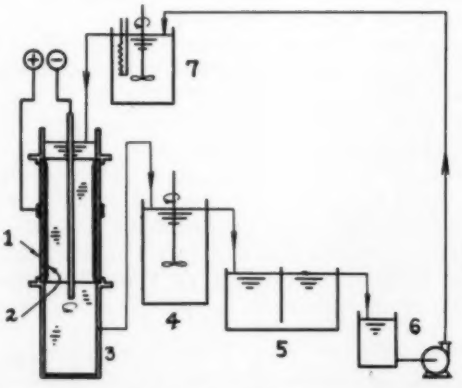

Fig. 1. Apparatus for electrodepositing lead peroxide layer. 1, Iron cylinder; 2, lead peroxide layer deposited; 3, electrolytic bath; 4, neutralization tank; 5, settling tank; 6, pump for recycling electrolyte; 7, preheating tank.

obtained (diameter, 200 mm; length, 350 mm). The lead peroxide cylinder was separated into twelve parts by cutting it again lengthwise. Each part of the lead peroxide thus obtained has the shape of a rectangular piece shown in Fig. 2. Its dimensions are as follows: length, 350 mm; width, 50 mm; thickness, 7-9 mm.

Important Factors in Electrochemical Formation of Bromate

Anodic reactions in bromate formation may be represented as follows.

$$2Br^- - 2e \rightarrow Br_2 \qquad (I)$$

$$Br_2 + OH^- \rightarrow HBrO + Br^- \qquad (II)$$

$$Br_2 + 2OH^- \rightarrow BrO^- + Br^- + H_2O \qquad (III)$$

$$2HBrO + BrO^- \rightarrow BrO_3^- + 2HBr \qquad (IV)$$

These reactions are similar to those in chlorate formation, but some differences are seen between the two cases. Reaction (IV) is about 100 times faster than that in chlorate formation according to Kretzschmar (3). On the other hand, reactions (II) and (III) seems to occur imperfectly as compared with those in chlorate formation by comparing the hydrolysis constant of Br with that of Cl_2 (4).[2] Therefore, in the case of bromate, it may be preferable to maintain the pH of the electrolyte slightly alkaline in order to favor these reactions and thus obtain high current efficiency. This condition can be attained easily by using a neutral or slightly alkaline solution of bromide at the start of the electrolysis. Efforts to keep the pH in the desirable range is not necessary except to avoid discharge of hydroxyl ion.

Reactions (II) and (III) may also be accelerated by high temperature, which has a favorable effect on current efficiency. When reactions (II) and (III) are still slow and imperfect as compared with reaction (I), the current concentration and current density may have a marked influence on the current efficiency. Preliminary experiments showed that high current concentration and also high current density [for example, 50 amp/l to 100 amp/l (13-28 amp/dm^2)] had no unfavorable effect on the current efficiency. This facilitates design of the cell and also the determination of the operating conditions.

[2] This was confirmed by the fact that bromine separated at the bottom of the cell when the initial pH of the electrolyte was less than 8 and the circulation of the electrolyte was inefficient.

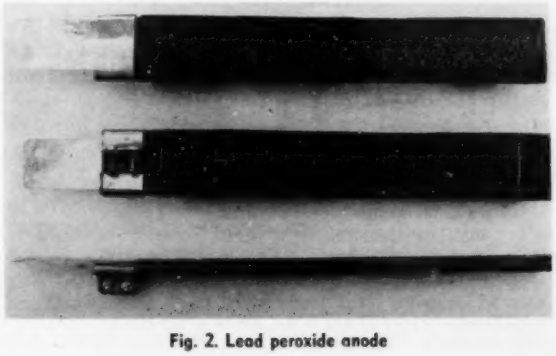

Fig. 2. Lead peroxide anode

Cell Design

The cell design depends on the use of vertical lead peroxide anodes of rectangular shape and stainless steel cathodes. A diagram of the bromate cell construction is shown in Fig. 3.

The cell body is constructed of a sheet iron rectangular tank 900 mm long x 500 mm wide x 400 mm high. All inside surfaces of the body are lined with concrete. Cell volume was determined so as to keep the cell temperature as constant as possible by balancing the internal heating with natural cooling. Three sheets of hard vinyl chloride polymer rested side by side on top of the cell and covered it entirely. The central cover supported 10 anodes and 20 cathodes. These were arranged in 6 rows running the length of the cover. Down the middle were two rows of 5 anodes, and on either side was a row of 5 cathodes. In each cell all anodes and all cathodes were in parallel.

The lead peroxide anodes were 50 mm wide, 7-8 mm thick, and 350 mm long, and extend about 55 mm above the cover. The stainless steel cathodes (Avesta 832-SV) were 35 mm wide, 2.5 mm thick, and 400 mm long. The distance from an anode to the nearest cathode was about 13 mm.

Hydrogen discharged at the cathodes caused sufficient circulation of the cell liquor. It was vented through the roof from each cell.

Batch Experiments

The cell was operated batchwise with 90-95 l of potassium bromide solution. To decrease anode loss, the temperature was kept as constant as possible. The pH was not controlled and reached a maximum of about 10 when a slightly alkaline solution (less than pH 9) of bromide was used at the start of the

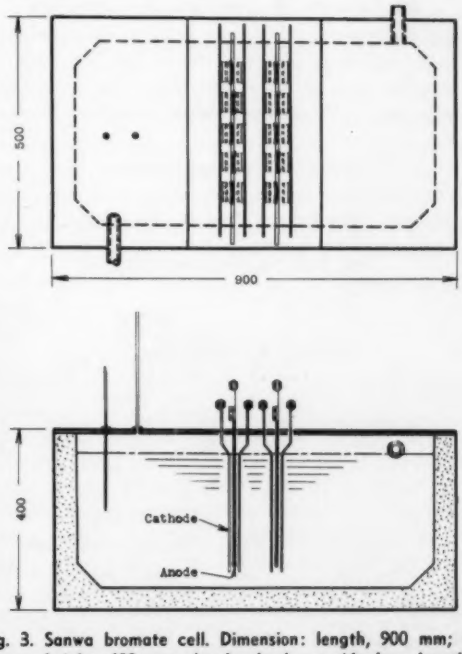

Fig. 3. Sanwa bromate cell. Dimension: length, 900 mm; width, 500 mm; height, 400 mm. Anode: lead peroxide bar; length, 350 mm; width, 50 mm; thickness, 7-9 mm. Cathode: stainless steel bar; length, 400 mm; width, 35 mm; thickness, 2.5 mm. Capacity: 95 l.

Table II. Operating conditions

Run No.	Starting electrolyte: KBr g/l	$KBrO_3$ g/l	Vol, l	Initial pH	Current, amp	Cell voltage, v	Temp, °C	Time, hr min	Amount of current, 1000 amp-hr
1	186	4	95	8.3	494	4.0	69	47 10	23.2
2	173	6	90	8.9	506	3.9*	66	44 00	22.2
3	229	9	95	6.9	500	3.8	67	56 40	28.3
4	232	9	95	8.9	500	3.7	66	56 40	28.3
5	233	9	95	9.2	500	4.0	70	56 40	28.3

* Voltage reached about 4.6 v at the end of the electrolysis.

Results

Run No.	$KBrO_3$ produced: Crystal obtained, kg	In solution, kg	Total kg	KBr unconverted, kg	Conversion of bromide to bromate, %	Current efficiency, %
1	17.3	5.6	22.9	1.0	94.2	94.6
2	15.7	5.4	21.1	0.4	97.4	91.3
3	22.7	3.9	26.6	2.7	87.4	90.5
4	22.7	4.4	27.1	2.4	88.9	92.2
5	24.0	3.1	27.1	3.0	86.7	92.2

electrolysis. All electrolyses were conducted at an anodic current density of 20 amp/dm². Operating conditions and results are given in Table II.

Two runs were made to determine what losses the anode might sustain (Table III).

Lead peroxide losses averaged 53-56 mg/1000 amp-hr and also 57-60 g/ton of product. It indicated that the loss amounted to about 2.2-2.6% of the original weight after the anode has been used for one year. Lead could not be detected in the product, the electrolyte, or in a black deposit which developed on the cathode. Lead was found in the slight amount of mud on the bottom of the cell.

An Example of Commercial Production

On a commercial scale, 24 cells were connected in series to make a circuit of 90 v and 500 amp. The cell system was divided into two solution series of 12 cells each. Electrolyte was introduced into the cell by means of a glass tube through the cover at one end and was discharged by the same means through the cover at the opposite end. The flow maintained good circulation.

A potassium bromide solution (pH 8-9), containing approximately 210-220 g/l KBr, 19-24 g/l $KBrO_3$, and 2 g/l $K_2Cr_2O_7$, was fed from a constant head tank into the cells. The concentration of bromide was adjusted so as to prevent crystallization of bromate during electrolysis. In a single pass through the cell, about 140 g/l of bromide was converted to bromate. The composition of cell effluent was approximately 270 g/l $KBrO_3$ and 90 g/l KBr. Results obtained are summarized in Table IV.

Cell effluent was a very clear solution due to the insolubility of the anode, and filtration was not necessary. After electrolysis, the electrolyte was cooled to 20°-25°C with circulating water. About 87% potassium bromate crystallized out. Almost all of the remaining potassium bromate in the mother liquor can be crystallized by adding a suitable amount of potassium bromide to return the electrolyte to the original concentration for a new cycle in the bromate cells. By this method, 97% of the bromate produced can be crystallized out without evaporation.

Potassium bromate crystal thus produced has excellent purity without recrystallization. Following

Table III. Operating conditions

Electrolyte: 180-220 g/l KBr, 15-25 g/l $KBrO_3$, 2 g/l $K_2Cr_2O_7$, pH 9-10 (during electrolysis)
Temp, 70°-85°C

Run No.	Current, amp	Amperage per one anode	Anodic current density, amp/dm²	Time, hr	Amount of current per one anode, 1000 amp-hr
Cell 1 (10 anodes)	600	60	30	2970	178
Cell 2 (15 anodes)	750	50	20	6170	308

Results

Run No.	Weight of anode* before electrolysis, g	after electrolysis, g	Loss, g	Loss per 1000 amp-hr mg	per ton $KBrO_3$ g
Cell 1	1146.5	1136.5	10.0	56.2	60
Cell 2	1043.6	1027.2	16.4	53.3	57

* Cell 1, mean value of 4 anodes; cell 2, mean value of 10 anodes.

Table IV. Characteristics of bromate production

Current: 510-550 amp
Voltage: 1st cell 3.8 v, 2nd cell 3.7 v, other cells 3.5 v in 12 cells
Current density, anodic: 20-22 amp/dm²
Temperature: 65°-72°C (1st to 4th cells, less than 60°C)
pH: alkaline, less than about 10
Rate of flow: 32 l/hr
Current efficiency: 90-92%
Energy consumption: 3.84 kwhr (d.c.)/kg $KBrO_3$
Cell feed: 210-220 g/l KBr, 19-24 g/l $KBrO_3$
Cell effluent: 260-280 g/l $KBrO_3$, 80-100 g/l KBr

are the chemical specifications of the final product currently being produced: colorless crystal, $KBrO_3$ assay, 99.2-99.5%; bromide as KBr, 0.05-0.1%; free acid, 0.35 cc 1/50*N* NaOH/5 g $KBrO_3$, max; total nitrogen, 0.002% max; sulfate, 0.005% max; heavy metals, 0.0005% max; iron, 0.0025% max.

Manuscript received April 30, 1956. This paper was prepared for delivery before the San Francisco Meeting, April 29 to May 3, 1956.

Any discussion of this paper will appear in a Discussion Section to be published in the June 1958 JOURNAL.

REFERENCES

1. For example: C. H. Martin and E. C. Hardy (Morton Salt Co.), U. S. Pat. 2191574 (1940).
2. K. Sugino, *Bull. Chem. Soc. Japan*, **23**, 115 (1950). [Method (I)].
3. H. Kretzschmar, *Z. Elektrochem.*, **10**, 789 (1904).
4. W. C. Bray, *J. Am. Chem. Soc.*, **32**, 932 (1910); **33**, 1485 (1911).

High Temperature Oxidation of High Purity Nickel between 750° and 1050°C

Earl A. Gulbransen and Kenneth F. Andrew

Research Laboratories, Westinghouse Electric Corporation, Pittsburgh, Pennsylvania

ABSTRACT

Kinetic studies on the oxidation of nickel using the vacuum microbalance method have been extended to 1050°C in order to determine the conditions and mechanisms of breakdown of the metal in oxidation. Below 900°C Ni oxidizes in the normal manner and the rate data fit in well with experimental rate relationship already established. At 900°C and higher, parabolic rate law plots of the data show increasing values of the constant with time. At 1000°C and higher, the oxide cracks away from the metal. It is suggested that Ni fails in protective oxidation due to a loss of adhesion at the oxide metal interface.

A number of studies have been reported on the oxidation of pure Ni. These studies were reviewed in an earlier paper (1). In recent years precise data have been obtained on the kinetics of the oxidation of pure Ni at temperatures up to 900°C. Moore (2), using a volumetric method, studied the reaction over the temperature range 400°-900°C while Gulbransen and Andrew (1), using a sensitive weight gain method, studied the reaction over the temperature range 400°-750°C. Considering the differences in method and metal, good agreement was found. In both studies the parabolic rate law was used to correlate the experimental data. Using the classical rate theory of oxidation, Gulbransen and Andrew (1) proposed a mechanism of reaction based on the diffusion of Ni ions through cation vacancies.

This paper extends the earlier work to 1050°C. Two objectives were of particular interest. First, to compare oxidation rate data with tracer studies (3) on the diffusion of Ni ions through nickel oxide and, second, to determine the conditions for transition in the mechanism of oxidation. Studies on several other metals (4) have shown that at some oxide thickness transition occurs from a slow protective oxide formation to a more rapid nonprotective type of oxide formation. If this transition phenomena is found to occur for all metals and alloys, we are dealing with a question of great technical importance.

Failure of metals in protective oxidation.—The use of metals and alloys at high temperature in many applications depends on the fact that the oxide film limits to a certain extent the rate of oxidation. In the protective range of reaction the rate of oxidation decreases as the oxide film thickens. However, at some temperature, time, and oxygen pressure, or film thickness, the rate of oxidation undergoes a transition to a more rapid reaction in which the rate of reaction does not depend on the oxide thickness. This phenomena has been termed "catastrophic reaction," "breakaway corrosion," "transition reaction," etc., depending on the degree of change in the reaction kinetics. The change in kinetics is referred to here as "failure in protective oxidation"; the film or scale is no longer rate controlling. The following physical and chemical factors have been related to the onset of transition in the kinetics of the reaction: (*a*) volatilization of the oxide; (*b*) volatilization of the metal; (*c*) phase transformations in the oxide; (*d*) phase transformations in the metal; (*e*) melting of the oxide; (*f*) loss of adhesion of the oxide to the metal; (*g*) combustion.

Apparatus and Method

Kinetic measurements were made using a vacuum microbalance method which has been described (5). However, to extend the range of the method, a low sensitivity balance was used as well as specimens of smaller area. In this way film thicknesses of 2000 μ g/cm^2 weight gain could be measured. In terms of film thickness for NiO, this weight gain is of the order of 126,000Å. The microbalance had a sensitivity of 4.75/division of 0.001 cm.

Samples were prepared from high purity nickel strip purchased from Johnson, Mathey and Company, London, and had no metallic impurities in excess of 0.0005%. Specimens were abraded through

4/0 polishing paper in a manner described previously (6).

Specimens had surface areas of 2.9 cm^2 and weighed about 0.1890 g.

Results and Discussion

The rate of oxidation of high purity Ni was studied as a function of time and temperature from 750° to 1050°C. Weight changes were calculated in units $\mu g/cm^2$ and converted to Å of film thickness (1).

To interpret the beginning of a transition in the kinetics of the reaction, careful observations were made on the color of the oxide and adherence of the oxide to the metal. Since these observations can be made only at room temperature after reaction has stopped, certain precautions were taken to assure the best experimental conditions. Thus, if the color of the oxide is used as a criteria of loss of contact between the oxide and metal, it is necessary to equilibrate the metal and the oxide when it is in good contact. The following procedure was adopted. After oxidation and before cooling, the oxygen atmosphere was removed and the system evacuated to a pressure of less than 10^{-4} mm Hg. Specimens were held at temperature for at least 15 min to assure equilibrium between the metal and that part of the oxide film in contact with the metal.

Fig. 1 shows oxidation curves for the temperature range of 750°-1050°C for 2 hr of reaction time and an oxygen pressure of 7.6 cm Hg of oxygen. Curves were reproducible at the higher temperatures to ±5%. Table I shows the thickness of the oxide film after 2 hr of reaction, the color of the oxide film formed, and visual evidence on the loss of adhesion of the oxide film as a result of cooling.

The color of the oxide film was gray for temperatures up to 850°C, while above 900°C the oxide film was green. The color of the oxide was determined by the conditions under which it was formed. Thus green colored oxide films were formed under strong oxidizing conditions as shown by the studies of Bénard (7) and Bogatskii (8) and were probably not formed when the oxide was in equilibrium with the metal phase. Since all oxide films were equilibrated with the metal, this is interpreted to mean that the green colored oxide films are caused by a lack of contact of the oxide with the metal phase.

Table I. Oxide film thickness vs. oxide color

Temp. °C	Thickness $\mu g/cm^2$	Thickness Å*	Color	Stability
750	102.5	6,450	Gray	Adherent
800	160.0	10,060	Gray	Adherent
850	224.0	14,090	Gray	Adherent
900	385.0	24,220	Dark green	Adherent
950	653.0	41,070	Green	Adherent
1000	1220.0	76,740	Green	Nonadherent
1050	1890.0	118,900	Green	Nonadherent

* Surface roughness ratio = 1.

If the metal and oxide lose contact over a large area, the oxide film can crack away from the metal and the oxide becomes nonadherent. Stresses developed between the metal and oxide as a result of cooling aid the process of cracking the oxide loose from the metal.

Table I suggests a definite relationship between the color and the loss of adherence of the oxide as a result of cooling. The 950°C experiment was an intermediate case.

The parabolic rate law was used to interpret the oxidation data. The equation states that $W^2 = At + C$. Here W is the weight gain, t is the time, and A and C are constants. Some of the oxidation experiments could be fitted to the cubic rate law. Since the cubic rate law has not been derived from accepted physical principles, this rate law has not been used here in interpretation of the mechanism of the reaction (1) or of the transition phenomenon.

To test the agreement of the data with the parabolic rate law, plots were made of the square of the weight gain as a function of time. Fig. 2 shows the plot for the 750°C experiment. Here the value of the slope or rate law constant A decreases with time as oxidation proceeds. For this experiment the cubic rate law gives a better empirical correlation. At 750°C, the oxide film increases in its protective properties with increasing thickness faster than that predicted by normal diffusion processes. After 2 hr of reaction the change in rate law constant with increasing amounts of oxidation becomes a smaller factor.

Fig. 3 shows a parabolic rate law plot for the 900°C experiment. A detailed analysis of the plot

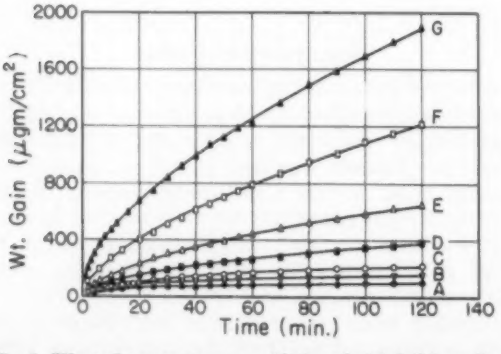

Fig. 1. Effect of temperature on oxidation of nickel, 7.6 cm Hg of O_2. A, 750°C; B, 800°C; C, 850°C; D, 900°C; E, 950°C; F, 1000°C; G, 1050°C.

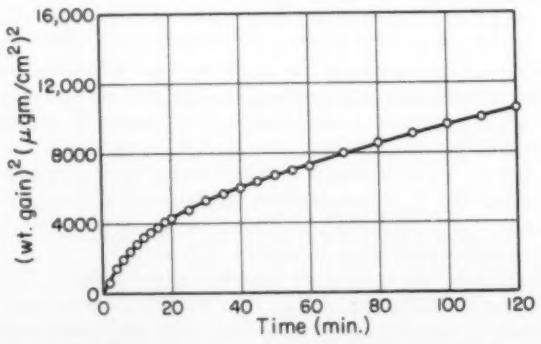

Fig. 2. Oxidation Ni, 750°C, 7.6 cm Hg of O_2, parabolic plot. Abraded through 4/0. $A = 9.03 \times 10^{-13}$ $(g/cm^2)^2/sec$.

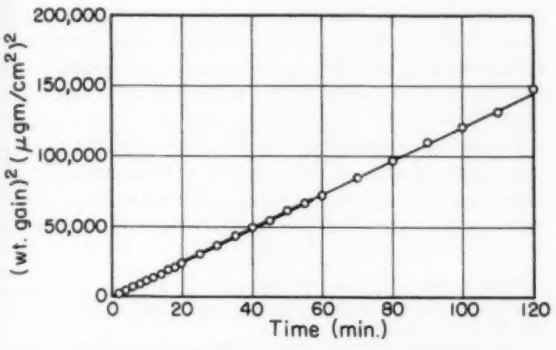

Fig. 3. Oxidation Ni, 900°C, 7.6 cm Hg of O_2, parabolic plot. Abraded through 4/0. $A_{initial} = 1.875 \times 10^{-11}$ (g/cm²)²/sec; $A_{1-2\ hr} = 2.01 \times 10^{-11}$ (g/cm²)²/sec.

shows a slightly increasing value of A as reaction proceeds.

Fig. 4 shows a parabolic rate law plot for the 1050°C experiment. Here, the slope A increases with the amount of oxidation. The increasing value of the slope A is taken as evidence for localized cracking of the oxide film and repair by oxidation. In the experiment the oxide was green and cracked away from the metal on cooling.

Table II shows a summary of the parabolic rate law constants taken from parabolic rate law plots. For temperatures of 850°C and higher, the initial and 1-2 hr values of the constants were tabulated. The initial slopes were determined during the first 10 min of reaction. Although the limiting slopes at times close to zero would be of theoretical interest, it was impossible to measure the reaction rate for these conditions. The very early stage of the reaction in addition was complicated by surface area and trace impurity effects.

Fig. 5 shows a plot of the parabolic rate law constants A on a log A vs. $1/T$ plot. The results of the earlier work at 550°-700°C as well as a recent measurement of Zima (9) were plotted together with the results of the present work. The data show the initial slope to be higher than the 1-2 hr slope. This was shown also earlier (1). However, above 900°C the initial slope was less than the final slope. The initial slopes above 900°C lie between the extrapolated values for the results below 900°C and

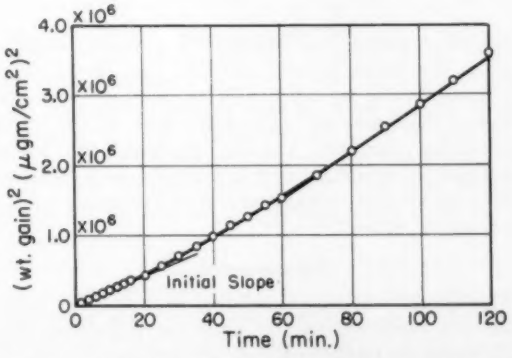

Fig. 4. Oxidation Ni, 1050°C, 7.6 cm Hg of O_2, parabolic plot. Abraded through 4/0. $A'_{initial} = 4.08 \times 10^{-10}$ (g/cm²)²/sec; $A_{1-2\ hr} = 5.56 \times 10^{-10}$ (g/cm²)²/sec.

Table II. Parabolic rate law constants, (g/cm²)²/sec

Temp, °C	Initial value	1-2 Hr value
750		9.03×10^{-13}
800		2.46×10^{-12}
850	7.67×10^{-12}	5.84×10^{-12}
900	1.875×10^{-11}	2.01×10^{-11}
950	3.75×10^{-11}	6.34×10^{-11}
1000	1.11×10^{-10}	2.41×10^{-10}
1050	4.083×10^{-10}	5.55×10^{-10}

the 1-2 hr slopes. If the initial values could be determined, it was suggested that these values would fall on an extrapolated line of BC in Fig. 5.

The data below 900°C fit in well with the earlier work, using a heat of activation of 41,200 cal/mole. Above 900°C, the data may be falling on a second line having a slope which yields a heat of activation of about 68,300 cal/mole. However, if the oxide loses contact with the metal, the slope of this line has little meaning.

The experimental heat of activation of 41,200 cal/mole was in agreement with some preliminary observations of Moore (3) on the heat of activation involved in the diffusion of nickel in nickel oxide at temperatures greater than 1000°C using a radioactive tracer method. Using the same grade of nickel as that used in this study, Moore (3) obtained a value of 44,200 cal/mole for the heat of activation of the diffusion process. These values can be compared since the experimental heat of activation for both the oxidation experiments and the diffusion experiments contains the same two heat terms. These were: the heat of formation of defects for diffusion and the heat of activation of diffusion. Since the parabolic rate law constant involves both the heat of formation of defects and the heat of activation of diffusion as exponential terms, the defect concentration at the oxide-metal and oxide-gas interface changes with the temperature.

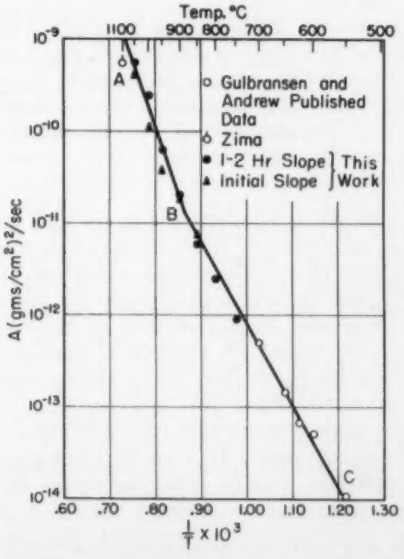

Fig. 5. Oxidation high purity nickel. Log A vs. $1/T$, 600°-875°C, $\Delta H_{BC} = 41{,}200$ cal/mole; 875°-1050°C, $\Delta H_{AB} = 68{,}300$ cal/mole.

This agreement of oxidation data obtained below 900°C and the diffusion data of Moore obtained above 1000°C suggests that deviations observed at 950°C and higher are due to a transition in the kinetics of the oxidation reaction. The transition in the kinetics was probably due to local loss of adhesion at the metal-oxide interface with a subsequent interruption of normal diffusion processes.

Conclusions

From experimental observations on (*a*) the color of the oxide film, (*b*) the cracking of the oxides on cooling, and (*c*) the deviations from the parabolic rate law it is concluded that the failure of nickel oxide in high temperature protective oxidation is due to a localized loss of adhesion at the interface between the oxide and metal. This failure occurs for this grade of nickel at about 900°C, at which temperature the parabolic rate law constant has a value of 1.88×10^{-11} $(g/cm^2)^2/sec$ and a film thickness value of 400-600 μ g/cm^2.

The failure of the oxide-metal adhesion may be related to one of several factors. (*A*) Stress may exist at the interface due to a mismatching of the nickel and nickel oxide lattice, which leads to failure as the oxide grows to a thick film. (*B*) Oxygen may dissolve in the nickel. This process could lead to small changes in the physical and chemical properties of the oxide-metal interface which could cause failure. (*C*) Since oxidation results from a diffusion of nickel through the oxide, the oxide must continuously collapse onto the metal as nickel diffuses from the oxide-metal interface. This process will not occur uniformly due to the different reaction rates on the several crystal orientations of the metal grains. Thus, cohesion between the oxide crystals and cohesion between the alloy and oxide would be diminished.

Manuscript received December 5, 1956. This paper was prepared for delivery before the Washington Meeting, May 12-16, 1957.

Any discussion of this paper will appear in a Discussion Section to be published in the June 1958 JOURNAL.

REFERENCES

1. E. A. Gulbransen and K. F. Andrew, *This Journal*, **101**, 128 (1954).
2. W. J. Moore, *J. Chem. Phys.*, **19**, 255 (1951).
3. M. T. Shim and W. J. Moore, *J. Chem. Phys.*, In press.
4. E. A. Gulbransen and K. F. Andrew, To be published.
5. E. A. Gulbransen, *Trans. Electrochem. Soc.*, **81**, 187 (1942).
6. E. A. Gulbransen and K. F. Andrew, *Trans. Am. Inst. Mining Met. Engrs.*, **185**, 515 (1949).
7. J. Bénard, *Ind. Chim. Belge*, **17**, 553 (1952).
8. D. P. Bogatskii, *Zhur. Olishchei Khim (J. Gen. Chem.)*, **21**, 3 (1951).
9. G. Zima, Private communication.

Impedance at Polarized Platinum Electrodes in Various Electrolytes

James N. Sarmousakis and Manfred J. Prager

William H. Nichols Chemical Laboratory, New York University, New York, New York

ABSTRACT

The results of alternating current bridge measurements of the impedances of bright Pt in contact with 1*N* aqueous solutions of KCl, KBr, and KI as functions of polarizing voltage and alternating current frequency are presented. The data may be interpreted in a manner similar to that for experiments with acid solutions. Various factors are discussed which may determine the dependence of the impedance on frequency for the electric double layer at rough surfaces.

The alternating current impedance of a polarized electrode immersed in an electrolyte can give much information (1-4) concerning conditions existing and processes occurring at or near the metal-electrolyte interface. Recent studies of this electrical property for bright Pt have been carried out by Ershler and his co-workers (5, 6) and by Schuldiner (7, 8) primarily from the kinetic point of view, while the work of Robertson (9), Wilburn (10), and Kheifets and Krasikov (11) on the same subject has been concerned mainly with the states of metal-solution systems at equilibrium. However, no systematic, comparative investigation has been reported as yet having to deal with bright Pt dipped in aqueous solutions of a number of halides of the same alkali metal. Accordingly the authors, employing an impedance bridge method, have determined the impedances of bright Pt in contact with 1*N* aqueous solutions of KCl, KBr, and KI to small alternating currents passing through the metal polarized at various direct potentials, as a function of the polarizing voltage and the frequency of the alternating current.

Experimental

The apparatus and procedures used for the measurements were essentially those of Robertson (9) with some modifications.

The glass assembly, Fig. 1, consisted of a Pyrex cell *A* attached to an evacuating assembly, *J* and *M*,

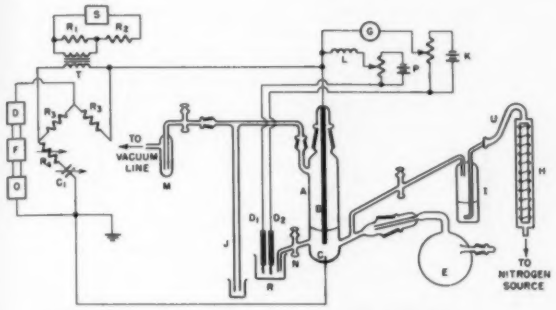

Fig. 1. Diagram of an apparatus for the determination of the impedance of a Pt microelectrode at fixed polarizing voltage. S, oscillator; D, amplifier; F, filters; O, oscilloscope; T, bridge transformer; R_1, 10 ohms; R_2, 10,000 ohms; R_3, 1000 ohms; G, galvanometer; R_4, 11111.1 ohms in steps of 0.01 ohm; C_1, 1.111 μf in steps of 0.0001 μf; A, cell; B, microelectrode; C, counterelectrode; D_1, D_2, reference electrodes; E, 500 ml flask; H, copper furnace; I gas wash bottle; J, mercury manometer; M, dry ice-acetone trap; N, ungreased stopcock; R, 50 ml beaker; U, Tygon connection; L, 62 Henry inductance; K, type K-2 potentiometer; P, Student's potentiometer.

and to a storage flask *E* in which the electrolyte could be degassed and then saturated with nitrogen entering from a train made up of a hot-copper furnace *H* and a saturator *I*. The electrolyte could then be transferred from flask *E* to cell *A* by a simple rotation, without coming into contact with grease. Contact between the electrolyte in the cell and the electrode vessel *R* was made through the closed ungreased stopcock *N*. Only the stopcocks leading to the dry-ice trap *M* and from the saturator *I* and the ground-glass joint from flask *E* to cell *A* were greased, the lubricant being Apiezon M grease.

There were two electrodes in cell *A*, the microelectrode *B* and the counter electrode *C*. The microelectrode *B* was made by sealing a length of Pt wire into a soft glass capillary tube so that only a cross section of the wire was exposed at the end of the capillary. The exposed end of the wire was then polished with successively finer grades of emery paper down to grade 0000 and finally on a metallurgist's wheel with a microcloth using first fine alumina and then Linde Air Products Type B-5125 Fine Abrasive. Measurement of a photomicrograph, made with a metallurgical microscope, gave the apparent area of the polished cross section of the Pt.

The counter electrode *C* was of much larger area than that of *B* so that its impedance compared with that of *B* was negligible. It was prepared by coating the bottom of the Pyrex cell, into which a Pt wire lead had been loosely sealed, with Liquid Bright Platinum No. 05.[1] After having been fired with a Tirrill burner flame, the mirror formed was plated (12) with a layer of Pt black. The seal through which the wire lead passed was made tight by the Pt deposited.

D_1 and D_2 in Fig. 1 were normal silver-silver halide reference electrodes. Ag-AgCl and Ag-AgBr electrodes were prepared according to the method of Harned (13), Ag-Ag I electrodes by the method of Owen (14). These electrodes were constantly checked, the chloride electrodes against calomel electrodes (15), the bromide and iodide electrodes by intercomparison of three electrodes of each type with each other.

The polarizing potential was applied across electrodes *B* and D_1 by means of a L&N Student's potentiometer *P* and measured across *B* and D_2 by means of a L&N Type K-2 potentiometer through a sensitive galvanometer *G*.

Electrodes *B* and *C* of cell *A* formed the unknown arm of a series-resistance bridge with equal ratio arms. The bridge was of the completely shielded type, cell *A* being the only component unshielded. The equal ratio arms were constructed as a Campbell-Shackleton unit (16). On measurement of L&N Type 106 mica capacitors in series with various values of resistance, it was found that the accuracy of the bridge was better than 1% and was independent of frequency.

The bridge was activated at a level of 2 mv by an oscillator *S* through a potential divider and an isolation transformer *T* with shield ungrounded. The detector circuit consisted of a high gain amplifier *D* tuned by means of a Wien bridge feedback circuit, of bridged-T line frequency filters *F*, and of an oscilloscope *O*.

The Pt was by report 99.5% pure.[2] All salts were reagent grade at least once recrystallized. Solutions were prepared from water obtained as a middle fraction on distillation of a solution of $KMnO_4$ in distilled water after long refluxing. N_2 was passed over Cu at 450°-500°C to remove oxygen.

An experiment began with the cleaning of the apparatus. The cell *A* and flask *E*, kept in concentrated HNO_3, were rinsed with water and then steamed for at least 1 hr over alkaline permanganate solution. The microelectrode, kept in distilled water, was immersed in warm concentrated HNO_3 for 5 min and then washed with water. The apparatus was assembled after the appropriate solution was poured into flask *E*. The system was then flushed with N_2 for ½ hr and evacuated for 2 hr with an oil pump to remove dissolved gases. N_2 was reintroduced to bring the system to atmospheric pressure. Solution was then transferred to the measuring cell from the flask. The reference electrodes were assembled to the apparatus and checked.

To remove trace impurities from the surface of the Pt electrode the procedure described by Robertson (9) was used. The Pt electrodes in contact with the KCl, KBr, and KI solutions were polarized repeatedly over the voltage ranges −0.6 to 1.0, −0.4 to 0.85, and −0.2 to 0.55, and back, respectively, the voltages given being referred to the corresponding silver-silver halide electrodes. This process was terminated when the capacity of the electrode, measured at a given desired potential, reached a permanent maximum value.

After the potential of the electrode was set at a given value, readings on the bridge were made every five min. The capacity generally decreased with time, at first rapidly, and then more slowly. A final reading was taken when its value was different

[1] Made by the Hanovia Chemical and Manufacturing Co., 100 Chestnut St., Newark, N. J.

[2] Supplied by the American Platinum Works, 231 New Jersey Railroad Ave., Newark, N. J.

by less than one-half of one per cent from the previous reading. This usually meant a change of no more than 0.0001 μf in capacity in 5 min. These values of capacity and those corresponding of resistance are discussed in the next sections.

The experiments were carried out at room temperature which varied from 24° to 31°C during the period of the investigation.

Experimental Results

When the equal-arm impedance bridge was brought to balance, the capacity and resistance in series in the standard arm were electrically equivalent to the microelectrode as a circuit component at the given frequency and polarizing voltage.

Capacity as a function of polarizing voltage.—In Fig. 2 are represented all the experimental values of the capacities, measured at a frequency of 980 cps, for a single microelectrode immersed in 1*N* KBr and in 1*N* KI solutions as a function of polarizing potential. The polarizing potentials are referred to the normal Ag-AgCl electrode as standard. In calculating these values of potential it was assumed, on the basis of computations employing the Lewis and Sargent equation (17), that the liquid junction potentials between the potassium halides were negligible (less than 0.01 v). The capacities are given in microfarads per square centimeter as calculated from the bridge readings and the area[3,4] of the electrode, 1.42×10^{-5} cm^2.

The curves are similar in form to those of Dolin and Ershler[5] for 1*N* solutions of HCl and H_2SO_4, and for 0.03*N* and 0.2*N* solutions of HCl 1*N* in KBr. In particular, the curves in Fig. 2 show a maximum at cathodic potentials near that for the reversible evolution of H_2 at unit activity. This maximum is followed by a decrease to a flat minimum at intermediate potentials. The minimum is followed by a sharp rise in capacity in the anodic region at potentials not far away from those at which the halogens would be evolved reversibly at unit activity. The sharp rise in capacity at highly anodic potentials has been followed in detail by Robertson (9) for 1*N* HCl. The minimum capacity for both salts appears to be about 18 μf/cm^2 to be compared with 19 μf/cm^2 for 1*N* HCl as found by Robertson (9).

Capacity as a function of frequency.—In Fig. 3 are represented the capactities in microfarads per square centimeter of the microelectrode as a function of the reciprocal of the square root of the frequency of the alternating current used in the measurement, at various polarizing voltages as indicated.

[3] Measurements of the capacity of this microelectrode, with KI as electrolyte, at the beginning and end of the work, had a maximum dispersion of 5%, indicating no change in effective area of the electrode surface within experimental error.

[4] Values of capacity per unit area were measured at nine different polarizing potentials for this electrode and for another of area, 2.05×10^{-5} cm^2 immersed in 1*N* KCl. The average of the various ratios of difference in capacity of the two electrodes to average capacity was approximately 7%. The data are not given in detail since the capacities were varying with time at a rate greater than one half of one per cent per five minutes.

[5] The bridge used by Dolin and Ershler in measuring impedance had a standard arm containing a capacitor and resistance in parallel. The values of capacity and resistance in series as used in this investigation may be converted by calculation with standard formulas to values in a parallel combination like that of Dolin and Ershler. The magnitudes of capacity in series and that in parallel differ from about 5% to about 12%. The shape of the curve in Fig. 2 would not be changed significantly by the transformation.

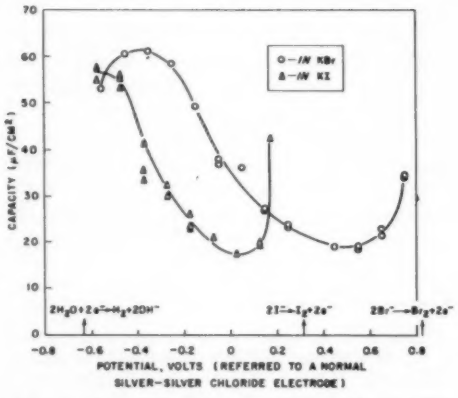

Fig. 2. Dependence on the polarizing potential, referred to a 1*N* Ag-AgCl electrode, of the capacity, measured at 980 cps, of a Pt electrode immersed in 1*N* KBr and 1*N* KI solutions.

At least 60% of the points at each potential represent averages of at least two independent measurements. However most of the points referring to KBr and polarizing potential, −0.55 v, and to KI and polarizing potential, 0.03 v, refer to the results of single measurements.

The reproducibility of the data used for Fig. 3 was no worse than that indicated by the scatter of the points in Fig. 2. It may then be presumed that the absorption of trace impurities does not play a very significant role in determining the frequency dependences as shown by the graphs. Inspection of the curves makes it appear possible that there is a

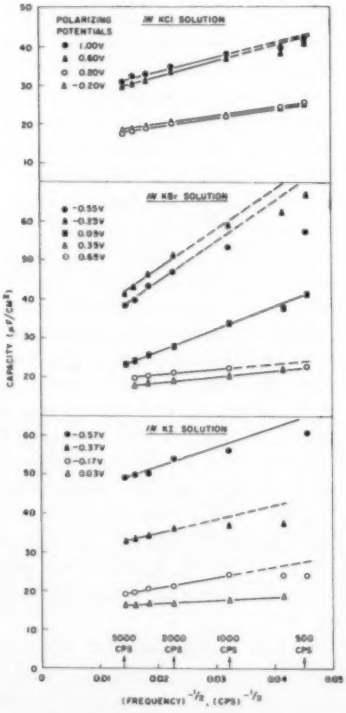

Fig. 3. Dependence on the frequency of the measuring alternating current, of the capacity of a Pt electrode immersed in aqueous 1*N* KCl, KBr, and KI solutions at various polarizing potentials referred to a 1*N* Ag-AgCl electrode.

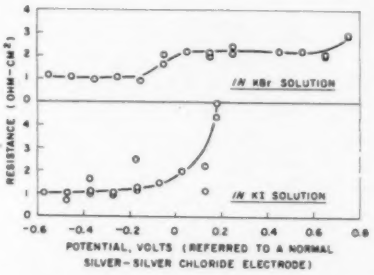
RESISTANCE (OHM-CM²)
1N KBr SOLUTION
1N KI SOLUTION
POTENTIAL, VOLTS (REFERRED TO A NORMAL SILVER-SILVER CHLORIDE ELECTRODE)

Fig. 4. Dependence on the polarizing voltage referred to a 1*N* Ag-AgCl electrode, of the resistance, measured at 980 cps, of a Pt electrode immersed in 1*N* KBr and KI solutions.

linear dependence of capacities on the reciprocal of the square root of the frequency at higher frequencies. At lower frequencies there is a tendency for the points to fall below the lines drawn through the points at higher frequencies. This trend, if continued, would lead to the maxima of capacity at lower frequencies found by Robertson (9).

Increase of frequency by a factor of ten from 480 cps produces an increase of about 35-45% for 1*N* KCl and of about 15-25% for 1*N* KI. The percentage increases for each of the two salt solutions are the same, within the experimental scatter, at all polarizing potentials studied. For 1*N* KBr, the corresponding increases are approximately 20% for the two most positive polarizing potentials and about 60-80% for the other potentials. This variation of the fractional increases in capacity, as potential varies, lies outside the experimental scatter of the measurements, and gives rise to an apparent anomaly in the results for the bromide solution for which no explanation can at present be offered.

Resistance.—Resistance measurements by the procedure described are highly irreproducible. The extent to which this statement is true may be seen in Fig. 4 in which are shown the apparent series resistances plotted as functions of the potential of

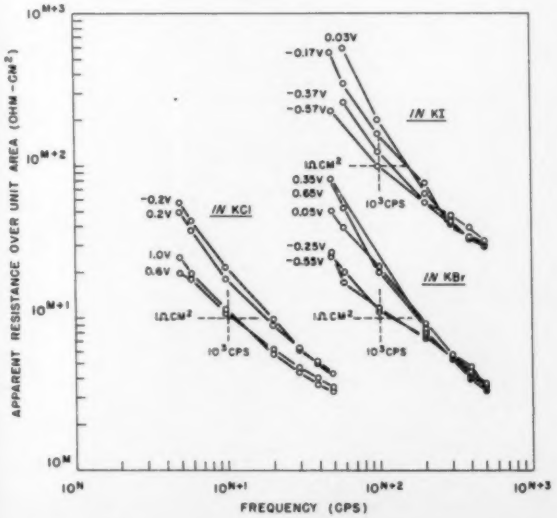

Fig. 5. Dependence on frequency of the apparent resistance of a Pt electrode immersed in 1*N* KCl, KBr, and KI solutions and for various polarizing potentials referred to a 1*N* Ag-AgCl electrode.

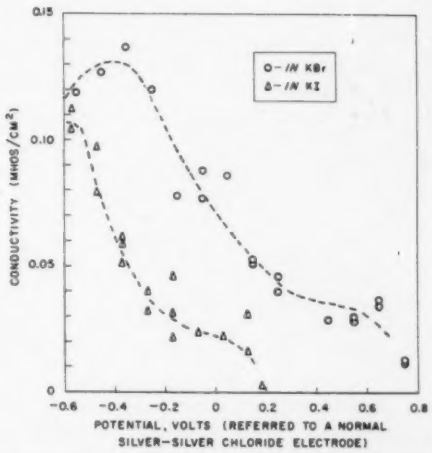

Fig. 6. Dependence on the polarizing potential referred to a 1*N* Ag-AgCl electrode, of the conductivity, in parallel with capacity, of a Pt electrode immersed in 1*N* KBr and 1*N* KI solutions. Measurements at 980 cps.

the microelectrode. These resistances in series with the capacities of Fig. 2 are equivalent to the microelectrode as electric circuit elements. Resistances are low at cathodic potentials and high at anodic potentials.

As already pointed out by Dolin and Ershler (6), Robertson (9), and Grahame (2) for systems involving solid electrodes which they studied, the series resistance is large at low frequencies and decreases very rapidly with increase of frequency for all the salts and at all potentials. Broken line graphs are drawn on a logarithmic scale in Fig. 5 to represent the resistance-area products in ohm cm² corresponding to the capacities shown in Fig. 3. The crossed dashed lines serve to indicate the values of the powers of ten, M and N, for the groups of curves closest to them, each of which corresponds to a different electrolyte as shown. The apparent resistance appears to be roughly inversely proportional to the first power of the frequency, the power being greater than one at low frequencies and less than one at higher frequencies.

The similarity in behavior, illustrated in Fig. 2, of the series capacity, as the polarizing potential changes, to that of the parallel capacity determined by Dolin and Ershler for their systems has already been noted. When the data for series capacity and resistance are used to calculate the equivalent combination of capacity and resistance in parallel and the reciprocal of resistance (conductivity) obtained therefrom, it is found that the resulting values of conductivity also change with polarizing potential in much the same way as do the corresponding quantities determined by Dolin and Ershler (*see* Fig. 6).

Discussion

The variables which may be considered to determine the combination of capacity and resistance equivalent to the microelectrode as an electrical circuit component are (*a*) type of electrolyte, (*b*) polarizing potential, (*c*) frequency, (*d*) roughness and nonhomogeneity of the electrode surface, (*e*)

shape of the electrode and its symmetry, and (*f*) presence of trace impurities at the surface.

The shape factor may be considered as not important on the presumption that the Pt electrode used in this work behaved much like those of Robertson (9) whose results indicate a similar behavior of plane and spherical electrodes with similar dependence of capacity on frequency at a given potential in 1*N* HCl. Further, considering the degree of reproducibility of the values of the capacity as shown in Fig. 2, the adsorption of trace impurities is probably not a significant factor.

As has already been pointed out for Fig. 2 and 4 the capacities and conductivities vary with polarizing potential in much the same manner as has been reported by Dolin and Ershler (6) with maxima at cathodic potentials and minima at intermediate potentials. In addition there is the sharp increase in capacity at anodic potentials which appeared in one experiment by Dolin and Ershler (6) and was followed in detail by Robertson (9) for 1*N* HCl at polarizing potentials close to that for the reversible evolution of Cl_2 at unit activity. There appears no reason to interpret the data in a way other than that of Dolin and Ershler. At cathodic potentials the discharge of hydrogen ion and reduction of water and adsorption of hydrogen together with production of hydroxyl ion give rise to a high capacity. At intermediate potentials where no reaction should be occurring, the electric double layer at the metal-solution interface should be the most important determining factor. At anodic potentials the sharp rise in capacity may be associated with a "pseudo-capacity" such as that described by Grahame (18) as occurring at the reversible potential of an electrode reaction. In this case the reversible potential should be that of the discharge of iodide and bromide ions.

The values of the potentials of the minima in capacity for the KBr and KI solutions are probably determined mainly by the rise in capacity due to reversible reaction commencing, so that they cannot be expected to have significance with respect to the structure of the double layer.

For the clean, smooth, and symmetrical surfaces presented by freshly formed mercury drops, there is no dependence on frequency of the measured capacities and resistances, which last are made up only of the bulk-electrolyte and lead resistances as components (19). It has further been shown experimentally that the variation of capacity with frequency for Tl, Cd, and Pb electrodes is much decreased by melting the electrode to form a smooth surface (20). If shape effects and the adsorption of trace impurities are to be assumed as not important in determining the variation with frequency of the capacity of the Pt electrode in contact with alkali halide solutions at potentials where no reaction can be occurring, then it may be presumed, as has already been emphasized by Grahame (1,2), that roughness is still an important factor even with the type of polishing previously described.

Any theory which is formulated to relate roughness to the frequency dependence of the measured impedance must be capable of explaining both the relatively small dispersion of the capacity and the much larger dispersion of series resistance of the electrode. For example, one might consider that, as the electric potential alternates during a measurement, the surface concentrations of ions in the hollows of the rough surface would oscillate, causing the hollows to become sources and sinks of ions moving out to and in from the bulk of the solution. The ease with which transfer by diffusion and migration would remove and supply these ions would then be frequency dependent. However, it would require an extensive mathematical procedure to determine whether this explanation would account for the differences in dispersion of the capacities and resistances just mentioned. Experimental work on surfaces of known roughness is desirable, together with theoretical analysis, before circuit components equivalent to the electrode can be set up unambiguously.

As has been pointed out by Grahame (1), double layer capacities for solid surfaces can be obtained by measurements at very high frequencies. The linear dependence of capacity on the square root of frequency which seems to be exhibited by the graphs of Fig. 3, especially for those curves involving small capacities, and corresponding to polarizing potentials in the double layer region, if continued to higher frequencies, may provide a means for carrying out extrapolations to infinite frequency.

Acknowledgment

The authors wish tc express their appreciation to the College Relations Department of the Western Electric Co. for donating equipment and arranging the provision of the facilities of the Bell Telephone Laboratories, Murray Hill, N. J., to calibrate the standard condenser. Acknowledgment is also made to Dr. Remsen T. Schenck for providing the design of the tuned amplifier, and to Dr. John Nielsen, of the Department of Metallurgical Engineering of New York University, for providing facilities for the polishing of the electrodes.

Manuscript received May 31, 1956. This paper was prepared for delivery before the Washington Meeting, May 12-16, 1957.

Any discussion of this paper will appear in a Discussion Section to be published in the June 1958 JOURNAL.

REFERENCES

1. D. C. Grahame, *This Journal*, **99**, 370C (1952).
2. D. C. Grahame, *Ann. Rev. Phys. Chem.*, **6**, 337 (1955).
3. J. O'M. Bockris, "Modern Aspects of Electrochemistry," pp. 103 to 276, Academic Press, Inc., New York (1954).
4. H. Gerischer, *Z. Elektrochem.*, **59**, 604 (1955).
5. B. Ershler, *Acta Physicochim. U.R.S.S.*, **7**, 327 (1937).
6. P. Dolin and B. Ershler, *ibid.*, **13**, 747 (1940).
7. S. Schuldiner, *This Journal*, **99**, 488 (1952).
8. S. Schuldiner, *ibid.*, **101**, 426 (1954).
9. W. D. Robertson, *ibid.*, **100**, 194 (1953).
10. R. L. Wilburn, *Univ. Microfilms, Publ. No.* 10,019; *Dissertation Abstr.*, **14**, 1943 (1954).
11. V. L. Kheifets and B. S. Krasikov, *Doklady Akad. Nauk. S.S.S.R.*, **94**, 101 (1954).
12. A. Weissberger, "Physical Methods of Organic Chemistry," 2nd ed., Vol. I, Part II, p. 1722, Interscience Publishers, New York (1949).
13. H. S. Harned, *J. Am. Chem. Soc.*, **51**, 416 (1929).
14. B. B. Owen, *ibid.*, **57**, 526 (1935).

15. I. M. Kolthoff and N. H. Furman, "Potentiometric Titrations," 2nd ed., p. 79, John Wiley & Sons, Inc., New York (1931).
16. L. Behr and A. Williams, *Proc. Inst. Radio Engrs.*, **20**, 969 (1932); T. Shedlovsky, *J. Am. Chem. Soc.*, **52**, 1793 (1930).
17. G. N. Lewis and L. W. Sargent, *J. Am. Chem. Soc.*, **31**, 363 (1909).
18. D. C. Grahame, *Chem. Rev.*, **41**, 441 (1947).
19. D. C. Grahame, *J. Am. Chem. Soc.*, **68**, 301 (1946).
20. T. Borisova and B. Ershler, *Zhur. Fiz. Chim.*, **24**, 337 (1950).

Technical Note

Electrodeposition of Lead from the Pyrophosphate Bath

J. Vaid and T. L. Rama Char

Department of General Chemistry, Indian Institute of Science, Bangalore, India

Lead is commonly plated from the fluosilicate, fluoborate, and sulfamate baths. Belyaer (1) used an alkaline bath containing lead acetate, sodium hydroxide, rochelle salt, rosin, and gelatin. Ferguson and Hovey (2) state that a solution containing sodium pyrophosphate, copper acetate, and lead acetate showed little promise for Cu-Pb alloy plating. This laboratory has undertaken a detailed investigation on the electrodeposition of various metals and alloys from the pyrophosphate bath. The plating of Pb was studied mainly in connection with work on Pb-Sn alloy deposition.

Experimental

Plating solutions were prepared by addition of sodium pyrophosphate to lead nitrate, a complex, $Na_2[Pb(P_2O_7)]$, being formed. Potentiometric and conductometric titrations showed that the ratio of pyrophosphate to Pb in the complex is 1:1. The Pb ion concentration in the solution and the instability constant K of the complex as found from potential measurements were of the order of 10^{-12} g ion/l and 10^{-13}, respectively (3). Rogers and Reynolds (4) reported a value of the same order for K of the 1:1 complex, whereas Halder (5) has stated that there are two complexes corresponding to 1:1 and 2:1 ratios, K for the latter being 10^{-6}. The pyrophosphate content of the bath was always in excess of that required for complex formation. The bath control did not present any difficulties.

Cylindrical Cu-plated Pt cathodes (diameter 5/8 in., length 1½ in.) and Pb anodes (diameter 1⅝ in., length 1 in.) were used, the immersed anode area being four times the cathode area (3 in.²). Plating time was 20-30 min; volume of solution used was 175 cc. The rest of the experimental procedure was the same as described before (6). Cathode potentials (hydrogen scale) were reproducible to ±5 mv. Photomicrographs of a thick coating of Pb on Cu plate were taken with a Vicker's projection microscope. X-ray powder patterns of the deposits were obtained from a Siemans Baujahr 1950 model unit, with a 57.3 mm diameter camera.

Experimental Results

Table I gives the effect of variation of electrolyte concentration and current density on the cathode efficiency and potential. Data recorded correspond to good quality deposits. The decomposition potential for the plating solution was 1.6-1.7 v.

Cathode efficiency was 90-100% throughout. Gelatin decreased the efficiency as well as the limiting current density (48-29 amp/ft²). A solution containing 0.05M $Pb(NO_3)_2$ could be regarded as optimum. The specific resistivity and cathode polarization decreased with increase in metal ion concentration. The increase in polarization with the addition of gelatin has also been observed in Sn deposition from the pyrophosphate bath (6). The throwing power of the solution was quite good, the

Table I. 1200 rpm cathode, 60°C, 0.2-1.1 v, pH 9.5, anode efficiency, close to 100%. For each concentration the first figure under current density gives the efficiency per cent and the second the cathode potential (— sign) in volts on H scale. Static potential, —0.45 v; reference electrode, saturated calomel

	Concentration, g/l		Sp. resistivity, ohm/cm³	Current density amp/ft²					
	Lead	Pyrophosphate		5	10	19	29	38	48
1.	2.1	7.0	55.1	93	94	89	88	—	—
				0.70	0.70	1.24	—	—	—
2.	5.2	17.5	29.2	92	95	97	92	90	—
				0.59	0.68	0.93	—	—	—
3.	10.4	35.0	15.9	95	96	99	98	94	93
				0.57	0.59	0.71	1.10	1.20	—
	10.4	35.0							
	(+ gelatin 0.5 g/l)		15.9	87	87	80	59	—	—
				0.59	1.37	1.64	1.74	—	—
4.	15.5	52.0	11.8	95	96	100	100	100	96
				0.56	0.57	0.66	0.74	1.03	—
5.	20.7	70.0	9.5	95	99	100	100	100	96
				0.54	0.57	0.65	0.73	0.93	1.06

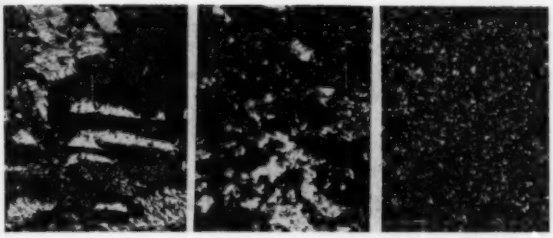

Fig. 1. (Left) Cu base; (center) Pb deposit under conditions of Table I-3, 19 amp/ft^2; (right) same with gelatin. Magnification, 500X before reduction for publication.

Schlotter-Korpiun value (7) being in the range 1.7-4.7.

The bath gave adherent and grayish-white deposits on Cu (steel or brass) cathodes. The deposit became finer grained and bright (matte) by adding gelatin (Fig. 1). It has a face centered cubic structure, with a = 4.93Å. The deposits (0.001 in.) were nonporous as indicated by the ferroxyl test (steel base), and the corrosion resistance was good in the laboratory atmosphere (0.001 in., 4 months). The time required to deposit 0.001 in. thickness at 25 amp/ft^2 was 18 min.

The performance of the pyrophosphate bath for Pb plating appears to be satisfactory. The deposition of Pb-Sn alloys from this bath will be reported later.

Acknowledgment

The author's thanks are due to K. R. Krishnaswami, Head of the Department, for his keen interest in the work. One of the authors (J. Vaid) is grateful to the Government of India for the award of a Senior Research Scholarship during the period of this investigation.

Manuscript received August 6, 1956.

Any discussion of this paper will appear in a Discussion Section to be published in the June 1958 JOURNAL.

REFERENCES

1. P. Belyaer, *Chem. Abs.*, **36**, 4031 (1942); *Korroziya i Borba s Nei*, **6**, [2], 15 (1940).
2. A. L. Ferguson and N. W. Hovey, *This Journal*, **98**, 146, (1951).
3. J. Vaid and T. L. Rama Char, *Proc. 41st Indian Science Congress*, Part 3, 86 (1954).
4. L. B. Rogers and C. A. Reynolds, *J. Am. Chem. Soc.*, **71**, 2081 (1949).
5. B. C. Halder, *Current Science*, **19**, 244 (1950).
6. J. Vaid and T. L. Rama Char, *This Journal*, 104,282 (1957).
7. M. Schlötter and J. Korpiun, *Trans. Electrochem. Soc.*, **62**, 129 (1932).

Technical Review

A Review of Patents on Silicon Carbide Furnacing

J. C. McMullen

Research and Development Division, The Carborundum Company, Niagara Falls, New York

The value of a good abrasive was brought to Edward Goodrich Achesons's attention by one of the members of Tiffany and Company. Remembering one of his early experiments in which clay, when heated in a gas-fired furnace, was converted to a hard, carbon-impregnated substance he decided to subject clay and carbon to the influence of electric heat. A small iron bowl was attached to one lead from a dynamo and filled with a mixture of clay and powdered coke. A carbon rod attached to the other lead was inserted. Current was passed through the mixture until the center was heated to a very high temperature. An examination of the cold mass revealed a few bright specks on the end of the carbon rod. When drawn across a pane of glass the rod tip cut like a diamond. The new material, he thought, was composed of carbon and corundum.

Acheson soon modified the furnace by constructing a horizontal one with firebrick walls. Between two electrodes he placed a conducting core of loose graphite surrounded by a mixture of clay, carbon, and salt. The first patent relating to SiC was issued to him in 1893 (1). It details the method of manufacture and correctly describes the product as SiC. While there have been improvements in furnacing and in mix proportions, the principles as developed by Acheson are still in use today in the commercial production of SiC.

To keep this review within bounds, only those United States patents which show marked changes over the original patent, at least in the writer's opinion, will be discussed. A complete list, comprising 59 of the subject patents reviewed, is given in the appendix. An attempt is made to arrange the subject matter in groups rather than chronologically.

Resistance Furnaces

In the original patent, a mix composed of 50% pure carbon, 25% clay, and 25% common salt was used. The salt was deemed necessary to act as a flux which on melting brought the particles of clay and carbon in intimate contact. The use of salt is mentioned frequently throughout the patent literature on SiC. Kirchner (48) described the action of salt as follows: "The salt tends to reduce the impurities in the resultant product, since it reacts at high temperatures with impurities containing iron and some other elements to form volatile chlorides."

In Acheson's second patent (2) issued in 1896, the clay is replaced by silica. Carbon is used in stoichiometric proportions rather than in excess as stated in the original patent. A generous amount of salt, 9%, is still added as a flux. Also 4% of sawdust was added to promote permeability to the mix.

F. J. Tone was issued 17 patents from 1902 to 1913. Two patents (9, 11) describe a furnace with movable sidewalls. These walls were made in sections composed of iron frames lined with firebrick. This eliminated repeated handling of individual bricks used in assembling the SiC furnace.

According to the accepted equation for the formation of silicon carbide ($SiO_2 + 3C = SiC + 2CO$), 1.4 tons of CO gas is generated for each ton of SiC produced. The heat value, on combustion, of this CO is equivalent to 3560 kwhr and, since 8000-12,000 kwhr is required to produce a ton of SiC in commercial furnaces, the recovery of the waste gas offers one method of reducing manufacturing costs.

Tone's patent (13) in 1908 described a furnace heated by a combination of electric power and combustion of gases generated during the operation. However, during one experiment an explosion occurred and further work on this method was abandoned.

Tone was granted two patents (16, 24) disclosing the use of a solid carbon core, which would be more consistent in physical properties than a loose core. However, the resistance of a solid rod is so low that either its length has to be greatly increased or its cross section reduced. Tone increased the length by the use of a zig-zag pattern. Since a loose graphite core, surrounded by the conventional sand-coke-sawdust mix, is used today, it indicates that a solid rod is not practical with this type of furnace loading.

In 1909 Tone patented (15) a pot-type furnace for producing SiC. As furnacing proceeds, mix is added, and vertically depending electrodes raised until a complete ingot is formed.

Ridgeway was an important contributor to the art. His patents (45, 47) disclose a radical departure from the conventional furnace method. He reasoned that SiC, since it becomes an excellent electrical conductor when heated, could be used as a core. A jointed graphite rod of small cross section is used to preheat the core composed of SiC-containing furnace by-products. A low voltage is used until the

graphite rod is consumed, and the remainder of the heat is made with increased voltage. It is claimed that the efficiency is improved by making use of the SiC by-products. The entire furnace charge tends to be heated electrically rather than by thermal radiation from a large central core.

Ridgeway also developed a closeable furnace (52, 55) for making abrasive metal carbides. The object here was to minimize losses by oxidation of the product and by volatilization. While the method is advantageous in making boron carbide, it is not particularly applicable for making SiC as losses, except for CO, are negligible.

Improved Product

According to Acheson's patent (22) of 1912, a new product different in appearance and having a toughness and hardness at least equal and perhaps greater than the normal product is formed when 5% boron oxide is incorporated in the furnace mix. Since the resultant SiC was found to be essentially boron-free, he postulated that the unusual properties are due to the modifying influence of the boron during the reaction. This suggests that other additives be tried to determine the effect on the crystal habit of SiC.

Tone's patents (17, 23) in 1910 and 1912 deal with making clear crystals of SiC using pure raw materials. Such crystals, it is claimed, possess double refraction and are of great value as gems, for they can be cut with regular facets and polished.

Hutchins in 1933 (44) described a method of producing a dense SiC, by adding 3% excess carbon to the mix and furnacing with a 30% increase in power rate over that normally used. Lumps of the new material, it is claimed, have an apparent density of 2.6 or greater while the ordinary variety is usually less than 1.8 g/cc. SiC made by the process is said to consist of densely compacted masses having a structure very similar to that of a material solidified from a molten state. It is also claimed that the dense material has a more uniform and also a lower electrical resistance than that of normaliy furnaced crystalline material.

Furnace Mix

A patent by Hutchins (34) in 1920 pertains to the more uniform production of SiC. During furnace operations the highly heated vapors of silicon and silica tend to rise through the charge. This results in a concentration of siliceous compounds in the upper part of the furnace, and a deficiency of these compounds in the lower part. In Hutchins' preferred method the bottom of the furnace is loaded with mix having a SiO_2/C ratio of 1.94 while mix with a 1.70 ratio is used in the top. Since both of these are in excess of the theoretical ratio of 1.67, it indicates that some Si leaves the reaction zone and is either condensed in the outer by-product material or is lost to the atmosphere.

A patent by Kirchner (48) in 1935 is the only one dealing with the pore forming material used to promote permeability in the raw mix. He advocates the use of buckwheat or other seed hulls to replace sawdust, since they are more consistent physically and chemically and allow better control of the furnace mix.

Use of Silicon Compounds

Four patents cover the use of materials other than free silica or silicon, with carbon, to form SiC.

Dorseman (5) in 1902 heated $ZnSiO_3$ and C in a closed arc furnace to produce metallic Zn and SiC. Zn vapors are condensed to a liquid and the CO is vented. The removal of the SiC from the closed furnace is not clearly described but it appears that this would present quite a problem.

Weber (8) in 1903 described a process for the manufacture of alumina and SiC from kaolin. Calcined clay and coke, both finely ground, are heated electrically forming a mixture of Al_4C_3 and SiC. In water, the former hydrolyzes and the inert SiC crystals settle out.

Thoms (25) in 1912 found a method of making a SiC in filament form as follows ". . . . admitting to an evacuating flashing jar a predetermined amount of the vapors of silicon tetrachloride, then a predetermined amount of a mixture of hydrogen and ethylene gases and then in flashing a carbon core in such atmosphere."

Peacock (30, 31) in 1915 heated feldspar and C to 2500°C in a N atmosphere to form carbo-nitrides of Al and K. After these gaseous products are collected, the temperature is raised to a purported 3500°C to form SiC.

Shaped Articles

Twelve patents relate to furnacing of definitely shaped articles of SiC. In most cases, the resistance-type furnace was used as a medium for heat-forming articles of SiC from preshaped carbon, wood, fine silicon carbide, or mixtures of silicon or various silicon compounds with C (4, 10, 14, 19, 20, 21, 27, and 28). In two patents (26, 46) articles are converted to SiC by an arc. In one case (42) the reaction is carried out in an induction furnace.

Geiger (58) in 1947 was successful in forming SiC at relatively low temperatures from an intimate mixture of finely divided C and Si previously molded to a desired shape. By maintaining non-oxidizing conditions the reaction was completed between 1200° and 1500°C in a fuel-fired furnace.

Continuous Furnaces

There have been numerous attempts to produce SiC continuously. The advantages of such a process might include a saving in labor and power through recuperation of waste heat, collection and use of the CO gas, as well as a saving in operating space required. However, there are many difficulties to be overcome due to the high temperatures involved, the lack of free flow of the materials and product, and the abrasive action of the moving materials.

Roberts (3) in 1897 patented a process using a modified arc furnace. A horizontal column of mix is fed by a mechanical conveyor between carbon electrodes. The electrodes are first positioned so as to strike an arc, then gradually separated as the SiC is formed and becomes the conductor. A ribbon of product emerges and there remains the problem of separating the SiC and the unconverted mix.

Tone (18) in 1910 illustrates two methods of making SiC continuously. In the first case granular core material is supplied at and around an upper electrode and is surrounded by the mix of carbon and siliceous material. The containing walls move downward, carrying with them the charge and core, at a rate governed by the ingot diameter representing most economical production. The lower electrode is tapered so that the core material and finished product move outward and may be removed readily from the furnace.

In Tone's alternate scheme, the mix, supported on cars, is moved continuously under two stationary vertically depending electrodes. After the charge passes the second electrode, the products are removed. The principal objection is again the difficulty of separating the SiC from the core and the unused mix.

Cox (49, 50) in 1937 patented an up-fed furnace. A screw arrangement pushes mix up through an inverted truncated cone-shaped furnace lined with refractory. Power is supplied through carbon electrodes projecting into the sides of the furnace.

Benner, Melton, and Boyer (56) in 1939 employed an electrically heated tunnel through which refractory trays, loaded with loose or briquetted mix, are passed. The tunnel may consist of a hollow carbonaceous conductor to act as a resistance heater, or may be heated by induction.

Van der Pyl (59) was issued a patent in 1956 covering a process to synthesize SiC. Claim #1 aptly describes the method as follows: "Process for the synthesis of silicon carbide comprising charging a mixture of carbon and silica into a plurality of open ended containers which are of a size and shape to be detachable joined at the open ends, mating a plurality of said containers and introducing them into a tube furnace having the shape of a long tube thereby forming a tube within the tube furnace which tube thereby formed constitutes a single compartment, advancing the containers through the tube furnace and removing the containers which have been advanced all the way through the tube furnace, said tube furnace being at a median location thereof heated to a temperature of at least 1800°C."

The SiC produced in Van der Pyl's furnace consists of discrete crystals which require only classification for use as abrasive grain, thus eliminating crushing operations. Costs are further reduced by the utilization of the waste gases.

Summary

In summary, the art of furnacing SiC has not departed radically from the method originated by Acheson. Today's furnaces are much larger but they still use his principle of heating from within, with the charge acting as a refractory container as well as a thermal insulator for the ingot being formed. Improvements in furnace design have facilitated loading and unloading operations. Large scale collection and utilization of waste gases have not yet been achieved. Changes in core composition and geometry have resulted in a moderate improvement in the over-all efficiency of the operation. Better physical and chemical properties of the product have been attained by controlling mix composition and power input. Several starts have been made toward a continuous commercial process for making SiC.

Manuscript received January 18, 1957. This paper was prepared for delivery before the Cleveland Meeting, Sept. 30 to Oct. 4, 1956.

Any discussion of this paper will appear in a Discussion Section to be published in the June 1958 JOURNAL.

REFERENCES

1. E. G. Acheson, U. S. Pat. 492,767, Feb. 28, 1893. Title: Production of artificial crystalline carbonaceous materials; content: substitute for diamonds.
2. E. G. Acheson, U. S. Pat. 560,291, May 19, 1896. Title: electrical furnace; content: improvement in design of furnace.
3. I. L. Roberts, U. S. Pat. 587,138, July 27, 1897. Title: process of and apparatus for manufacturing metallic carbides; content: continuous furnace.
4. F. J. Tone, U. S. Pat. 709,808, Sept. 23, 1902. Title: Carborundum® articles and process of making same; content: crystallized shapes.
5. A. Dorsemagen, U. S. Pat. 716,008, Dec. 16, 1902. Title: working zinc and substances containing silicic acid in electric furnaces; content: use of zinc silicate as raw material.
6. E. G. Acheson, U. S. Pat. 722,792, March 17, 1903. Title: method of producing compounds containing silicon, oxygen and carbon.
7. E. G. Acheson, U. S. Pat. 723,631, March 24, 1903. Title: method of heating material; content: multiple cores.
8. F. C. Weber, U. S. Pat. 728,528, May 19, 1903. Title: process of treating kaolin for the production of Carborundum® and alumina; content: Al_4C_3 and SiC from clay.
9. F. J. Tone, U. S. Pat. 800,515, Sept. 26, 1905. Title: incandescent electrical furnace; content: furnace with movable sides.
10. F. Bolling, U. S. Pat. 801,296, Oct. 10, 1905. Title: process for the production of molded blocks of SiC; content: SiC shapes made from C.
11. F. J. Tone, U. S. Pat. 834,948, Nov. 6, 1906. Title: electrical furnace; content: movable sidewalls and air-cooled base.
12. H. N. Potter, U. S. Pat. 875,673, Dec. 31, 1907. Title: method of making SiC; content: SiC from SiO and C.
13. F. J. Tone, U. S. Pat. 908,357, Dec. 29, 1908. Title: method of producing SiC; content: use of waste gases.
14. F. J. Tone, U. S. Pat. 913,324, Feb. 23, 1909. Title: manufacture of SiC; content: dense SiC.
15. F. J. Tone, U. S. Pat. 937,119, Oct. 19, 1909. Title: process of producing SiC; content: arc furnacing SiC.
16. F. J. Tone, U. S. Pat. 941,339, Nov. 23, 1909. Title: process of producing SiC; content: zig-zag core.
17. F. J. Tone, U. S. Pat. 949,386, Feb. 15, 1910. Title: method for the production of SiC; content: pure SiC.
18. F. J. Tone, U. S. Pat. 965,142, July 19, 1910. Title: method of making SiC; content: continuous furnace process.
19. F. J. Tone, U. S. Pat. 992,698, May 16, 1911. Title: method for the production of dense compacted SiC; content: dense SiC shapes.
20. F. J. Tone, U. S. Pat. 1,013,700, Jan. 2, 1912. Title: SiC; content: dense SiC shapes.
21. F. J. Tone, U. S. Pat. 1,013,701, Jan. 2, 1912. Title: manufacture of SiC; content: dense SiC shapes.
22. E. G. Acheson, U. S. Pat. 1,014,199, Jan. 9, 1912. Title: refractory body and process of making same content: B_2O_3 in furnace mix.
23. F. J. Tone, U. S. Pat. 1,015,598, Jan. 23, 1912. Title: light refracting material; content: pure SiC.
24. F. J. Tone, U. S. Pat. 1,044,295, Nov. 12, 1912. Title: process for producing SiC; content: zig-zag core.
25. F. C. Thoms, U. S. Pat. 1,048,231, Dec. 24, 1912. Title: method of manufacturing Carborundum® filaments; content: use of $SiCl_4$.

26. F. J. Tone and T. B. Allen, U. S. Pat. 1,054,372, Feb. 25, 1913. Title: process of silicidizing; content: SiC shapes in arc furnace.
27. F. J. Tone, U. S. Pat. 1,054,373, Feb. 25, 1913. Title: method of silicidizing articles containing C; content: SiC shapes in resistance furnace.
28. E. S. Smith and F. J. Tone, U. S. Pat. 1,058,800, April 15, 1913. Title: SiC article and method of making the same; content: porous article from blocks of wood.
29. G. Egly, U. S. Pat. 1,075,634, Oct. 14, 1913. Title: process for production of refractory, electrically conducting molded bodies; content: refractory shape.
30. S. Peacock, U. S. Pat. 1,129,506, Feb. 23, 1915. Title: process of making silicon compounds and by-products; content: use of feldspar.
31. S. Peacock, U. S. Pat. 1,134,081, March 30, 1915. Title: process for producing carbide of silicon and by-products; content: use of feldspar.
32. W. K. Booth, U. S. Pat. 1,299,110, April 1, 1919. Title: electric furnace; content: SiC lining formed *in situ*.
33. F. Jacoviello, U. S. Pat. 1,324,156, Dec. 9, 1919. Title: electric furnace; content: resistance furnace.
34. O. Hutchins, U. S. Pat. 1,331,435, Feb. 17, 1920. Title: manufacture of SiC; content: SiO_2/C ratio in mix.
35. H. E. Schabacker, U. S. 1,381,346, June 14, 1921. Title: SiC and method of making same; content: use of high purity coke.
36. M. O. Sem and E. Lund, U. S. Pat. 1,442,033, Jan. 9, 1923. Title: method of operating electric furnaces; content: self-baking electrode.
37. J. H. Reid, U. S. Pat. 1,445,645, Feb. 20, 1923. Title: process of and material for production of metal hydrate and gas; content: feldspar and bituminous coal.
38. L. Burgess, U. S. Pat. 1,512,271, Oct. 21, 1924. Title: reduction of oxides; content: furnace under pressure.
39. H. E. White, U. S. Pat. 1,660,144, Feb. 21, 1928. Title: process for production of SiC and CaC_2; content: tapping furnace CaC_2 and SiC.
40. T. F. Baily, U. S. Pat. 1,675,744, July 3, 1928. Title: shaft-type electric furnace; content, shaft furnace.
41. H. E. White, U. S. Pat. 1,684,611, Sept. 18, 1928. Title: electric furnace for producing SiC; content: concrete sidewalls and ends for SiC furnace.
42. M. J. Marcin, U. S. Pat. 1,804,361, May 5, 1931. Title: process of treating carbonaceous articles; content: coating articles with SiC.
43. H. E. White, U. S. Pat. 1,859,856, May 24, 1932. Title: process for production of SiC and CaC_2; content: tapping furnace for CaC_2 and SiC.
44. O. Hutchins, U. S. Pat. 1,937,060, Nov. 28, 1933. Title: SiC and the manufacture thereof; content: dense SiC ingot.
45. R. R. Ridgeway, U. S. Pat. 1,979,052, Oct. 30, 1934. Title: electric resistance furnace; content: solid rod.
46. A. L. Mingard, U. S. Pat. 1,982,012, Nov. 27, 1934; Title: process for manufacture of hard objects in silicidized carbon or other similar substances; content: SiC shapes.
47. R. R. Ridgeway, U. S. Pat. 2,005,956, June 25, 1935. Title: method of making abrasive metal carbides and an apparatus therefor; content: solid rod.
48. H. P. Kirchner, U. S. Pat. 2,018,133, Oct. 22, 1935. Title: manufacture of SiC; content: hulls as pore formers.
49. G. C. Cox, U. S. Pat. 2,068,447, Jan. 19, 1937. Title: continuous high temperature electrothermal furnace; content: upfed continuous furnace.
50. G. C. Cox, U. S. Pat. 2,068,448, Jan. 19, 1937. Title: continuous high temperature electrothermal furnace; content: upfed continuous furnace.
51. L. E. Ward, U. S. Pat. 2,122,446, July 5, 1938. Title: manufacture of calcium metal; content: making Ca metal.
52. R. R. Ridgeway, U. S. Pat. 2,123,158, July 5, 1938. Title: electric furnace structure for making abrasive metal carbides; content: closeable furnace.
53. M. Frankl, U. S. Pat. 2,131,102, Sept. 27, 1938. Title: process for operation of smelting and reducing furnaces; content: fuel fired furnace.
54. M. Frankl, U. S. Pat. 2,136,430, Nov. 15, 1938. Title: process for smelting and reduction of minerals; content: fuel fired furnace.
55. R. R. Ridgeway, U. S. Pat. 2,155,682, April 25, 1939. Title: method of making abrasive metal carbides; content: closeable furnace.
56. R. C. Benner, R. L. Melton, and J. A. Boyer, U. S. Pat. 2,178,773, Nov. 7, 1939. Title: SiC and manufacture thereof; content: continuous furnace.
57. R. R. Ridgeway, U. S. Pat. 2,285,837, June 9, 1942. Title: method of producing the abrasive metal carbides; content: deep furnace—arc type.
58. C. F. Geiger, U. S. Pat. 2,431,327, Nov. 25, 1947. Title: refractory and method of making same; content: low temperature, SiC shapes.
59. E. Van der Pyl, U. S. Pat. 2,729,542, Jan. 3, 1956. Title: synthesis of SiC; content: continuous tube furnace.

FUTURE MEETINGS OF
The Electrochemical Society

Buffalo, October 6, 7, 8, 9, and 10, 1957

Headquarters at the Statler Hotel

Sessions will be scheduled on
Batteries, Corrosion, Electrodeposition (symposium on "Metal Powders"),
Electrodeposition—Corrosion (Joint Symposium on
"Corrosion of Electrodeposited Metals"),
Electronics (Semiconductors),
Electro-Organics, and Electrothermics and Metallurgy

* * *

New York, April 27, 28, 29, 30, and May 1, 1958

Headquarters at the Statler Hotel

Sessions probably will be scheduled on
Electric Insulation, Electronics,
Electrothermics and Metallurgy, Industrial Electrolytics,
and Theoretical Electrochemistry

* * *

Ottawa, September 28, 29, 30, October 1, and 2, 1958

Headquarters at the Chateau Laurier

* * *

Philadelphia, Pa., May 3, 4, 5, 6, and 7, 1959

Headquarters at the Sheraton Hotel

* * *

Papers are now being solicited for the meeting to be held in New York, N. Y., April 27-May 1, 1958. Triplicate copies of each abstract (*not exceeding 75 words in length*) are due at the Secretary's Office, 1860 Broadway, New York 23, N. Y., *not later than January 2, 1958* in order to be included in the program. *Please indicate on abstract for which Division's symposium the paper is to be scheduled.* Complete manuscripts should be sent in triplicate to the Managing Editor of the JOURNAL at 1860 Broadway, New York 23, N. Y.

Current Affairs

R. J. McKay Appointed Publication Committee Chairman

Robert J. McKay was appointed Chairman of the Publication Committee by the Board of Directors at the Washington Meeting of the Society, May 12, 1957. Mr. McKay has been a vice-president of the Society and was president in 1953. He had previously served as Chairman of the New York Section, Chairman of the Corrosion Division, and in various other capacities.

Mr. McKay was born in Washington County, New York, in 1887. He received his B.A. degree at Butler College in 1910 and while there was assistant to Dr. R. B. Moore who was beginning his work on radioactivity and atomic fission. His B.S. degree, in physical chemistry, was received from the University of California in 1913, at which time he was an instructor at this university. After early work with western smelters, he joined the International Nickel Company in 1916. Following experimental work which led to the use of pH control in nickel refining, he did work at Mellon Institute on corrosion of nickel alloys for the International Nickel Company, which was

Robert J. McKay

the basis for early papers on these alloys and the effect of concentration cells in corrosion.

Later, as the company's Superintendent of Technical Service Mr. McKay was active in the development of new products, such as nickel clad steel and the alloy, Inconel, which has had recent attention in connection with jet and other high temperature engines—and he was author of the first paper describing the properties of Inconel. From 1938 until his retirement in 1954 Mr. McKay was Chemical Engineer in charge of Plating Sales and Development; while there he became interested in new industrial uses involving corrosion, heat resistance, and mechanical strength as contrasted with the more commonly known decorative uses of nickel plating.

Mr. McKay's publications include some 40 technical papers on the corrosion properties of nickel alloys, many of them in the TRANSACTIONS of the Society. He is co-author of the American Chemical Society Monograph on "Corrosion Resistance of Metals and Alloys."

Since retiring from the Nickel Company Mr. McKay has been occupied with further studies on concentration cells, the corrosion of nickel plated coatings, and helping with a current revision of the A.C.S. Monograph.

Buffalo Meeting, October 6 to 10, 1957

Leep Zelones Photograph.

Aerial view of Metal Research Labs. and Plant of Electro Metallurgical Co. and Strategic Udy Lab. (lower left) at Niagara Falls, N. Y., which members will visit during Buffalo Meeting.

The Fall Meeting of the Society will be held at the Statler Hotel, Buffalo, N. Y., October 6 to 10, 1957.

A varied and interesting program of technical sessions and trips is promised for the Fall Meeting. The Niagara Falls Section, host of this meeting, has taken full advantage of the concentration of electrochemical and electrothermic industries in the Niagara Frontier in organizing plant visits.

Technical Sessions

The technical program will be conducted by several Divisions, including Battery, Corrosion, Electrodeposition, Electronics (semiconductors), Electro-Organics, and Electrothermics and Metallurgy. Several special symposia have been arranged, on "Metal Powders" by the Electrodeposition Division; on "Corrosion of

Electrodeposited Metals" jointly sponsored by Electrodeposition and Corrosion Divisions; "Ferroalloys and Slag" by the Electrothermics and Metallurgy Division; and a joint symposium and Round Table sponsored by the Electro-Organic and Theoretical Electrochemistry Divisions.

The complete program, including general information, technical sessions, and abstracts, will appear in the August JOURNAL. Additional details will be published in the September issue.

Plant and Laboratory Visits

The world renowned Cornell Aeronautical Lab., Inc., carrying out many programs for government and also for industry, will show its wind tunnels and other unclassified facilities. Carborundum Metals Division of The Carborundum Company at Akron, New York, will open its doors for those interested in zirconium and hafnium production.

On Niagara Falls Day, October 9, there will be a choice of three trips. One will be to the International Nickel Co. plant at Port Colborne, Ont. A second will include part of the plant of Hooker Electrochemical Co., to see its chlor-alkali production facilities, followed by a trip through the Metals Research Labs. of the Electro Metallurgical Co. A third trip will again cross the border for an inspection of the plant of North American Cyanamid Ltd., followed by a tour of the new Sir Adam Beck No. 2 Hydroelectric Plant of the Ontario-Hydro Commission.

Ladies' Program

At the Fall Meeting, in addition to coffee each morning in the ladies' lounge, several activities for the visiting ladies are being arranged. Luncheons will be held at the Park Lane on Monday, October 7, and at the Buffalo Country Club on Tuesday, October 8, to be followed by bridge in the afternoon. The next day, Niagara Falls Day, ladies will be taken by bus to the Niagara Falls Country Club and later on a trip through famous old Fort Niagara and sightseeing along the Niagara River. In the evening the group will join the men for dinner at the Sheraton Brock Hotel.

Abstracts of "Recent News" Papers

Presented at Electronics Division Semiconductor Symposium at Washington Meeting, May 14 and 15

Electrical Properties of High-Purity Indium Phosphide*

T. C. Harman and E. P. Stambaugh, Battelle Memorial Institute, Columbus, Ohio

The technique used for measurement of the electrical properties of InP is discussed. High purity single crystal InP was shown to be electrically and optically homogeneous. The purest specimen contains approximately $4 \times 10^{16}/cm^3$ donor impurities and the behavior of the mobility as a function of temperature suggests negligible compensation. The electron mobility is proportional to $T^{-1.5}$ from high temperatures down to 200°K and reaches a maximum of 14,000 cm^2/volt-sec at 110°K.

* The research reported was supported jointly by the Army, Navy, and Air Force under contract with the Massachusetts Institute of Technology and performed under subcontract with M.I.T.

Pulse Properties and Reliability of Diffused Junction Rectifiers

H. S. Veloric, Bell Telephone Labs., Inc., Murray Hill, N. J.

Experiments on breakdown phenomena in high voltage rectifiers are described and the results related to recent work on surface and body breakdown. The results show that some devices break down uniformly over the area of the junction, others at a few spots on the surface. Most junctions show a negative resistance at power levels from a watt to several kw. Units with avalanche body breakdown are able to dissipate several kw instantaneously. Devices with surface breakdown collapse at a few watts. Devices which collapse under operation at much lower power levels are thought to break down initially at the surface. Some device implications of the data are discussed briefly.

Diffusion of Oxygen in Silicon

R. A. Logan and A. J. Peters, Bell Telephone Labs., Inc., Murray Hill, N. J.

Diffused oxygen layers have been formed in Si at temperatures of 1200°-1400°C. The diffused oxygen layer can be recognized by its etching characteristics. Using Dash's etching technique,[1] the rate of development of the etch-pits associated with edge dislocations in Si is shown to vary with oxygen concentration in the crystal. Pits in oxygen-rich Si (pulled with rotation from a silica crucible) are small compared to those in oxygen-free Si (floating zone). Changes in oxygen concentration caused by heat treatment have been observed in terms of etch-pit size and the results indicate that the precipitation of oxygen on heating near 1000°C does not occur at dislocations.

The diffused oxygen layer can also be converted to low n-type resistivity by heating[2] at 450°C, and is readily demarcated from the p-type floating zone base material which does not change resistivity in this heat treatment. The effective diffusion constant of the donors formed is about 10^{-30} cm^2/sec at 1300°C and has an activation energy of about 3 ev.

[1] W. C. Dash, *J. Appl. Phys.*, **27**, 1193 (1956).

[2] C. S. Fuller, J. A. Ditzenberger, N. B. Hannay, and E. Buehler, *Acta Met.*, **3**, 1 (1955).

Volatile Impurities in Silicon and Germanium

H. A. Papazian* and S. P. Wolsky, Raytheon Manufacturing Co., Waltham, Mass.

A mass spectrographic investigation of the nature and amounts of volatile impurities in Si and Ge has been performed. Concentrations of hydrogen, oxygen, and carbon were found to be as large as 10^{19} atoms/cc in Si and 10^{18} atoms/cc in Ge.

* Present address: Convair Scientific Research Lab., San Diego, Calif.

Vacuum Microbalance Experiments on Germanium and Silicon

S. P. Wolsky, Raytheon Manufacturing Co., Waltham, Mass.

A quartz microbalance capable of detecting weight differences of 0.15 μg has been set up in an ultra-high vacuum system. The argon ion bombardment of Ge and Si has been studied. The rates of sputtering of Ge and Si have been determined as a function of ion energy. Bombardment and oxidation data have been used to obtain information concerning the nature of the Ge and Si surfaces.

Photoengraving in Transistor Fabrication

J. Andrus and W. L. Bond, Bell Telephone Labs., Inc., Murray Hill, N. J.

Photoengraving as adapted to transistor fabrication is described. Methods are given for grinding, lapping, and polishing crystal plates; cleaning and coating them; exposing them to light through a stencil; developing the image, dyeing it, and etching the pattern into the crystal. Chemical formulas are given for etches that retain flatness and remove material controllable to a micron. The method produces strain-free surfaces and allows one to use patterns too small and complicated to be cut mechanically.

Selective Bath Etching of Germanium to Produce Very Narrow Base Regions*

D. E. Sawyer, R. H. Rediker, and J. Lowen, Lincoln Lab., Massachusetts Institute of Technology, Lexington, Mass.

Since holes are necessary in the electrolyte etching of n-type Ge, etching will preferentially occur opposite a hole-injecting rectifying contact. By varying electric circuit parameters, the spatial distribution of the injected holes can be varied and the etched depression made concave, convex, or flat. The etching is periodically interrupted in order to sense the base width. During sensing, the rectifying junction is back biased and a plate is deposited on the etched surface. Monitoring the voltage at

which the junction space charge region punches through to below the plate allows base widths to be etched to as small as 1 μ.

* The research reported was supported jointly by the Army, Navy, and Air Force under contract with the Massachusetts Institute of Technology.

Field Modulation of Liquid Induced Excess Surface Currents on Germanium Diodes

W. T. Erikson, Raytheon Manufacturing Co., Waltham, Mass.

An investigation of the fieldistor effect has been made in light of a recently proposed mechanism for liquid induced excess currents.[1] Field modulation occurs only when the liquid is polar, but high values of reverse current are obtained for nonpolar liquids in which case no field modulation is obtained. The field dependent portion of the excess current is highly temperature dependent, and the field dependent fraction of the total current increases with decreasing temperature down to the freezing point of the polar liquid. The phenomenon is discussed from the point of view that the liquid induced excess current is flowing outside of the semiconductor in the liquid and that this current is being modulated by the field.

[1] W. T. Erikson, H. Statz, and G. A. deMars, *J. Appl. Phys.*, **28**, 133 (1957).

Effect of Gaseous Ambients on the Interface Structure of Germanium

A. Many* and D. Gerlich, Dept. of Physics, The Hebrew University, Jerusalem, Israel

Simultaneous measurements of surface recombination velocity and trapped charged density in the fast states as a function of surface potential are reported. The surface potential is varied over a wide range by the application of large a-c fields normal to the surface. It is found that the distribution and characteristics of the fast states are markedly affected by the surrounding ambients. Initially, with the sample in vacuo, rapid changes in interface structure take place. After a few days, stabilization is essentially reached; following that, repeated exposures to different ambients result in reproducible changes which persist for many weeks.

* On leave of absence. Present address: Physics Lab., Sylvania Electric Products Inc., Bayside, N. Y.

Section News

Council of Local Sections

At its meeting in Washington, D. C., on May 13, 1957, the Council of Local Sections elected the following officers:

Representative of the Council on the Board of Directors—Lee O. Case, 1245 Chemical Bldg., University of Michigan, Ann Arbor, Mich.

Chairman—Howard T. Francis, 107 Walnut St., Park Forest, Ill.

Vice-Chairman—Martin F. Quaely, 88 Mt. Hebron Rd., Montclair, N. J.

Secretary—Karl S. Willson, 3785 W. Thirty-third St., Cleveland 9, Ohio.

Completing the second year of his term is the other representative on the Board of Directors, Fred W. Koerker, 4103 Dyckman Rd., Midland, Mich.

Boston Section

The sixth meeting of the Boston Section was held on March 21, 1957 at the M.I.T. Graduate House, where Dr. Miles V. Sullivan, Bell Telephone Labs., Inc., Murray Hill, N. J. presented a paper on "New Sources of Electrical Energy—The Bell Solar Battery."

The first experimental application of the Bell Solar Battery was the powering of a telephone repeater in an area where conventional power sources are not available. Small solar cells are now available commercially. It is assumed that solar cells will last indefinitely. Demonstrations were given of a solar-powered portable receiver, an FM transmitter, and a toy automobile.

Charles Levy, *Secretary*

Chicago Section

The Chicago Section had as its speaker at the April 8, 1957 meeting Dr. Richard F. Humphreys, Assistant Director for Technical Development, Armour Research Foundation. The title of his talk was "A Nuclear Reactor for Industrial Research." The meeting was held at The Chicago Engineers Club.

Dr. Humphreys was, in large measure, responsible for obtaining the initial operation of the reactor now operating at Armour Research Foundation. He described some of the things one could do with a reactor. First, it gives a ready source of isotopes. Long-life isotopes can, of course, be easily purchased, but short-life isotopes decay too rapidly to permit shipment. The reactor can fill this need. Further, research is in high gear now to study the effects of radiation on matter, such as polymerization, curing, etc. Finally, much work is being done using the neutron as an analyzer, such as neutron diffraction.

W. H. Colner, *Secretary*

India Section

A business meeting of the Section was held on March 17, 1957 at the Indian Institute of Science, Bangalore, with Mr. P. S. Marayana as chairman. The minutes of the Aug. 27, 1956 meeting were confirmed, and the Statement of Accounts for 1956 was approved. The following were nominated Officers of the Section for 1957-58, as per the report of the Nominating Committee:

Chairman—M. S. Thacker
Vice-Chairmen—S. Ramaswamy, K. Srinivas
Secretary—J. Balachandra
Treasurer—T. L. Rama Char

It was decided to communicate the thanks of the Section to the Asia Foundation for continuing the financial assistance to members over Society dues, and to the President and Board of Directors of the Society for their help in the matter.

T. L. Rama Char

Manuscripts and Abstracts for Spring 1958 Meeting

Papers are now being solicited for the Spring 1958 Meeting of the Society, to be held at the Statler Hotel in New York City, April 27, 28, 29, 30, and May 1, 1958. Technical Sessions probably will be scheduled on Electric Insulation, Electronics, Electrothermics and Metallurgy, Industrial Electrolytics, and Theoretical Electrochemistry.

To be considered for this meeting, triplicate copies of abstracts *(not to exceed 75 words in length)* must be received at Society Headquarters, 1860 Broadway, New York 23, N. Y., *not later than January 2, 1958. Please indicate on abstract for which Division's symposium the paper is to be scheduled.* Complete manuscripts should be sent to the Managing Editor of the JOURNAL at 1860 Broadway, New York 23, N. Y.

* * *

The Fall 1958 Meeting will be held in Ottawa, Canada, September 28, 29, 30, October 1, and 2, 1958, at the Chateau Laurier.

Ontario-Quebec Section

The third meeting of the 1956-57 season held in Toronto on the afternoon of March 22 at the Wallberg Building of the University of Toronto was well attended. It was the first time the Section met outside Montreal. Speakers were Dr. H. R. Copson, who is in charge of the Corrosion Section, Research Lab., International Nickel Co., Inc., Bayonne, N. J., whose subject was "Relationship between Stress and Corrosion," and Mr. F. J. Rutland, Sales Engineer for the Electro-Chemical Div., Norton Co., Niagara Falls, Ont., who spoke on "High Temperature Refractories, Manufacture, Properties, and Uses." Dr. L. M. Pidgeon, Head of the Dept. of Metallurgy, University of Toronto, acted as Technical Chairman of the meeting.

H. A. Timm, *Secretary-Treasurer*

Philadelphia Section

The May meeting of the Philadelphia Section was held on the campus of Bryn Mawr college. Cocktails and dinner were enjoyed in the deanery by members and their wives, who afterward adjourned to the chemistry building for the meeting.

The single item of business transacted was the election of officers for 1957-58. Elected were:

Chairman—George Temple
Vice-Chairman—George Bodamer
Treasurer—Albert Ware
Secretary—H. C. Mandell, Jr., Pennsalt Chemicals Corp., Technical Division, 3 Penn Center Plaza, Philadelphia 2, Pa.

A rising vote of thanks was tendered the retiring chairman, Ned Eckfeldt.

Dr. Robert E. Maynard then gave a talk on "Skin Diving—Entrance into Another World," illustrated by slides, movies and equipment on hand for inspection. Dr. Maynard pointed out the attractions to be found beneath the sea for the naturalist, adventurer, artist, and fisherman, and emphasized the lack of danger involved in skin diving, even in the most extreme cases.

Pittsburgh Section

The second meeting of the year was held on March 25, 1957 jointly with the Physical and Inorganic Group of the Pittsburgh Section of the American Chemical Society at Mellon Institute for Industrial Research. After dinner at the Pittsburgh Playhouse, Dr. Virginia Griffing of Catholic University spoke on "The Molecular Orbital Theory of Activation Energies." She presented a formal procedure for discussing the qualitative aspects of chemical binding and chemical interaction between atoms and molecules within the framework of the molecular orbital theory. The procedure was illustrated for a few simple four-atom systems and some quantitative calculations on simple systems were reviewed. It was emphasized that the occurrence and removal of degeneracy of molecular wave function by changing the internuclear parameters should be an important factor in all chemical problems.

Ling Yang, *Secretary-Treasurer*

1956 Directory

The 1956 Directory of Members of The Electrochemical Society is available. The Directory contains an alphabetical and geographical list of members of the Society as of March 1, 1956, and a list of Patron and Sustaining Members, Past Presidents, and winners of Society prizes and awards.

In the Classification of Members preceding page 1, under Type of Membership Affiliation, the following should be added: 7—Emeritus, 8—Life.

Members who wish to receive the Directory are requested to fill in and return the order form below, accompanied by check, to Society Headquarters, 1860 Broadway, New York 23, N. Y.

Please send ..... copy (ies) of the 1956 Membership Directory to:

Name .....

Company .....

Street .....

City ..... Zone ..... State .....

Attached is check for $ ..... for Directory. (Single copies cost $2.00.)

Southern California-Nevada Section

A regular Section meeting was held on April 2, 1957 at the Roger Young Auditorium in Los Angeles, at which the speaker was Mr. Wilbur C. Myers, Director of Research of the Electronic Div. of National Cash Register Co. His topic was "Ferroelectrics." Mr. Myers defined the properties of ferroelectric materials and explained where they fit into the field of solid state physics. Slides showing photographs of the material and the more unusual devices employed were presented.

Lee John Droege,
Secretary-Treasurer

Back Volumes Available

Bound Volumes **12** (1907) through **102** (1955) complete, together with the 5 volumes of Indexes from 1902 through 1951, are available. Anyone interested in obtaining back volumes should contact Dr. Oliver W. Storey, 2 Santa Cruz Blvd., Santa Barbara, Calif.

New Members

In May 1957 the following were approved for membership in The Electrochemical Society by the Admissions Committee:

Active Member Sponsored by a Sustaining Member

Joseph H. Carter, Jr., American Machine & Foundry Co., 509 W. North St., Raleigh, N. C. (Battery)

Active Members

John J. Adams, Tung-Sol Electric, Inc.; Mail add: 55 Walnut St., Belleville 9, N. J. (Electronics, Electrothermics & Metallurgy)

Akio Amaya, Tokyo Tsushin Kogyo Ltd., 351, 6-Kitashinagawa, Shinagawa-ku, Tokyo, Japan (Electronics)

George A. Bartholomew, Applied Research Lab., U. S. Steel Corp., Monroeville, Pa. (Electrodeposition)

Leonard M. Bianchi, Westinghouse Electric Corp.; Mail add: R. D. #6, Iowa St., Greensberg, Pa. (Electrothermics & Metallurgy)

John D. Carroll, Hughes Aircraft Co.; Mail add: 13024 Cimarron Ave., Gardena, Calif. (Electronics, Industrial Electrolytic)

Earl E. Chadsey, Jr., National Research Corp.; Mail add: Concord Rd., Sudbury, Mass. (Corrosion, Electrodeposition, Electrothermics & Metallurgy)

Hung-Chi Chang, Westinghouse Electric Corp., 7325 Penn Ave., Pittsburgh 9, Pa. (Electronics)

Clifford B. Collins, General Electric Co., Nela Park, Cleveland 12, Ohio (Electronics)

Carl E. Coy, Carl E. Coy & Associates; Mail add: 121 Louise Terrace, Glen Burnie, Md. (Electric Insulation, Electronics)

George A. Cypher, General Electric Co.; Mail add: 1524 Myron St., Schenectady 9, N. Y. (Electric Insulation)

George G. Harman, Jr., National Bureau of Standards; Mail add: 4413 Lowell St., S.W., Washington 16, D. C. (Electronics)

Mario M. Jacopetti, University of Naples; Mail add: Via Mezzocannone 4, Naples, Italy (Corrosion, Theoretical Electrochemistry)

Edward T. Johnson, Pittsburgh Metallurgical Co.; Mail add: 4727 Rapids Blvd., Niagara Falls, N. Y. (Electrothermics & Metallurgy)

Howard Lawrence, Bell Telephone Labs.; Mail add: 24 Hibernia Rd., Rockaway, N. J. (Electronics)

Luther D. Loch, Carborundum Co., Research & Development, Niagara Falls, N. Y. (Electrothermics & Metallurgy)

Charles P. Marsden, National Bureau of Standards, Section 1.2, Washington 25, D. C. (Electronics)

Donald R. Mason, University of Michigan, 2028 East Engineering Bldg., Ann Arbor, Mich. (Electronics)

George Mayurnik, Grace Research & Development; Mail add: 139 Union Ave., Garfield, N. J. (Electronics)

James J. McMullen, Dept. of Metallurgical Research, Kaiser Aluminum & Chemical Corp, Spokane 69, Wash. (Theoretical Electrochemistry)

Nelson P. Nies, U. S. Borax & Chemical Corp., 630 Shatto Place, Los Angeles 5, Calif. (Electrothermics & Metallurgy, Industrial Electrolytic)

Remo Pellin, E. I. du Pont de Nemours & Co., Inc.; Mail add: 302 Plymouth Rd., Wilmington 3, Del. (Electronics)

Roger J. A. Potvin, Faculty of Sciences, Laval University, Quebec, P. Q., Canada (Corrosion, Electrothermics & Metallurgy, Theoretical Electrochemistry)

Morton B. Prince, Hoffman Semiconductor Div.; Mail add: 930 Pitner Ave., Evanston, Ill. (Electronics)

Joseph M. Rafferty, Northrop Aircraft Inc.; Mail add: 11818 Crenshaw Blvd., Inglewood, Calif. (Corrosion, Electrodeposition)

Howard L. Recht, Pittsburgh Consolidation Coal Co.; Mail add: 711 Riehl Dr., Pittsburgh 34, Pa. (Battery, Corrosion, Theoretical Electrochemistry)

Wesley W. Riches, E. I. du Pont de Nemours & Co., Inc.; Mail add: 112 Banbury Dr., Wilmington 3, Del. (Electronics)

Dibyendra L. Roy, Central Electrochemical Research Institute, P. O. Alagappa College, Karaikudi (S. Rly), India (Battery, Corrosion, Electrodeposition, Electronics, Electrothermics & Metallurgy, Industrial Electrolytic, Theoretical Electrochemistry)

Roswell J. Ruka, Westinghouse Electric Corp., Churchill Boro., Beulah Rd., Pittsburgh 35, Pa. (Electronics)

Edward Sailer, Radio Corp. of America, Somerville, N. J. (Electronics)

Glenn R. Schaer, Battelle Memorial Institute, 505 King Ave., Columbus 1, Ohio (Electrodeposition)

Bernard F. Schoen, Nepera Chemical Co., Inc.; Mail add: 200 Woodstone Rd., Rockaway, N. J. (Electro-Organic)

Bertram Schwartz, Hughes Aircraft Co.; Mail add: 5315 W. 102 St., Los Angeles 45, Calif. (Electronics)

Ralph L. Sherwood, Semiconductor Div., Radio Corp. of America; Mail add: 63 No. Hamilton Ave., Trenton 9, N. J. (Electronics)

George A. Snow, Simplex Wire & Cable Co.; Mail add: Cross St., Hopkinton, Mass. (Corrosion, Electrothermics & Metallurgy)

Mark von Stackelberg, University of Bonn, Wittelsbacher Ring 1, Bonn, Germany (Theoretical Electrochemistry)

William A. Sterner, American Smelting & Refining Co.; Mail add: 12 MacArthur Dr., Fords, N. J. (Electrodeposition, Electronics, Industrial Electrolytic)

Delbert M. Van Winkle, Hughes Aircraft Co., International Airport Station, Los Angeles 45, Calif. (Electronics)

Robert C. Walker, Dow Chemical Co.; Mail add: 2461 Letts Rd., R.R. #3, Midland, Mich. (Industrial Electrolytic)

John W. Ward, Los Alamos Scientific Lab.; Mail add: 107 Acorn St., Los Alamos, N. Mex. (Theoretical Electrochemistry)

Mary W. Wegner, Hughes Aircraft Co.; Mail add: 3662 Cardiff Ave., Los Angeles 34, Calif. (Electronics)

Joseph Weissbart, Research Labs., Westinghouse Electric Corp., Pittsburgh 35, Pa. (Corrosion, Theoretical Electrochemistry)

Joseph G. Wurm, Faculty of Sciences, Laval University, Quebec, P. Q., Canada (Industrial Electrolytic)

Student Associate Members

William E. Garrison, Jr., University of Illinois, 14 East Chemistry Bldg., Urbana, Ill. (Electronics, Electro-Organic)

Ralf Koslow, New York University; Mail add: 785 West End Ave., New York 25, N. Y. (Corrosion, Electrodeposition, Electronics, Theoretical Electrochemistry)

Donald E. Nisbett, Hiram College; Mail add: 630 Vienna Ave., Niles, Ohio (Electrothermics & Metallurgy, Theoretical Electrochemistry)

Larry L. Schwartz, Western Reserve University; Mail add: 315 No. Buchanan St., Fremont, Ohio

By action of the Board of Directors of the Society, all prospective members must include first year's dues with their applications for membership.

Also, please note that, if sponsors sign the application form itself, processing can be expedited considerably.

December 1957 Discussion Section

A Discussion Section, covering papers published in the January—June 1957 JOURNALS, is scheduled for publication in the December 1957 issue. Any discussion which did not reach the Editor in time for inclusion in the June 1957 Discussion Section will be included in the December 1957 issue.

Those who plan to contribute remarks for this Discussion Section should submit their comments or questions in triplicate to the Managing Editor of the JOURNAL, 216 W. 102 St., New York 25, N. Y., *not later than September 1, 1957*. All discussion will be forwarded to the author, or authors, for reply before being printed in the JOURNAL.

New Address

for

The Electrochemical Society, Inc.

1860 Broadway New York 23, N. Y.

Telephones—CIrcle 5-6282, CIrcle 5-6283

The Electrochemical Society has moved its offices to new quarters, located on the northeast corner of 61st Street and Broadway. All communications to the Society and the JOURNAL should be addressed to the new address, 1860 Broadway.

Associate Member

Richard E. Henriks, Hughes Products; Mail add: 3630 Motor Ave., Los Angeles 34, Calif. (Electronics)

Reinstatements to Active Membership

Charles D. Coxe, Handy & Harman, Bridgeport 1, Conn. (Battery, Corrosion, Electrodeposition, Electronics, Electrothermics & Metallurgy, Theoretical Electrochemistry)

Palmer H. Langdon, Finishing Publications, Inc., 381 Broadway, Westwood, N. J. (Electronics)

Charles E. MacKinnon, International Salt Co., Inc., Marine Trust Bldg., Buffalo 2, N. Y. (Industrial Electrolytic)

James S. Sconce, Hooker Electrochemical Co.; Mail add: Forest Rd., Lewiston, N. Y. (Industrial Electrolytic)

Thottuvelil J. Varkey, St. Joseph's College; Mail add: 13 Nanjappa Rd., Shantinagar, Bangalore, India (Corrosion, Electrodeposition, Electrothermics & Metallurgy)

Transfer from Associate to Active Membership

Henry B. Maier, Devenco, Inc.; Mail add: 415 W. 118 St., New York 27, N. Y. (Corrosion, Electrodeposition, Electronics, Electrothermics & Metallurgy)

Deceased Reported during April 1957

Fernand Portail, Neuilly, Seine, France

Correction

There was an omission in the monograph series published in 1956 in the Annual Report of the Board of Directors for 1956, given at the Society's Annual Business Meeting held on May 14, 1957 in Washington, D. C. "Arcs in Inert Atmospheres and Vacuum," W. E. Kuhn, Editor, was published by John Wiley & Sons, Inc., in 1956.

Personals

John Frederick Gall has been advanced from Director of Inorganic Research to the newly-created position of Assistant Manager of the Research and Development Dept. at Pennsalt Chemicals Corp., Philadelphia. Associated with Pennsalt since 1939, he is well-known professionally in the fields of electrochemistry and fluorine chemistry and is the author of numerous scientific publications.

H. C. Mandell, Jr., has been promoted to Group Leader in the Inorganic Research Dept. of Pennsalt Chemicals Corp. In his new post Dr. Mandell will supervise research in inorganic synthesis. Previously, he was Senior Research Chemist. Although broadly experienced in inorganic and electrochemistry, his more recent interests are in the field of high energy fuels and oxidants.

John J. Lander has been appointed Manager, Basic Battery Research, and **Raymond C. Haefner** assumes new duties as an Assistant Chief Engineer within the Battery Engineering Div. in charge of research and development functions of the division, in a series of appointments within Central Engineering of The Electric Auto-Lite Co., Toledo, O. Mr. Haefner will direct the Commercial Engineering and Customer Engineering Contact functions of the battery division.

E. Robert Breining has joined the Commonwealth Engineering Co. of Ohio, Dayton, O., as Technical Director of Gas Plating Activities. Formerly he had been Supervisor of Electrochemistry Research at General Motors Research Staff.

P. S. Narayana has been nominated a member of the Council of the All India Management Associations.

S. D. Gokhale has joined the Chemistry Div., Atomic Energy Establishment, Bombay, India.

News Items

Union Carbide Changes Name

The name of Union Carbide and Carbon Corp. has been shortened to Union Carbide Corp. Stockholders approved this change at the Annual Meeting of the Corporation on April 16.

The names of three divisions of Union Carbide have also been changed. Carbide and Carbon Chemicals Co. has become Union Carbide Chemicals Co.; Linde Air Products Co. is changing its name to Linde Co., and Carbide and Carbon Realty

Co. will be known as Union Carbide Realty Co.

Cleveland to Get $1,500,000 Engineering Center

Construction of a $1,525,000 Cleveland Engineering and Scientific Center on Chester Avenue near East Thirtieth Street is to begin immediately, representing the largest money commitment of its type to be made in Cleveland since the 1930's. The new structure will provide adequate meeting facilities for more than 53 engineering and technical groups and through its over-all program of individually organized activities will be a Center for continuing technical education.

The Cleveland Engineering and Scientific Center will have approximately 50,000 square feet of floor space or about three times the space now available at the Cleveland Engineering Society's present building, a remodeled telephone exchange at 2136 East Nineteenth street.

The Center will have an auditorium of approximately 900 seating capacity, a single-purpose, slanted floor auditorium to accommodate 150 people, a main dining room serving 350 people, and three special dining-meeting rooms and class rooms. The auditorium, and an adjacent future dining room, are designed for heavy loading for exhibition purposes. Office space is also available for society offices, and special services, such as mailing and duplication, will also be offered.

Silicon Carbide Rectifier Operates up to 1200°F

A silicon carbide rectifier has been operated at temperatures up to 1200°F, the General Electric Research Lab. recently announced. Similar devices made with other semiconductor materials, notably silicon, have been able to operate only up to the 400-500°F range.

"Although currents of several amperes have been rectified with usable efficiency, the practical future of silicon carbide in rectifiers and other solid-state devices will depend on progress in the preparation of this highly stable but extremely stubborn material," according to Dr. Guy Suits, GE vice-president and director of research.

Basic studies of silicon carbide, a material best known as an abrasive, are part of a GE research program aimed at exploring a variety of compound materials for use in solid-state electronic devices.

"Most of the semiconductor devices now on the market have been made from single-element materials —principally germanium and silicon —but future progress appears to depend on learning more about compounds," Dr. Suits said. "A major problem in all semiconductor research, that of achieving extremely pure materials, becomes increasingly difficult when more than one element is involved."

The GE research director emphasized that the silicon carbide rectifier is still in laboratory development and that the announcement was "simply to affirm the important scientific fact that solid-state rectification has been observed in the range of temperatures from —100° to 1200°F."

Ratings up to 140 amperes per cell are available in the new high power silicon component rectifiers announced by General Electric Rectifier Dept. at Lynn, Mass. Heart of the new rectifier is a small silicon wafer in a hermetically sealed enclosure of ceramic and welded stainless steel.

Additional information on high-current silicon rectifiers may be ob-

Opening for ELECTROCHEMIST

Interested In Development Work in aqueous and fused salt electrolysis, including all aspects of cell operation

A program is being established in a new laboratory devoted to these fields of investigation, and contacts will be had with Management, Research, Sales, Production, and Customer organizations.

The man we want should be well grounded in theoretical and applied electrochemistry and preferably should have had one or more years experience in the electrolysis of alkali halides and metal compounds. Emphasis will be placed on the commercial application of the work.

This is a challenging opportunity to establish yourself with a Development program in electrolysis where the future is practically unlimited.

Please submit full details of qualifications to:

NATIONAL CARBON COMPANY

Division of Union Carbide Corporation • Development Laboratory
3625 Highland Avenue, Niagara Falls, New York—Attention: Dr. H. J. Johnson

RESEARCH AND DEVELOPMENT

Research program requires experienced electrochemists to work in electrolytic process development. Excellent laboratory facilities located twenty miles East of Los Angeles.

GROUP LEADER

Electrochemical engineer, three to four years experience desired. The man we are seeking need not be acting in this capacity at the present time, but desires more responsibility based on successful performance in electrochemical research and process development.

ELECTROCHEMIST

Position open in electrochemical process development. Degree in chemistry or chemical engineering with two to three years experience required. Salary commensurate with experience.

Send resume to: Personnel Manager

American Potash & Chemical Corporation

3030 W. 6th St., Los Angeles 54, Calif.

Just Published!

SEMICONDUCTOR SURFACE PHYSICS

Proceedings of the Conference on the Physics of Semiconductor Surfaces, June, 1956.

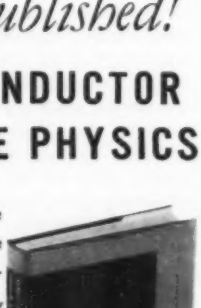

Edited by R. H. KINGSTON, with the assistance of E. Burstein, A. L. McWhorter, P. H. Miller, Jr., D. T. Stevenson, and P. B. Weisz.

This important new work of paramount interest to physicists and physical chemists is a collection of invited papers devoted to the latest developments in the significant field of research which led to the discovery of the transistor, and which directly concerns the specialist in catalysis.

For the physicist, there are detailed reports on the most recent interpretation of surface state, surface conductance, and related phenomena on germanium and silicon surfaces, plus a description of the experimental techniques being used to study the newer semiconductor materials, and those aspects of surface phenomena related to the chemical structure of the surface.

For the physical chemist, there is valuable information on the effect of electronic properties of the semiconductor surface on oxidation and catalysis.

The book is divided into four sections: CLEAN SURFACES - REAL SURFACES - ADSORPTION AND CATALYSIS - OXIDATION — each full of detailed and dependable information.

1957 405 pages, 130 figures $8.00

Mail this coupon for a 10-day Free examination copy!

University of Pennsylvania Press
Dept. 2210
3436 Walnut Street, Philadelphia 4, Pa.

Please send me a copy of SEMICONDUCTOR SURFACE PHYSICS to read and examine free of charge. In 10 days I will return the book, or I will remit $8.00, plus postage.

Name .....
Address .....
City ..... Zone ..... State .....

( ) SAVE MONEY! Check here if you ENCLOSE payment, in which case we pay postage. Same return privilege, refund guaranteed.

tained by writing for bulletin GET-2689, General Electric Co., Schenectady 5, N. Y.

Distribution of Certain Short-Lived Radioisotope Standards

Effective May 6, 1957, the National Bureau of Standards discontinued the distribution of the following radioactivity standard samples of short-lived radioisotopes, which are now commercially available: NBS Standard Sample No. 4916 Phosphorus-32; NBS Standard Sample No. 4917 Iodine-131; NBS Standard Sample No. 4918 Gold-198; NBS Standard Sample No. 4923 Sodium-24; NBS Standard Sample No. 4933 Potassium-42.

Standardized samples of these nuclides may be obtained from the Nuclear-Chicago Corp., 223 West Erie Street, Chicago 10, Ill. The standards to be issued by this firm will be derived from comparisons made with the primary standards of the National Bureau of Standards. The firm, however, has accepted full responsibility for the standardization of the samples that it distributes.

Discontinuance of this activity will permit the Bureau to devote more of its resources toward meeting the demands of science and industry for new and more accurate standards. The Bureau's action also conforms with the Federal Government's general policy of withdrawing from activities that can be carried on by private business. The Bureau will, however, continue to maintain the primary disintegration-rate standards of these nuclides, with which commercially available secondary standards may be compared. It is anticipated that there will be no interruption in the distribution schedules of the above standards.

Olin Mathieson International Corp. Formed

Formation of Olin Mathieson International Corp. and appointment of Henry A. Arnold as the new corporation's president has been announced by Thomas S. Nichols, chairman of Olin Mathieson Chemical Corp., and Stanley de J. Osborne, president. The new company is a wholly owned subsidiary.

Book Reviews

Essentials of Qualitative Analysis, An Introduction to the Basic Unit Operations by A. A. Benedetti-Pichler. Published by the Ronald Press Co., New York, 1956. XIV + 666 pages, $15.00.

The point of view adopted by the well-known analyst who is the author of this book is that trustworthy analyses depend on an understanding and mastery of a variety of simple operations and techniques. Each of these is discussed lucidly in great detail with many references to other published material. Approximately two-thirds of the book is devoted to these unit operations, after which follows a series of experiments sufficient for a two-term course. The suggested experiments are characterized by a statement of the principle involved and unusually clear directions. A final feature of the book is the inclusion of nearly 30 useful tables in the appendices.

The author believes that the function of a text in a formal course is to relieve the instructor of long discussions of techniques and procedures but not to provide a set of lecture notes. Thus, there are no discussions of the theory of acidimetry, oxidation titrations, electrochemistry, etc., since the individual instructor is expected to have his own preferred method of presenting such material.

The book will serve many useful purposes not only in analysis directly but in many other laboratory activities since the so-called unit operations are involved whenever a careful experiment is planned.

John E. Vance

Photoconductivity Conference, Edited by R. G. Breckenridge, B. R. Russell and the late E. E. Hahn. Published by John Wiley & Sons, Inc., New York, 1956. XIII + 365 pages, $13.50.

This comprehensive volume includes 30 papers presented at the November, 1954 Photoconductivity Conference at Atlantic City, N. J. Although two years passed between the Conference and the appearance of this book its papers include numerous references to published work through 1955 and with few exceptions (notably in the area of magnetic interactions in the fundamental optical absorption) represent a summary of the available information on photoconductivity.

The book is divided into five major sections. The first section, Phenomenological Theory of Photoconductivity, discusses the important parameters affecting the properties of photoconductors and the relationship from an information theory point of view between lifetime, limit of sensitivity and information rate in photoconductors. The second section, Photon Absorption Process, includes theoretical treatments of localized energy levels in solids, transition properties of electrons and holes in such trapping levels, indi-

rect photon transitions (those involving phonons) between bands, absorption near band edges, and the experimental status of infrared absorption in germanium and silicon and its implications for the band structure of these materials. The third section, Electron Processes, treats the motion, trapping, and recombination of holes and electrons in photoconductors, surface photoeffects, the photoelectromagnetic effect, and in considerable detail minority carrier trapping in silicon. The fourth section, Photoconducting Materials, considers the properties of silicon, germanium, the intermetallic compounds, ionic crystals, the lead salt photoconductors, and zinc oxide. The fifth section, Current Topics, discusses more recent photoconductivity results on indium and antimonide, gold-doped germanium, tellurium, cadmium selenide, lead sulfide, and lead telluride.

The majority of the papers are a review of important areas within the photoconductivity field. The outstanding contribution to the book is one of these: the paper by Burstein, Picus, and Sclar on the Optical and Photoconductive Properties of Silicon and Germanium. There are, however, a number of papers which treat particular aspects of specific photoconductors in detail. The paper by Haynes and Hornbeck on The Trapping of Minority Carriers in Silicon is an excellent example.

The book does not have the organization or the uniform presentation one would expect in a volume by one author. It does cover the photoconductivity field with adequate reference to the literature and with very little duplication in spite of the number of its authors. The overlapping of the study of the optical properties of germanium and silicon by Burstein, Picus, and Sclar and by Fan, Shepherd, and Spitzer is clearly justified and the two papers on gold-doped germanium by Dunlap and by Morton, Hahn, and Schultz are not objectionable.

As a whole the book is an excellent reference source for the photoconductivity field though it is scarcely a good text book on the subject.

Walter L. Brown

Announcements from Publishers

The Effects of Interstitial Contaminants on the Notch-Tensile Properties of Titanium and Titanium Alloys. Part 2—Alloy Titanium. E. P. Klier and N. J. Feola, Syracuse University, for Wright Air Development Center, Aug. 1956. Report PB 121575,* 202 pages, $5.50.

Surface Hardening of Titanium with Metalloid Elements. Armour Research Foundation, for Watertown Arsenal, U. S. Army, May 1953. Report PB 111821,* 151 pages, $4.00.

This final report describes the surface hardening of titanium and titanium alloys with the metalloid elements oxygen, carbon, hydrogen, boron, and nitrogen.

Heat of Formation and Entropy of Titanium Tetrachloride, W. F. Krieve and others, California Institute of Technology, for Ordnance Corps., U. S. Army, Jan. 1954. PB 121734,* 17 pages, 50 cents.

Vapor Deposited Coatings. Final Report, L. M. Schetky, H. S. Spacil, and J. Wulff, Massachusetts Institute of Technology, for Watertown Arsenal, U. S. Army, Aug. 1955. PB 121725,* 64 pages, $1.75.

Volume Change and Gas Evolution on Heating Electrolytic Chromium, K. A. Moon and G. A. Consolazio, Watertown Arsenal, U. S. Army, Jan. 1956. PB 121768,* 15 pages, 50 cents.

A Study of the Feasibility of Coating Magnesium with High-Purity Aluminum, C. F. Powell and I. E. Campbell, Battelle Memorial Institute, for Wright Air Development Center, Nov. 1956. PB 121860,* 28 pages, 75 cents.

Electricity and Magnetism by J. Newton. Philosophical Library, New York, 1956. ix + 613 pages. $10.00.

Scientific French by William N. Locke. John Wiley & Sons, Inc., New York, 1957. x + 112 pages, $2.25.

Meant to supplement elementary courses in learning to read and translate scientific French.

Thermodynamic Properties of Chlorine by R. M. Kapoor and J. J. Martin. University of Michigan Press, Ann Arbor, 1957. 40 pages, $2.25.

Development of equations for PVT relations, vapor pressure, saturated liquid density, specific heat; calculation and tabulation of PVT, enthalpy and entropy for saturated liquid and vapor from m. p. to crit. temp. Same for superheated vapor up to P = 1400 psi. P-H and T-S diagrams. Units are °F, °R, cu ft/lb, Btu/lb, psi etc.

Semiconductor Surface Physics, Proceedings of the Conference on the Physics of Semiconductor Surfaces, June 1956. Edited by R. H. Kingston, with the assistance of E. Burstein, A. L. McWhorter, P. H. Miller Jr., D. T. Stevenson, and P. B. Weisz. University of Pennsylvania Press, Philadelphia. 405 pages, more than 130 graphs and figures, index, $8.00.

A collection of invited papers and contributed discussion on the latest interpretation of surface states surface conductance, and related phenomena on germanium and silicon. Attention is given to those aspects of surface phenomena related to the chemical structure of the surface, in particular the electron-transfer mechanism between the bulk and the surface layer, and information on the effect of the semiconductor surface on oxidation and catalysis. The book is divided into four sections, Clean Surfaces, Real Surfaces, Adsorption and Catalysis, and Oxidation.

Chemical Apparatus Standard Revised. A revision, TS-5354, of the Commercial Standard for Interchangeable Ground-Glass Joints, Stopcocks and Stoppers CS21-39 recommended by a Standing Committee of the Industry, may be obtained while the supply lasts by addressing a request to F. W. Reynolds, Commodity Standards Div., Office of Technical Services, U. S. Dept. of Commerce, Washington 25, D. C.

Bibliography on Applications and Properties of Zirconium and Alloys, a seven-page bibliography giving up-to-date source material on properties of zirconium and its alloys will be furnished on request by J. W. Blanton, Columbia-National Corp., 70 Memorial Drive, Cambridge 42, Mass.

Gmelins Handbuch der anorganischen Chemie, Eighth edition. The volumes of this Handbuch are prepared by the Gmelin Institute and are published by Verlag Chemie, GmbH, Weinheim/Bergstrasse. They are available through book importers such as Walter J. Johnson, Inc., and Stechert-Hafner, Inc., New York.

Calcium. System No. 28, Part A, Sect. 2, 1957. xii + 420 pages, $55.68. Occurrence, geochemistry, and economic geography of calcium compounds (313 pages); physical, elec-

* Order from Office of Technical Services, U.S. Dept. of Commerce, Washington 25, D. C.

trochemical and chemical properties of the metal (91 pages); calcium alloys.

Zinc. System No. 32, Supplement Volume, 1956. xxxvi + 1025 pages. $138.00. The previous volume on Zinc was published in 1924, and this Supplement presents material appearing in the literature from 1924 to 1949. It covers occurrence, metallurgy, purification, preparation of salts; physics of the metal (124 pages), electrochemical behavior (137 pages), chemical properties (68 pages), etc.

Platinum. System No. 68, Part D, 1957. Liv + 638 pages, $90.00. Complex compounds of platinum with neutral ligands. Describes 2880 platinum compounds of this type, covering the literature through 1953. The whole of the Russian literature, which predominates in this field, is surveyed.

Symposium on Corrosion Fundamentals, edited by A. de S. Brasunas and E. E. Stansbury. University of Tennessee Press, Knoxville, 1956. v + 255 pages, $5.00. A series of lectures given at the University of Tennessee Corrosion Conference in March, 1955.

Not a textbook on corrosion, but very well planned to cover most of the important principles, illustrated with examples which should make the application to industrial corrosion control obvious. Some of the topics included are: effect of metal structure (Stansbury); atmospheric corrosion (H. R. Copson); coatings (J. I. Richardson, R. B. Seymour); cathodic protection (Milton Stern, H. C. Van Nouhuys); inhibition (H. C. Gatos); mechanical factors (J. J. Harwood); passivation (N. A. Nielsen).

Project Engineering of Process Plants, by Howard F. Rase and M. H. Barrow. John Wiley & Sons, Inc., New York, 1957. xii + 692 pages, $14.25.

Emphasizes the importance of the trained project engineer to coordinate efforts in modern complex plant design.

V.H.F. Television Tuners, by D. H. Fisher. Philosophical Library, Inc., New York, 1957. vii + 136 pages, $6.00.

Frequency Modulation Receivers, by J. D. Jones. Philosophical Library, Inc., New York, 1957. ix + 114 pages, $6.00.

Light, Vegetation and Chlorophyll, by J. Terrien, G. Truffaut and J. Carles. Philosophical Library, Inc., New York, 1957. 228 pages, $6.00.

Meetings of Other Organizations

Sept. 8-13—American Chemical Society, National Meeting, New York, N. Y.

Sept. 15-18—American Institute of Chemical Engineers, Regional Meeting, Lord Baltimore Hotel, Baltimore, Md.

Oct. 1-4—National Association of Corrosion Engineers, North Central Regional Meeting, Chicago, Ill.

Oct. 1-4—National Association of Corrosion Engineers, South Central Regional Meeting, Oklahoma City, Okla.

Oct. 7-9—National Association of Corrosion Engineers Northeast Regional Meeting, Pittsburgh, Pa.

Employment Situations

Please address replies to box shown, c/o The Electrochemical Society, Inc., 1860 Broadway, New York 23, N. Y.

Positions Wanted

Chemist, 15 years' creative and responsible work in metal finishing, corrosion, with experience in the continuous anodizing and dyeing of aluminum, seeks position in or near Metropolitan New York. *Reply to Box 361.*

Storage Battery Chemist is interested in a responsible position in research and development. Has a long and successful record in lead-acid battery field, and a good understanding of problems facing the industry, coupled with imagination and a scientific approach to practical problems. Publications and patents. *Reply to Box 362.*

Advertisers' Index

American Potash & Chemical Corporation 147C
Baker & Adamson, General Chemical Division, Allied Chemical & Dye Corporation 137C
Bell Telephone Laboratories, Inc. 139C
Continental Can Company, Inc. 150C
Dow Chemical Company..... 140C
Enthone, Incorporated.....Cover 4
Great Lakes Carbon Corporation ..... Cover 2
National Carbon Company..... 147C
University of Pennsylvania Press 148C

CORROSION RESEARCH

For long range and fundamental research work in container corrosion problems, encompassing practically all types of corrosion principles and investigational techniques. Good understanding of electrochemical fundamentals required. Applicant must have Ph.D. degree or equivalent ability.

Excellent working conditions in well-equipped laboratory with high-caliber associates. Company has liberal benefit plans and will pay salary commensurate with abilities. Write to:

Director, Electrochemical Metallurgy Laboratory
Central Research and Engineering Division

Continental Can Company, Inc.
7622 South Racine Avenue
Chicago 20, Illinois